

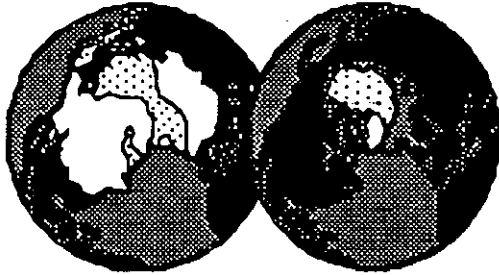
GEOMORPHOLOGICAL WATERSHED ANALYSIS PROJECT
ANNUAL REPORT FOR THE PERIOD FROM 10/91 TO 5/92

By

David Montgomery



May 18, 1992



QUATERNARY RESEARCH CENTER

University of Washington, Seattle, Washington 98195
(206) 543-1166 FAX 543-3836

Geomorphological Watershed Analysis Project

Annual Report for the period from 10/91 to 5/92

Submitted to the Sediment, Hydrology and Mass Wasting Committee
of the Timber/Fish/Wildlife Agreement

compiled by

David R. Montgomery
Quaternary Research Center and Department of Geological Sciences
University of Washington
Seattle, WA 98195

5/18/92

Nancy Sturhan
DNR Forest Practice Division
P.O. Box 47012
Olympia, WA 98504-7012

Dear Ms. Sturhan,

This document constitutes the first annual report for the Geomorphological Watershed Analysis project funded by the SHAMW committee under the Timber/Fish/Wildlife agreement. The report covers the seven month period from October 1, 1991, to May 1, 1992. The format of this report may differ from the standard TFW report format, but it is intended to communicate our progress in research on the geomorphology of mountain watersheds. We present a brief overview of our project, review the objectives defined in our proposal, compare progress to date with the projected targets, and briefly discuss some objectives for research in the upcoming year. Finally, in an appendix format we present a series of draft research papers and preliminary results produced by the project to date. One of these papers has been accepted for publication by a scientific journal. Two others are draft manuscripts. The abstract of a third draft manuscript that is almost completed is also included. The draft manuscripts are presented in this report with the understanding that they are not for distribution outside of the SHAMW committee at this time. We include them to allow assessment of project progress. In the immediate future we will be soliciting preliminary reviews from experts both within and external to the TFW process. Reviewers comments and revisions based on our upcoming field work will be incorporated at a later date when these draft manuscripts are presented in a formal report. It is our intention to publish our results in the scientific literature, as well as in TFW reports, and we have chosen this presentation format for our annual report to facilitate ongoing dialog with the SHAMW committee while maintaining progress toward our research objectives. Our final biennial report will be more formal.

Geomorphological Watershed Analysis

The overall goal of the Geomorphological Watershed Analysis project is to provide the scientific basis for predicting the response of hillslopes and channel systems in forested mountains to both long-term average conditions [climate, geology, topography, vegetation] and short-term perturbations [fire, extreme storm events, and timber harvest]. Our approach is oriented toward developing objective, physically-based procedures for assessing and interpreting the current condition of channels and hillslopes, and for predicting response to watershed perturbations such as accompany timber harvesting. Conceptually, we view

potential hillslope and channel responses as linked through the processes controlling sediment mobilization, routing, and storage within a watershed. While maintaining this watershed context, we have divided our study into three distinct components: shallow sediment sources, deep-seated landslides, and channel condition and response. Study plans and schedules for each of these components are presented in our original proposal. A brief review of progress toward our objectives follows.

Interactive Team of Researchers

A major goal of our project is the development of an interactive team of faculty and graduate student researchers studying the geomorphology of mountain drainage basins. Personnel directly funded by the project include one of the PI's [Montgomery] and three graduate students [Bauer, Buffington, and Schmidt], one working on each aspect of our project. Two computer programmers [Greenberg and Reiss] are partially supported by TFW funding. A fourth student has been admitted to UW to work on the channel assessment component starting in Fall, 1992. A post-doctoral fellow [Miller] will be funded in academic year 92-93 to work on the deep-seated mass wasting component of the project. The timing of recent budget uncertainties relative to our admission process and the subsequent elimination of \$28k from our project precluded further expansion of the program.

Communication between the PI's [Dunne, Montgomery, and Dietrich] occurs frequently and the entire project met at UW on April 5th to discuss progress and research directions. The TFW salaried personnel and the other PI's [Dunne and Dietrich] also have brought several collaborators to work on projects directly relating to project goals. Dr. Weihua Zhang (Univ. of Washington postdoctoral researcher funded from federal sources) has been working with Dr. Montgomery on examining the effects of digital elevation model (DEM) resolution on simulations of surface and hydrologic processes. Dr. Efi Foufoula (Univ. of Minnesota) has begun a collaborative effort with Dr. Montgomery focused on investigating methods to delineate the hillslope/channel network transition from DEM's. Dr. Montgomery also has been coordinating research efforts on channel assessment and response with Dr.'s Lee MacDonald and Ellen Wohl at Colorado State University with the goal of standardizing data collection procedures so as to maximize the usefulness of data collected by both groups. Communication is continuing with Dr. Cathy Wilson of CSIRO (Australia). She is working with the research group that developed the digital terrain model TOPOG, which we are using as the basis for our shallow debris flow prediction model. Their group is trying to develop a dynamic version of TOPOG. Dr. Wilson will be visiting UW at the expense of the Australian government during mid-June to discuss our research.

We also have provided input to other TFW funded, or related, projects through consultations, collaboration, and loans of equipment. The Ambient Monitoring Project approached us for advice on data collection methodologies and analysis in October and November, 1991. Prior to the program's termination, we suggested revisions to their field methods that would have increased the utility of their data for use in our analyses and those of other resource management professionals. We also suggested revisions in their analysis procedures that they have incorporated with productive results. A desired set of data for collection in any future efforts was transmitted to the Ambient Monitoring Committee through Jeff Light and Kate Sullivan. We also provided input for Ed Rashin's project on BMP evaluation at Washington State Department of Ecology, JoAnne Metzler's peak discharge channel damage assessment methodology, and Phil Peterson's response thresholds review. Additionally, we are pursuing plans for collaborative research on the history of landsliding in the Hoh River basin with Susan Calder, the DNR geologist located in Forks. In an effort to stimulate collaboration between fisheries biologists and geomorphologists we have been working on field measurements with, and loaning equipment to, Phil Peterson of the TFW "Big Fish" project for his study on channel scour and bed modifications at Kennedy Creek. Also, at the request of the SHAMW committee we have been developing a process-based channel classification that we hope will encourage further interdisciplinary research and provide insight into watershed analysis. In summary, we have established an interactive research group that extends well beyond the size of our TFW-funded personnel and we are involved in projects that extend beyond the scope of our original proposal.

Shallow Sediment Sources

Progress toward the objectives outlined in our proposal is summarized below.

- 1) Develop a method for determining how well digital elevation data represent actual watershed topography to the degree necessary for locating sediment sources.

We have developed two methods for examining the quality of landscape representation in digital elevation models. These methods are outlined in two of the draft manuscripts included in this report as appendices 1 and 2 [Bauer, in prep., Zhang and Montgomery, in prep.]. The method developed by Bauer is based on calculating the signal to noise ratio of a digital elevation surface. This approach provides a method for determining the quality with which an object of a given size (a hillslope or a debris flow source area, for

example) is represented in a DEM. The approach developed by Zhang and Montgomery examines the effect of DEM grid size on the distribution of the topographic parameters that influence both runoff generation and surface process models and on hydrologic simulations based on these models. Both of these studies have fundamental implications for the use of DEM's in surface process models and point to the need to use a DEM scale that is appropriate for resolving landscape features and processes of interest.

- 2) Test the use of a steady state shallow subsurface runoff model to predict spatial distribution of ground saturation in steep, realistically complex terrain.

We recently had a paper accepted in the journal "Geology" based on TFW-supported work on predicting the spatial pattern of runoff production and erosion mechanisms using the steady state shallow subsurface runoff model TOPOG. This paper discusses the partitioning of landscapes into different process regimes on the basis of slope, contributing drainage area, and threshold process theories. These thresholds provide the theoretical underpinnings of the DEM-based watershed modelling approach that we are developing. The paper is included in this report as Appendix 3. Also we are conducting steady state sprinkler experiments on a small catchment in Coos Bay, Oregon, from May 26 to June 14, 1992, in part to provide a data set against which to test the predictions of steady state shallow subsurface runoff models. Together with an earlier set of sprinkler experiments this data set will allow examination of the utility of the hydrologic model for use in steep terrain.

- 3) Develop a method for predicting areas prone to shallow landsliding in a watershed through the use of topographic analysis software.

We have developed a DEM-based method for predicting relative debris flow hazard in a catchment. A draft manuscript describing the model and documenting model predictions [Montgomery and Dietrich, in prep.] is included in this report as Appendix 4. To date, this model has been tested in two catchments: one in Marin County, California, and one in the Oregon Coast Range near Coos Bay. Model results are quite encouraging and are detailed in the draft manuscript. We have acquired high-resolution DEM data for another catchment in the Hoh River basin on the Olympic Peninsula and are commencing analysis of this data set. We also intend to test the method at an as yet undetermined catchment in the Cascades.

- 4) Develop and test DEM-based predictions of channels most likely to be affected by debris flows.

In the debris flow model manuscript we outline a method for identifying channels subject to potential debris flow scour [Montgomery and Dietrich, in prep.]. The method has been used for two catchments and we anticipate expanding this aspect of our study in conjunction with further predictions of relative debris flow initiation hazard in other catchments.

In summary, we have made significant progress toward the objectives of the shallow sediment source component of our project. Further development, testing, and refinement of model predictions and investigations of the effect of DEM scale on process models are anticipated to proceed according to our originally proposed schedule.

Deep-Seated Mass Failures

Our research in deep-seated mass failures is oriented toward three objectives:

- 1) Developing a method for systematic prediction of potential sites of deep-seated mass failures in a watershed.

Kevin Schmidt, a TFW-supported graduate student in Geological Sciences at UW, is examining controls on large-scale mass wasting in the Cascades. He is working in the Chuckanut formation in the Nooksak River basin and is currently analyzing initial data derived from air photographs and topographic maps. Comparing empirical observations with predictions of a two-dimensional slope stability model he has found evidence for both topographic and local structural/hydrologic controls on the size of stable hillslopes. A summary of his research to date is presented in Appendix 5. Dan Miller, currently a Ph.D. candidate in Geological Sciences at UW, will begin a TFW-supported post-doctoral fellowship in Fall 1992 to work on further developing models for the controls on deep-seated mass failures.

- 2) Developing a method for predicting the alteration of stability as a result of changes in hydrology due to natural weather fluctuations or to management.

Progress toward this objective is predicated upon satisfactorily testing a model for controls on deep-seated mass wasting and will be pursued later in the project.

- 3) Development of guidelines for field studies to refine predictions in areas that have been flagged as potentially unstable.

Progress toward this objective is predicated upon the previous two objectives and will be pursued later in the project.

Assessment of Channel Condition and Response

In addition to the objectives listed below, we have been working on developing a process-based channel classification. The abstract of the manuscript is included as Appendix 6 [Montgomery and Buffington, in prep.]. The proposed classification was developed in response to enthusiasm from the SHAMW committee when presented with our initial ideas on the subject. We have pursued further development of the scheme in addition to our other projects. Although the manuscript is quite long, it is essentially 80% completed. We estimate that it will take at least 3 to 4 more weeks to generate a rough draft. We hope to solicit TFW review of a draft in late June or early July, 1992. We anticipate completion of the paper [incorporation of reviewers comments, experience gained through field application, etc...] by late summer or early fall, 1992, and will be using the system to guide data collection this upcoming summer. Research groups at Colorado State University and the University of Montana have expressed interest in the system and will also be testing its utility independent of our effort. Thus we hope to have a field-tested version available within the next six months. We plan on publishing the manuscript as a TFW report upon incorporation of reviewers comments and after testing its utility in the field.

Progress toward our other objectives in the channel assessment project is outlined below.

- 1) Test the ability of digital elevation data to resolve local channel slope with sufficient accuracy to be useful for geomorphic modelling and habitat classification.

Field data necessary to conduct this comparison will be collected this upcoming summer. U.S.G.S. 7.5' DEM's (30 m resolution) have been obtained for the Hoh River, Tennessee Valley, and Coos Bay study sites. Appropriate DEM's will be obtained for other study areas after completion of summer field work.

- 2) Produce a summary of existing data on channel properties from forested mountainous watersheds that can be used to test our threshold and transport controlled characterization of channels.

John Buffington, a TFW-supported graduate student in Geological Sciences at UW, has collected and analyzed much of the available data pertinent to assessing our threshold channel model for predicting sediment size from channel slope and bankfull depth. A summary of his research is included as Appendix 7. Results to date are encouraging and illustrate the probable effects of bedform roughness, bed armoring, and large woody debris. Much of the available data from previous studies, however, is unsatisfactory because we either do not know exactly how it was collected, or do not approve of the methods used during data collection. John will be collecting and analyzing a field data set to address these effects this summer.

- 3) Develop a method for prediction of channel attributes from a digital elevation model (DEM) and field observations that test the predictions.

We outline a hypothesis for predicting channel type from digital elevation models in our draft manuscript on channel classification (Appendix 6) [Montgomery and Buffington, in prep.]. Data necessary to test this hypothesis will be collected this upcoming summer.

- 4) Develop methods for predicting sediment flux through a channel network.

One of the dominant effects on sediment routing and storage in low-order channels is the interaction between large woody debris and sediment. This interaction, however, has not been studied systematically and there exists no coherent theoretical context within which to view this interaction. Tim Abbe, currently a consulting hydrologist in San Francisco, California, has been admitted to the Department of Geological Sciences at UW with RA support to study this interaction. He will begin graduate studies in the fall of 1992.

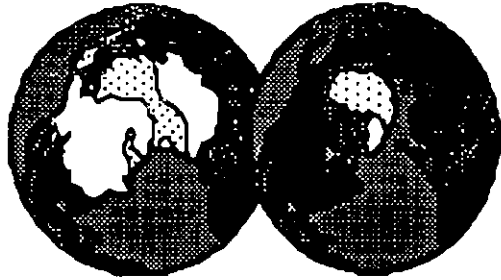
Another control on sediment routing through channel networks is the spatial distribution of sediment contributed across channel banks. Bill Dietrich is developing methods for predicting the flux of sediment into channels from across channel banks. This is a crucial component of any spatially distributed sediment budget and progress to date is summarized in Appendix 8.

Goals for FY 1992-1993

In fiscal year 1992-1993 we plan on continuing the studies outlined above and on achieving the objectives of our proposed work. We anticipate that some components will be effectively completed by the end of the biennium (June, 1993). For example, we anticipate that the debris flow prediction and runout model will be essentially tested by then. Other components of this study lend themselves to further development. For example, we see great value in continuing to develop methods for predicting and modelling sediment flux through channel networks. Field work on sediment storage and transport processes in steep low-order channels is especially needed and provides an avenue for future research. We can continue to build on existing models and new findings to refine our capabilities. Similarly, the coupling of large woody debris and sediment transport will likely require significant effort to document and model. Further studies of the influence of bedform roughness and woody debris on sediment transport mechanics and channel morphology are likely to be productive. Consequently, we anticipate continuing our efforts in each of our project subcomponents:

We value the input and involvement of the SHAMW committee and look forward to our scheduled briefing in the fall, at which time we hope to discuss preliminary interpretations of our summer field work. Additional copies of the appended manuscripts will be available upon their completion. Copies for review purposes are available on request. We look forward to continued progress toward our project goals.

TFW-SH10-92-001



QUATERNARY RESEA

University of Washington, Seattle, Washington 98195
(206) 543-1166 FAX 543-3836

Geomorphological Watershed Analysis Project

Annual Report for the period from 10/91 to 5/92

Submitted to the Sediment, Hydrology and Mass Wasting Committee
of the Timber/Fish/Wildlife Agreement

compiled by

David R. Montgomery
Quaternary Research Center and Department of Geological Sciences
University of Washington
Seattle, WA 98195

5/18/92

NOT FOR
DISTRIBUTION
OUTSIDE SHAMW
EXCEPT 1ST
SECTION
(up to appendix 1)



QUATERNARY RESEARCH CENTER

University of Washington, Seattle, Washington 98195
(206) 543-1166 FAX 543-3836

Geomorphological Watershed Analysis Project

Annual Report for the period from 10/91 to 5/92

Submitted to the Sediment, Hydrology and Mass Wasting Committee
of the Timber/Fish/Wildlife Agreement

compiled by

David R. Montgomery
Quaternary Research Center and Department of Geological Sciences
University of Washington
Seattle, WA 98195

5/18/92

Nancy Sturhan
DNR Forest Practice Division
P.O. Box 47012
Olympia, WA 98504-7012

Dear Ms. Sturhan,

This document constitutes the first annual report for the Geomorphological Watershed Analysis project funded by the SHAMW committee under the Timber/Fish/Wildlife agreement. The report covers the seven month period from October 1, 1991, to May 1, 1992. The format of this report may differ from the standard TFW report format, but it is intended to communicate our progress in research on the geomorphology of mountain watersheds. We present a brief overview of our project, review the objectives defined in our proposal, compare progress to date with the projected targets, and briefly discuss some objectives for research in the upcoming year. Finally, in an appendix format we present a series of draft research papers and preliminary results produced by the project to date. One of these papers has been accepted for publication by a scientific journal. Two others are draft manuscripts. The abstract of a third draft manuscript that is almost completed is also included. The draft manuscripts are presented in this report with the understanding that they are not for distribution outside of the SHAMW committee at this time. We include them to allow assessment of project progress. In the immediate future we will be soliciting preliminary reviews from experts both within and external to the TFW process. Reviewers comments and revisions based on our upcoming field work will be incorporated at a later date when these draft manuscripts are presented in a formal report. It is our intention to publish our results in the scientific literature, as well as in TFW reports, and we have chosen this presentation format for our annual report to facilitate ongoing dialog with the SHAMW committee while maintaining progress toward our research objectives. Our final biennial report will be more formal.

Geomorphological Watershed Analysis

The overall goal of the Geomorphological Watershed Analysis project is to provide the scientific basis for predicting the response of hillslopes and channel systems in forested mountains to both long-term average conditions [climate, geology, topography, vegetation] and short-term perturbations [fire, extreme storm events, and timber harvest]. Our approach is oriented toward developing objective, physically-based procedures for assessing and interpreting the current condition of channels and hillslopes, and for predicting response to watershed perturbations such as accompany timber harvesting. Conceptually, we view

potential hillslope and channel responses as linked through the processes controlling sediment mobilization, routing, and storage within a watershed. While maintaining this watershed context, we have divided our study into three distinct components: shallow sediment sources, deep-seated landslides, and channel condition and response. Study plans and schedules for each of these components are presented in our original proposal. A brief review of progress toward our objectives follows.

Interactive Team of Researchers

A major goal of our project is the development of an interactive team of faculty and graduate student researchers studying the geomorphology of mountain drainage basins. Personnel directly funded by the project include one of the PI's [Montgomery] and three graduate students [Bauer, Buffington, and Schmidt], one working on each aspect of our project. Two computer programmers [Greenberg and Reiss] are partially supported by TFW funding. A fourth student has been admitted to UW to work on the channel assessment component starting in Fall, 1992. A post-doctoral fellow [Miller] will be funded in academic year 92-93 to work on the deep-seated mass wasting component of the project. The timing of recent budget uncertainties relative to our admission process and the subsequent elimination of \$28k from our project precluded further expansion of the program.

Communication between the PI's [Dunne, Montgomery, and Dietrich] occurs frequently and the entire project met at UW on April 5th to discuss progress and research directions. The TFW salaried personnel and the other PI's [Dunne and Dietrich] also have brought several collaborators to work on projects directly relating to project goals. Dr. Weihua Zhang (Univ. of Washington postdoctoral researcher funded from federal sources) has been working with Dr. Montgomery on examining the effects of digital elevation model (DEM) resolution on simulations of surface and hydrologic processes. Dr. Efi Foufoula (Univ. of Minnesota) has begun a collaborative effort with Dr. Montgomery focused on investigating methods to delineate the hillslope/channel network transition from DEM's. Dr. Montgomery also has been coordinating research efforts on channel assessment and response with Dr.'s Lee MacDonald and Ellen Wohl at Colorado State University with the goal of standardizing data collection procedures so as to maximize the usefulness of data collected by both groups. Communication is continuing with Dr. Cathy Wilson of CSIRO (Australia). She is working with the research group that developed the digital terrain model TOPOG, which we are using as the basis for our shallow debris flow prediction model. Their group is trying to develop a dynamic version of TOPOG. Dr. Wilson will be visiting UW at the expense of the Australian government during mid-June to discuss our research.

We also have provided input to other TFW funded, or related, projects through consultations, collaboration, and loans of equipment. The Ambient Monitoring Project approached us for advice on data collection methodologies and analysis in October and November, 1991. Prior to the program's termination, we suggested revisions to their field methods that would have increased the utility of their data for use in our analyses and those of other resource management professionals. We also suggested revisions in their analysis procedures that they have incorporated with productive results. A desired set of data for collection in any future efforts was transmitted to the Ambient Monitoring Committee through Jeff Light and Kate Sullivan. We also provided input for Ed Rashin's project on BMP evaluation at Washington State Department of Ecology, JoAnne Metzler's peak discharge channel damage assessment methodology, and Phil Peterson's response thresholds review. Additionally, we are pursuing plans for collaborative research on the history of landsliding in the Hoh River basin with Susan Calder, the DNR geologist located in Forks. In an effort to stimulate collaboration between fisheries biologists and geomorphologists we have been working on field measurements with, and loaning equipment to, Phil Peterson of the TFW "Big Fish" project for his study on channel scour and bed modifications at Kennedy Creek. Also, at the request of the SHAMW committee we have been developing a process-based channel classification that we hope will encourage further interdisciplinary research and provide insight into watershed analysis. In summary, we have established an interactive research group that extends well beyond the size of our TFW-funded personnel and we are involved in projects that extend beyond the scope of our original proposal.

Shallow Sediment Sources

Progress toward the objectives outlined in our proposal is summarized below.

- 1) Develop a method for determining how well digital elevation data represent actual watershed topography to the degree necessary for locating sediment sources.

We have developed two methods for examining the quality of landscape representation in digital elevation models. These methods are outlined in two of the draft manuscripts included in this report as appendices 1 and 2 [Bauer, in prep., Zhang and Montgomery, in prep.]. The method developed by Bauer is based on calculating the signal to noise ratio of a digital elevation surface. This approach provides a method for determining the quality with which an object of a given size (a hillslope or a debris flow source area, for

example) is represented in a DEM. The approach developed by Zhang and Montgomery examines the effect of DEM grid size on the distribution of the topographic parameters that influence both runoff generation and surface process models and on hydrologic simulations based on these models. Both of these studies have fundamental implications for the use of DEM's in surface process models and point to the need to use a DEM scale that is appropriate for resolving landscape features and processes of interest.

- 2) Test the use of a steady state shallow subsurface runoff model to predict spatial distribution of ground saturation in steep, realistically complex terrain.

We recently had a paper accepted in the journal "Geology" based on TFW-supported work on predicting the spatial pattern of runoff production and erosion mechanisms using the steady state shallow subsurface runoff model TOPOG. This paper discusses the partitioning of landscapes into different process regimes on the basis of slope, contributing drainage area, and threshold process theories. These thresholds provide the theoretical underpinnings of the DEM-based watershed modelling approach that we are developing. The paper is included in this report as Appendix 3. Also we are conducting steady state sprinkler experiments on a small catchment in Coos Bay, Oregon, from May 26 to June 14, 1992, in part to provide a data set against which to test the predictions of steady state shallow subsurface runoff models. Together with an earlier set of sprinkler experiments this data set will allow examination of the utility of the hydrologic model for use in steep terrain.

- 3) Develop a method for predicting areas prone to shallow landsliding in a watershed through the use of topographic analysis software.

We have developed a DEM-based method for predicting relative debris flow hazard in a catchment. A draft manuscript describing the model and documenting model predictions [Montgomery and Dietrich, in prep.] is included in this report as Appendix 4. To date, this model has been tested in two catchments: one in Marin County, California, and one in the Oregon Coast Range near Coos Bay. Model results are quite encouraging and are detailed in the draft manuscript. We have acquired high-resolution DEM data for another catchment in the Hoh River basin on the Olympic Peninsula and are commencing analysis of this data set. We also intend to test the method at an as yet undetermined catchment in the Cascades.

- 4) Develop and test DEM-based predictions of channels most likely to be affected by debris flows.

In the debris flow model manuscript we outline a method for identifying channels subject to potential debris flow scour [Montgomery and Dietrich, in prep.]. The method has been used for two catchments and we anticipate expanding this aspect of our study in conjunction with further predictions of relative debris flow initiation hazard in other catchments.

In summary, we have made significant progress toward the objectives of the shallow sediment source component of our project. Further development, testing, and refinement of model predictions and investigations of the effect of DEM scale on process models are anticipated to proceed according to our originally proposed schedule.

Deep-Seated Mass Failures

Our research in deep-seated mass failures is oriented toward three objectives:

- 1) Developing a method for systematic prediction of potential sites of deep-seated mass failures in a watershed.

Kevin Schmidt, a TFW-supported graduate student in Geological Sciences at UW, is examining controls on large-scale mass wasting in the Cascades. He is working in the Chuckanut formation in the Nooksak River basin and is currently analyzing initial data derived from air photographs and topographic maps. Comparing empirical observations with predictions of a two-dimensional slope stability model he has found evidence for both topographic and local structural/hydrologic controls on the size of stable hillslopes. A summary of his research to date is presented in Appendix 5. Dan Miller, currently a Ph.D. candidate in Geological Sciences at UW, will begin a TFW-supported post-doctoral fellowship in Fall 1992 to work on further developing models for the controls on deep-seated mass failures.

- 2) Developing a method for predicting the alteration of stability as a result of changes in hydrology due to natural weather fluctuations or to management.

Progress toward this objective is predicated upon satisfactorily testing a model for controls on deep-seated mass wasting and will be pursued later in the project.

- 3) Development of guidelines for field studies to refine predictions in areas that have been flagged as potentially unstable.

Progress toward this objective is predicated upon the previous two objectives and will be pursued later in the project.

Assessment of Channel Condition and Response

In addition to the objectives listed below, we have been working on developing a process-based channel classification. The abstract of the manuscript is included as Appendix 6 [Montgomery and Buffington, in prep.]. The proposed classification was developed in response to enthusiasm from the SHAMW committee when presented with our initial ideas on the subject. We have pursued further development of the scheme in addition to our other projects. Although the manuscript is quite long, it is essentially 80% completed. We estimate that it will take at least 3 to 4 more weeks to generate a rough draft. We hope to solicit TFW review of a draft in late June or early July, 1992. We anticipate completion of the paper [incorporation of reviewers comments, experience gained through field application, etc...] by late summer or early fall, 1992, and will be using the system to guide data collection this upcoming summer. Research groups at Colorado State University and the University of Montana have expressed interest in the system and will also be testing it's utility independent of our effort. Thus we hope to have a field-tested version available within the next six months. We plan on publishing the manuscript as a TFW report upon incorporation of reviewers comments and after testing its utility in the field.

Progress toward our other objectives in the channel assessment project is outlined below.

- 1) Test the ability of digital elevation data to resolve local channel slope with sufficient accuracy to be useful for geomorphic modelling and habitat classification.

Field data necessary to conduct this comparison will be collected this upcoming summer. U.S.G.S. 7.5' DEM's (30 m resolution) have been obtained for the Hoh River, Tennessee Valley, and Coos Bay study sites. Appropriate DEM's will be obtained for other study areas after completion of summer field work.

- 2) Produce a summary of existing data on channel properties from forested mountainous watersheds that can be used to test our threshold and transport controlled characterization of channels.

John Buffington, a TFW-supported graduate student in Geological Sciences at UW, has collected and analyzed much of the available data pertinent to assessing our threshold channel model for predicting sediment size from channel slope and bankfull depth. A summary of his research is included as Appendix 7. Results to date are encouraging and illustrate the probable effects of bedform roughness, bed armoring, and large woody debris. Much of the available data from previous studies, however, is unsatisfactory because we either do not know exactly how it was collected, or do not approve of the methods used during data collection. John will be collecting and analyzing a field data set to address these effects this summer.

- 3) Develop a method for prediction of channel attributes from a digital elevation model (DEM) and field observations that test the predictions.

We outline a hypothesis for predicting channel type from digital elevation models in our draft manuscript on channel classification (Appendix 6) [Montgomery and Buffington, in prep.]. Data necessary to test this hypothesis will be collected this upcoming summer.

- 4) Develop methods for predicting sediment flux through a channel network.

One of the dominant effects on sediment routing and storage in low-order channels is the interaction between large woody debris and sediment. This interaction, however, has not been studied systematically and there exists no coherent theoretical context within which to view this interaction. Tim Abbe, currently a consulting hydrologist in San Francisco, California, has been admitted to the Department of Geological Sciences at UW with RA support to study this interaction. He will begin graduate studies in the fall of 1992.

Another control on sediment routing through channel networks is the spatial distribution of sediment contributed across channel banks. Bill Dietrich is developing methods for predicting the flux of sediment into channels from across channel banks. This is a crucial component of any spatially distributed sediment budget and progress to date is summarized in Appendix 8.

Goals for FY 1992-1993

In fiscal year 1992-1993 we plan on continuing the studies outlined above and on achieving the objectives of our proposed work. We anticipate that some components will be effectively completed by the end of the biennium (June, 1993). For example, we anticipate that the debris flow prediction and runout model will be essentially tested by then. Other components of this study lend themselves to further development. For example, we see great value in continuing to develop methods for predicting and modelling sediment flux through channel networks. Field work on sediment storage and transport processes in steep low-order channels is especially needed and provides an avenue for future research. We can continue to build on existing models and new findings to refine our capabilities. Similarly, the coupling of large woody debris and sediment transport will likely require significant effort to document and model. Further studies of the influence of bedform roughness and woody debris on sediment transport mechanics and channel morphology are likely to be productive. Consequently, we anticipate continuing our efforts in each of our project subcomponents.

We value the input and involvement of the SHAMW committee and look forward to our scheduled briefing in the fall, at which time we hope to discuss preliminary interpretations of our summer field work. Additional copies of the appended manuscripts will be available upon their completion. Copies for review purposes are available on request. We look forward to continued progress toward our project goals.

List of Appendices

- 1 Bauer, R., Evaluating digital elevation models, draft manuscript for submission to Water Resources Research.
- 2 Zhang, W., and Montgomery, D. R., Effect of DEM grid scale on landscape representation and hydrologic simulations: draft manuscript for submission to Water Resources Research.
- 3 Dietrich, W. E., Wilson, C. J., Montgomery, D. R., McKean, J., and Bauer, R., in press, Erosional Thresholds and Land Surface Morphology: Geology.
- 4 Montgomery, D. R., and Dietrich, W. E., in prep., A digital elevation model for predicting debris flow source areas and run out paths: draft manuscript for submission to Water Resources Research.
- 5 Schmidt, K. M., Application of slope/height relationships to identification of deep-seated mass failures, review of progress to date on identification of sites of deep-seated mass failures.
- 6 Montgomery, D. R., and Buffington, J. M., in prep., Channel classification, assessment of channel conditions, and the prediction of channel response: abstract of a draft manuscript for submission as a TFW report.
- 7 Buffington, J. M., Threshold channel predictions, review of progress to date.
- 8 Dietrich, W. E., Soil depth, slope stability and sediment production, review of progress to date.

Appendix 1

Evaluating Digital Elevation Models

draft, to be submitted to Water Resource Research

Romy Bauer

Department of Geology and Geophysics
University of California, Berkeley
Berkeley, CA. 94720

May 14, 1992

ABSTRACT

1. INTRODUCTION

Geomorphologists and hydrologists often use digital elevation models (DEMs) in their research (e.g. Moore et al., 1988a,b; Vertessy et al., 1990; Tarboton et al., 1991). However, a DEM is merely an approximation to the real landscape, and conclusions based on DEMs may not be valid for the actual terrain. Sources of error include inadequate density and distribution of samples, sampling error, and quantization error.

DEMs are usually evaluated qualitatively; a DEM is "good" if it "looks" like the terrain. However, how much it "looks" like the terrain is dependent on the observer and his or her application. What looks good to the global climate modeller probably looks terrible to the hillslope modeller. In addition, given two DEMs that look "good" for example, it is hard to say qualitatively which is better and why. A more useful method of evaluation would allow DEMs to be directly compared and would allow DEMs to be evaluated only over those scales deemed important.

In this paper, I suggest using the power signal to noise ratio (SNR) as a measure of quality of a DEM. The SNR is the ratio of the integrated power spectral density (PSD) of the *signal* to the integrated PSD of the *noise*, where the signal is the Fourier transform of the terrain and the noise is the Fourier transform of the difference between the DEM and terrain. The SNR is a quantitative measure which would allow DEMs to be directly compared. Also, the SNR can be computed over any range of frequencies desired.

First, I motivate this work with an example. I then briefly discuss DEMs and how they are produced. I then provide some simple background in harmonic analysis, followed by a development of an expression for the SNR. I then discuss practical considerations in computing a SNR, and present both theoretical and real-world examples. Finally I discuss how to determine the frequency range and minimum SNR needed to study a particular problem.

2. MOTIVATION

Tennessee Valley is a 1.2 km^2 catchment located in the hilly grass and chaparral lands of Marin County, California. Extensive mapping and hydrologic studies have been conducted at this site (Wilson and Dietrich, 1987; Montgomery and Dietrich, 1988, 1989; Black and Montgomery, 1991; Montgomery, 1991). To study this site using a computer model, digital elevation data were obtained by stereo digitization of aerial photographs. Approximately 15,000 points were digitized with an average separation of 10 m. I created *TVAL*, a USGS-style DEM, by converting these data to a rectangular array of data points spaced 30 m apart. Figures 1 and 2 show, respectively, a contour map and a perspective surface map of Tennessee Valley using *TVAL*.

For comparison, I obtained the USGS Point Bonita 7.5' quadrangle DEM, which I'll call *BONITA*. Like *TVAL*, *BONITA* is a rectangular array with 30 m grid spacing, but it covers the entire Point Bonita quadrangle. Figures 3 and 4 show, respectively, a contour map and a perspective surface map of Tennessee Valley using a subset of *BONITA*. For comparison, Figure 5 shows the contour map of Tennessee Valley taken from the printed Point Bonita 7.5' quadrangle. Qualitatively, it is obvious that there is a large difference between the two DEMs. Although the grid spacing is the same in both, *BONITA* clearly lacks much of the detail present in *TVAL* and the printed quadrangle.

The differences in these two DEMs raise a number of questions. Why are these two data sets different even though the grid spacing is the same? Which one is closer to reality? How can I measure the difference between the two datasets and reality? Is either one of them "good enough" to study the phenomena we are trying to study?

3. DIGITAL ELEVATION MODELS

In this paper a *digital elevation model (DEM)* is a two dimensional rectangular grid of elevations. The ideas I present can easily be used to evaluate other kinds of DEMs, such as triangular irregular networks (TINs) and contour-based digital line graphs (DLGs). A *height function* is a continuous function of two variables.

There are three steps involved in producing a DEM:

- First, the height function of the terrain is *sampled*. This can be done using a variety of methods, including surveying from the ground and from aerial photographs.
- Second, the sampled data is *filtered* to produce a new height function. For example, converting the sampled data to a surface consisting of triangles is a form of filtering. A more complicated filter function may produce a smooth, non-planar height function.
- Third, the new function is sampled at regular intervals to form a rectangular grid of elevations.

If the sample points already form a rectangular grid, filtering and resampling may not be necessary.

Sampling a function f , and then filtering the samples to produce a new function g , generates errors. That is, in most cases g is not identically equal to f . The SNR is one measure of the difference between g and f .

4. HARMONIC ANALYSIS

4.1. The Fourier Transform

It is often useful to transform a set of data into another domain for ease of manipulation or interpretation. The *Fourier transform* transforms a function in the spatial domain (x,y) to a function in the frequency domain (s,t)

$$F(s,t) = \int_{-\infty}^{\infty} \int_{-\infty}^{\infty} f(x,y) e^{-i2\pi(xs+yt)} dx dy$$

The inverse Fourier transform is a Fourier transform with a positive exponent

$$f(x,y) = \int_{-\infty}^{\infty} \int_{-\infty}^{\infty} F(s,t) e^{i2\pi(xs+yt)} ds dt$$

If $F(s,t) = q(s,t) + ir(s,t)$, then $|F(s,t)|$ is the *magnitude* and $r(s,t)/q(s,t)$ is the *phase* of frequency (s,t) in $f(x,y)$ (see Bracewell, 1978 for a complete discussion of Fourier analysis).

4.2. Convolution

The *convolution* operation is used in producing a DEM. The convolution of two functions f and g is

$$\int_{-\infty}^{\infty} \int_{-\infty}^{\infty} f(\sigma-x, \tau-y) g(x,y) dx dy$$

and is usually denoted by a *

$$h(\sigma, \tau) = f(x,y) * g(x,y)$$

If $h = f * g$ then the *convolution theorem* states that

$$H(s,t) = F(s,t) G(s,t)$$

That is, the Fourier transform of the convolution of two functions is the product of the Fourier transforms of each function (Bracewell, 1978).

4.3. Sampling and Filtering

I will now formalize the notion of sampling and filtering. A function $f(x,y)$ is *sampled* by multiplying it by a *sampling function* $s(x,y)$. In this paper, a sampling function has the following form:

$$s(x,y) = \sum_{j=0}^J \sum_{k=0}^K \delta(x - x_k, y - y_j)$$

where $\delta(x,y)$ is the *Dirac delta function*:

$$\delta(x,y) = 0, \quad x \neq 0$$

$$\int_{-\infty}^{+\infty} \delta(x,y) = 1$$

(Bracewell, 1978). The type of sampling function determines the (x_k, y_j) .

In practice, sampling is not error-free and the sampling product is

$$f(x,y) s(x,y)' = f(x,y) s(x,y) + error$$

This product is *filtered* to generate a new function $g(x)$ by convolving it with a *filter function* $h(x,y)$:

$$g(x,y) = (f(x,y) s(x,y)') * h(x,y)$$

or in frequency space:

$$G(s,t) = (F(s,t) * S(s,t)') H(s,t)$$

4.4. Signal to Noise Ratio

The *signal* $A(s,t)$, is the Fourier transform of the original function multiplied by the Fourier transform of the filter function:

$$A(s,t) = F(s,t) H(s,t)$$

The *noise* $B(s,t)$, is the Fourier transform of the sampled and filtered function minus the signal:

$$B(s,t) = G(s,t) - A(s,t)$$

The *power spectral density (PSD)* $\Phi_f(s,t)$, of a function f is the squared magnitude of the Fourier transform, $F(s,t)$:

$$\Phi_f(s,t) = |F(s,t)|^2$$

The PSD can also be represented as $\Phi_f(f,\theta)$ where f and θ are *polar* coordinates:

$$f = \sqrt{s^2 + t^2}$$

$$\theta = \tan^{-1} \left[\frac{t}{s} \right]$$

The *power signal to noise ratio (SNR)* $R(f_1, f_2)$ of g relative to f over a range of frequencies is the integral of the PSD of the signal divided by the integral of the PSD of the noise in polar coordinates:

$$R(f_1, f_2) = \frac{\int_0^{2\pi} \int_{f_1}^{f_2} \Phi_a(f, \theta) df d\theta}{\int_0^{2\pi} \int_{f_1}^{f_2} \Phi_b(f, \theta) df d\theta}$$

If $G(s,t)$ equals $A(s,t)$ over a range of frequencies, then the corresponding SNR is infinite. Intuitively, the higher the SNR, the closer G is to F within that range of frequencies.

The SNR may be measured at a single frequency as follows:

$$R(f_1) = \frac{\int_0^{2\pi} \Phi_a(f_1, \theta) d\theta}{\int_0^{2\pi} \Phi_b(f_1, \theta) d\theta}$$

4.5. Band-limited vs. Non Band-limited Functions

A function is *band-limited* if it has no power in frequencies higher than some finite frequency c . The *sampling theorem* says that if a band-limited function, f , is sampled at a rate N that is twice that of c , then it is possible to generate a new function g that is identically equal to f by filtering the samples with a low-pass filter with the same frequency (Bracewell, 1978). Thus, a band-limited function can be sampled at rate N , also called the Nyquist rate, and reconstructed with no loss of information.

If a function f is not band-limited, then in general, it cannot be identically reconstructed from a finite set of samples. That is, there is power at *all* frequencies, so no matter how high the sampling rate, there will still be noise in the the resulting function. In general $G(s, t)$ will not be identically equal to $F(s, t)$ over any range of frequencies.

5. COMPUTING A SNR FOR REAL TERRAIN

Elevation E, can be thought of as a non band-limited continuous function of two variables, latitude and longitude. Therefore, any DEM D , of E will have a finite SNR due to noise incurred by sampling and filtering E . To quantitatively describe how close D is to E , one must compute a SNR. This requires a knowledge of the sampling, filtering, and elevation functions, as well as a desired frequency range.

5.1. PSD of the Terrain

To determine the SNR, one needs to know the PSD of the elevation function (the terrain). If we knew the PSD (plus phase information) exactly, we would not have to sample the terrain in the first place. One way of attacking the problem is to estimate the PSD of the terrain. For example, one could assume that real terrain is fractal and therefore use a function of the form $(s^2+t^2)^{-\frac{\beta}{2}}$ as the PSD of the terrain (Saupe, 1988). Another way is to sample the terrain very densely over a small area and estimate a PSD using that. I go through an example of fitting a PSD to a real landscape in the next section.

5.2. Sampling Function

To compute a SNR, it is also necessary to determine what sampling function was used. The types of sampling fall into three categories: regularly spaced sampling, irregularly spaced sampling, and sampling from contour maps. I will briefly discuss the first two.

5.2.1. Regularly Spaced Sampling

The most common method of regularly spaced sampling is manual or automatic profiling of the terrain from stereo photographs. Points are sampled at even intervals

along a straight line (*profile*), and the profiles are evenly spaced. The sampling along a particular profile is:

$$s(x,y) = \sum_{k=-\infty}^{+\infty} \sum_{l=-\infty}^{+\infty} \delta(x-mk, y-nl)$$

where m and n are the sampling intervals in the x and y directions respectively. Although only a finite number of points will be sampled, one can assume that these points are reflected about the edges and repeated infinitely in both directions. This greatly facilitates the analysis.

The Fourier transform of an infinite row of δ functions is itself an infinite row of δ functions, scaled by m :

$$S(s,t) = \frac{1}{|n| |m|} \sum_{k=-\infty}^{+\infty} \sum_{l=-\infty}^{+\infty} \delta\left(s - \frac{1}{m}k, t - \frac{1}{n}l\right)$$

Figure 6 shows a one dimensional example of evenly spaced sampling in the spatial and frequency domains. Note that the Fourier transform of the sampled terrain is the Fourier transform of the terrain plus copies shifted by integer multiples of the sampling rate.

5.2.2. Non-Regularly Spaced Sampling

Most survey methods use non regular spacing of samples. It is impractical and usually impossible to survey in an evenly spaced fashion when surveying on the ground. Also, much stereo photograph digitizing is done non-regularly. Although the sample points are certainly not distributed randomly, the only way to analyze them quantitatively is to assume that they are random with some distribution. Dippe and Wold (1985) analyzed the PSDs of several random sampling processes followed by analyses of the SNR when using these sampling processes. One such process is *Poisson sampling*. In one dimension, a Poisson sampling process is defined as follows:

$$s(x) = \sum_{k=0}^{\infty} \delta(x-x_k)$$

where

$$x_{k+1} = x_k + l_k$$

and the l_k have a probability density function

$$p(l_k) = \beta e^{-\beta l_k}$$

β is the *average sampling rate*. In this case the PSD of the sampling process is as follows:

$$\Phi_s(s) = \beta + 2\pi\beta^2\delta(s)$$

The SNR when using a Poisson sampling process and filtering function $h(x)$ is:

$$R(f_1, f_2) = (2\pi\beta)^{\frac{1}{2}} \frac{\int_{f_1}^{f_2} \Phi_f(s) \Phi_h(s) ds}{\int_{f_1}^{f_2} \left[\int_{-\infty}^{+\infty} \Phi_f(u) du \right] \Phi_h(s) ds}$$

I will leave out the derivation for the PSD and the SNR; see Dippe and Wold (1985) for derivations and for other sampling processes.

5.3. Filter Function

It is also necessary to determine what filter function was used in generating a given DEM. Two examples of filter functions are the *sinc* function and the *triangle* function.

In one dimension, the sinc function is defined as

$$\text{sinc}(x) = \frac{\sin(\pi x)}{\pi x}$$

The Fourier transform of $\text{sinc}(x)$ is the rectangle function

$$\Pi(s) = \begin{cases} 1 & |s| < f_c \\ 0 & \text{elsewhere} \end{cases}$$

The *sinc* function is called a *low-pass* filter because it is non-zero only for frequencies below a certain cutoff frequency. Figure 7 shows a one dimensional example of filtering using the *sinc* function. Note that in the frequency domain, the multiplication of $\Pi(x)$ and $F(s) * S(s)$ removes all frequencies higher than the cutoff frequency. The result $G(s)$ is equal to $F(s)$ plus the shifted copies of $F(s)$ incurred in sampling. This addition is called *aliasing* (Dippe and Wold, 1985).

Another filter function is the *triangle function*. The triangle function is often used to linearly interpolate when the samples are evenly spaced:

$$\Lambda(x, y) = \Lambda(x) \Lambda(y)$$

where

$$\Lambda(x) = \begin{cases} 1+x & -1 < x < 0 \\ 1-x & 0 \leq x < 1 \end{cases}$$

It is a faster computation to filter using the triangle function, but unlike the *sinc* function, it is non-zero at high frequencies. The Fourier transform of $\Lambda(x, y)$ is $\text{sinc}^2(s) \text{sinc}^2(t)$.

6. EXAMPLES

6.1. SNR of a Fractal Terrain DEM

In this first example I use a theoretical fractal terrain to illustrate the effect of different sampling rates. I present this because, unlike a real terrain, we know precisely the PSD of a fractal terrain. For ease of visualization, I will consider a fractal curve rather than a fractal surface. It is straightforward to extend this analysis to a higher dimension. If a curve is fractal with fractal dimension D , then the PSD of that curve is proportional to $f^{-(5-2D)}$ (Saupe, 1988). Figure 8 shows the PSD of a fractal curve with $D = 1.5$. Suppose we generate a function g_m by sampling and filtering the fractal curve. g_m can then

be sampled to generate a DEM. Let's assume that g_m is generated by sampling the fractal curve with an evenly spaced sampling function of the form described earlier:

$$s(x) = \sum_{k=-\infty}^{\infty} \delta(x - mk)$$

where m is the sample spacing, and filtering with a perfect low pass filter:

$$h(x) = \text{sinc}\left(\frac{x}{m}\right) = m \frac{\sin\left[\pi \frac{x}{m}\right]}{\pi x}$$

The PSDs of g_{120} , g_{60} , and g_{30} (in meters) are shown in figures 9a-c along with the PSD of the fractal curve. Qualitatively, one can see how the PSD of g_{30} (the higher sampling rate) is much closer to the PSD of the real curve than the PSD of g_{120} . The SNR between $\frac{1}{24000}m^{-1}$ and $\frac{1}{240}m^{-1}$ is 10.67 for g_{120} , 45.82 for g_{60} , and 181.99 for g_{30} . The SNR decreases significantly if we look at just the higher frequencies: the SNR between $\frac{1}{2000}m^{-1}$ and $\frac{1}{240}m^{-1}$ is 1.56 for g_{120} , 7.97 for g_{60} , and 34.47 for g_{30} . Figure 11 shows how the SNR computed at a single frequency varies with sampling rate and frequency.

6.2. SNR Estimation of Tennessee Valley DEMs

Let us consider more carefully the examples presented in Section 2. I will first go over the sampling and filtering methods used to generate *BONITA* and *TVAL*. I will then derive an estimate for the PSD of the terrain using the *TVAL* data set and use this PSD to compute SNRs for the two data sets.

6.2.1. Sampling and Filtering Methods

The USGS data set *BONITA* was generated as follows: using stereo photographs, elevations were sampled every 25m along north-south profiles. These north-south profiles were spaced every 150m apart. To generate a 30m grid, grid points were bilinearly interpolated from the samples. More precisely, the sampling function is

$$s(x,y) = \sum_{k=-\infty}^{\infty} \sum_{l=-\infty}^{\infty} \delta(x - 150k, y - 25l)$$

and the filter function is

$$h(x,y) = \Lambda\left[\frac{x}{150}\right] \Lambda\left[\frac{y}{25}\right]$$

The *TVAL* data set is a bit trickier to evaluate. Elevations were sampled irregularly using stereo digitization from aerial photographs. Average sample spacing was 10m. If we assume the samples were distributed as a Poisson process with an average sampling rate of β we can use the theory developed by Dippe and Wold (Dippe and Wold, 1985). A 30m grid was generated using an inverse distance squared filter function

$$h(x) = \frac{1}{|\vec{x}|^2}$$

where \vec{x} is the distance from the center of the filter (this isn't necessarily the best way to interpolate; I chose it because it was easier to analyze for this paper. A better method

might be a Delauney triangulation). Properly normalized, the new height function is

$$g(x) = \frac{(f(x)s(x)) * h(x)}{s(x)*r(x)}$$

6.2.2. PSD and SNR Estimation

The PSD of Tennessee Valley is required to compute a SNR for any DEM of Tennessee Valley. I estimated a one dimensional PSD as follows: I computed the Fourier transform of the *TVAL* data set. I then rotationally averaged the transform, thus reducing it down to one dimension, and computed its PSD. I then fit this PSD to a function of the form

$$\Phi_{TV}(s) = \frac{a}{s^b}$$

plus copies shifted by multiples of 30m to take into account aliasing. This fitted function is an estimate of the rotationally averaged PSD of Tennessee Valley. This is a very crude approximation and assumes that the grid points of *TVAL* are actual sample points and that the PSD can be modelled as a fractal. In addition, the aliasing shift isn't exactly 30m, because in rotationally averaging, the sampling rate varies from $30m^{-1}$ to $30\sqrt{2}m^{-1}$.

In any case, the best fit b was 2.2, corresponding to a fractal dimension of 1.4. I computed the PSDs and SNRs of *BONITA* and *TVAL* using $\Phi_{TV}(s)$ as the PSD of the terrain and the previously described sampling and filtering functions (reduced to 1-D). The PSDs are shown in figures 10a and 10b.

The SNR computed from $\frac{1}{10000}m^{-1}$ to $\frac{1}{300}m^{-1}$ is 305.81 for *TVAL* and 8.32 for *BONITA*. If we just consider the higher frequencies, the SNR computed from $\frac{1}{1000}m^{-1}$ to $\frac{1}{300}m^{-1}$ is 20.72 for *TVAL* and .55 for *BONITA*.

Let's consider the questions raised in section 2:

1) Why are these two data sets different although the grid spacing is the same? Recall that there are three steps in generating a DEM: sampling, filtering, and resampling. Although the *resampling* method was the same for both (i.e. every 30m), the sampling and filtering methods (described above) were different.

2) Which one is closer to reality? How can I measure the difference between the two datasets and reality? The SNR is one measure of the difference between a DEM and the terrain it represents. Assuming that the PSD of the terrain is the PSD we derived in the previous section, figures 10a and 10b show pictorially that the PSD of *TVAL* is closer to the PSD of the terrain than the PSD of *BONITA*. The SNR calculations quantify the difference between these PSDs.

3) Is either one of them good enough to study the phenomena we are trying to study? Unfortunately, we haven't answered that question yet, but I will discuss it briefly in the conclusion.

7. CONCLUSION

The SNR is a measure of the difference between a DEM and the terrain it represents. In developing an expression for the SNR, I have also described the processes used in generating a DEM. I would recommend that anyone interested in using a DEM

find out exactly how the terrain was sampled, filtered and resampled. It may be impractical to compute a SNR, but I hope that the user would at least qualitatively consider the aforementioned processes. If one does compute a SNR, then one faces the question: for a particular application, what is the minimum SNR needed measured over what range of frequencies?



Figure 1: Tennessee Valley from hand-digitized points, 30m grid spacing
contour interval 10 m, 1" = 330m

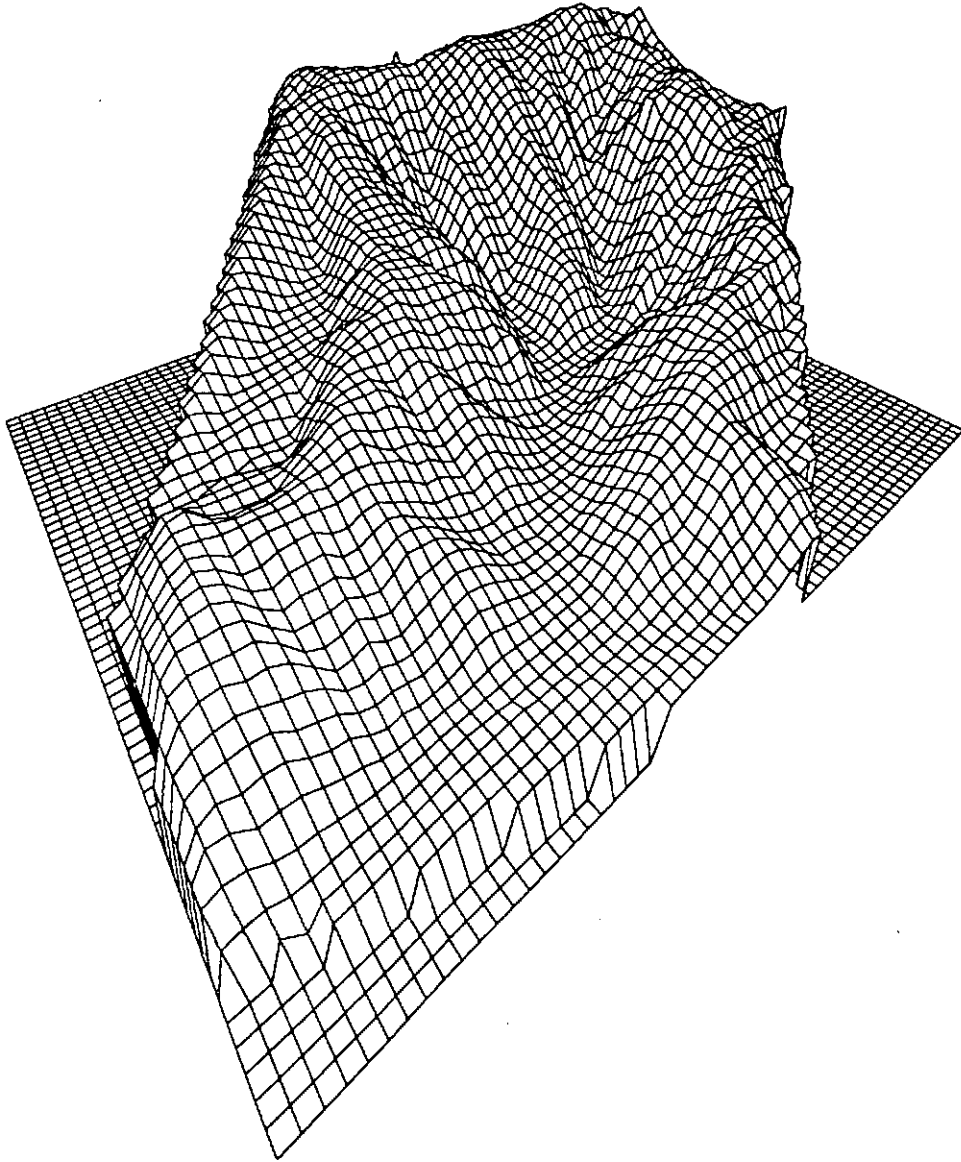


Figure 2: Tennessee Valley from hand-digitized points, 30m grid spacing
3x vertical exaggeration

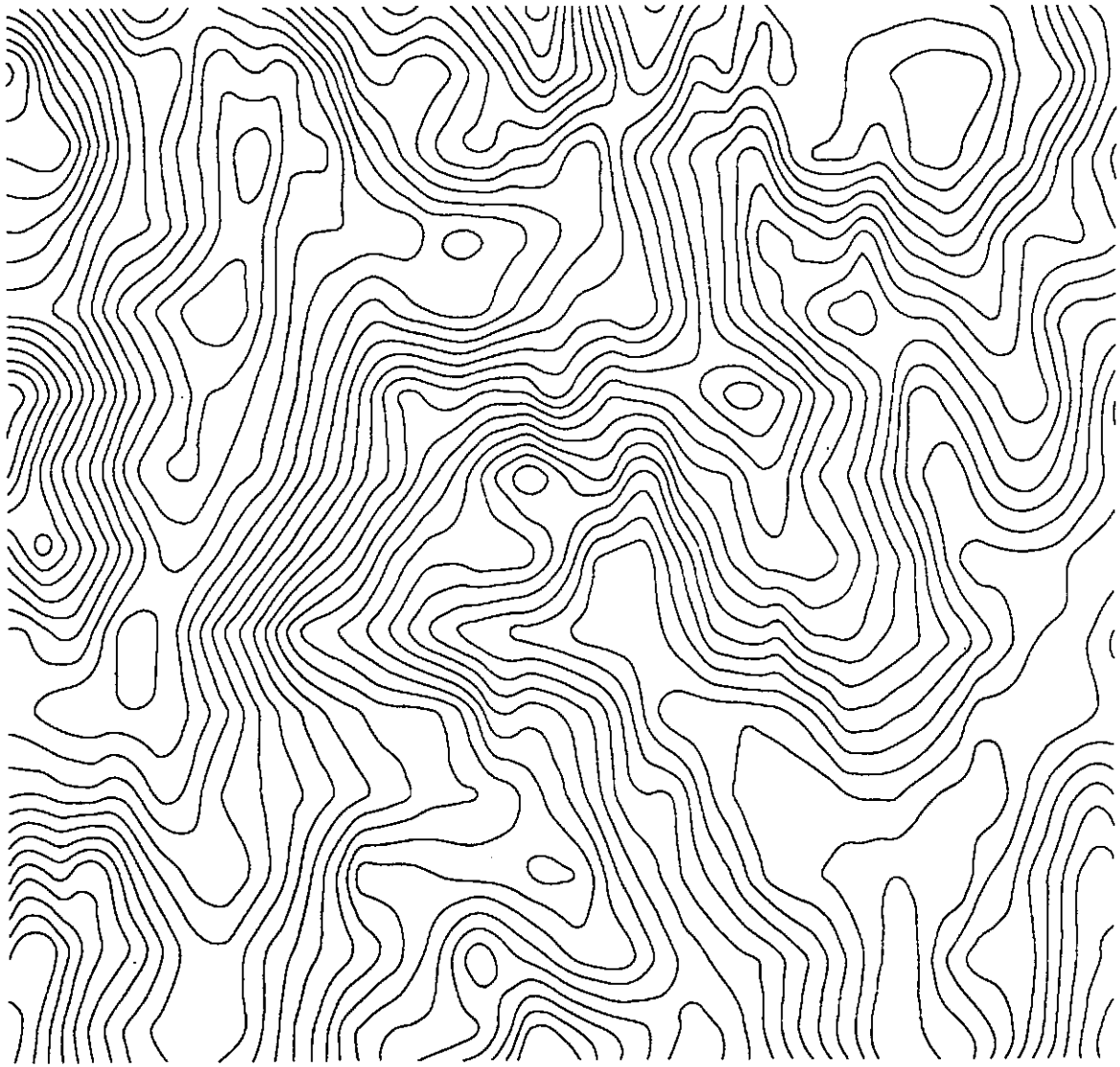


Figure 3: Tennessee Valley from USGS DEM data, 30m grid spacing
contour interval 10 m, 1" = 330m

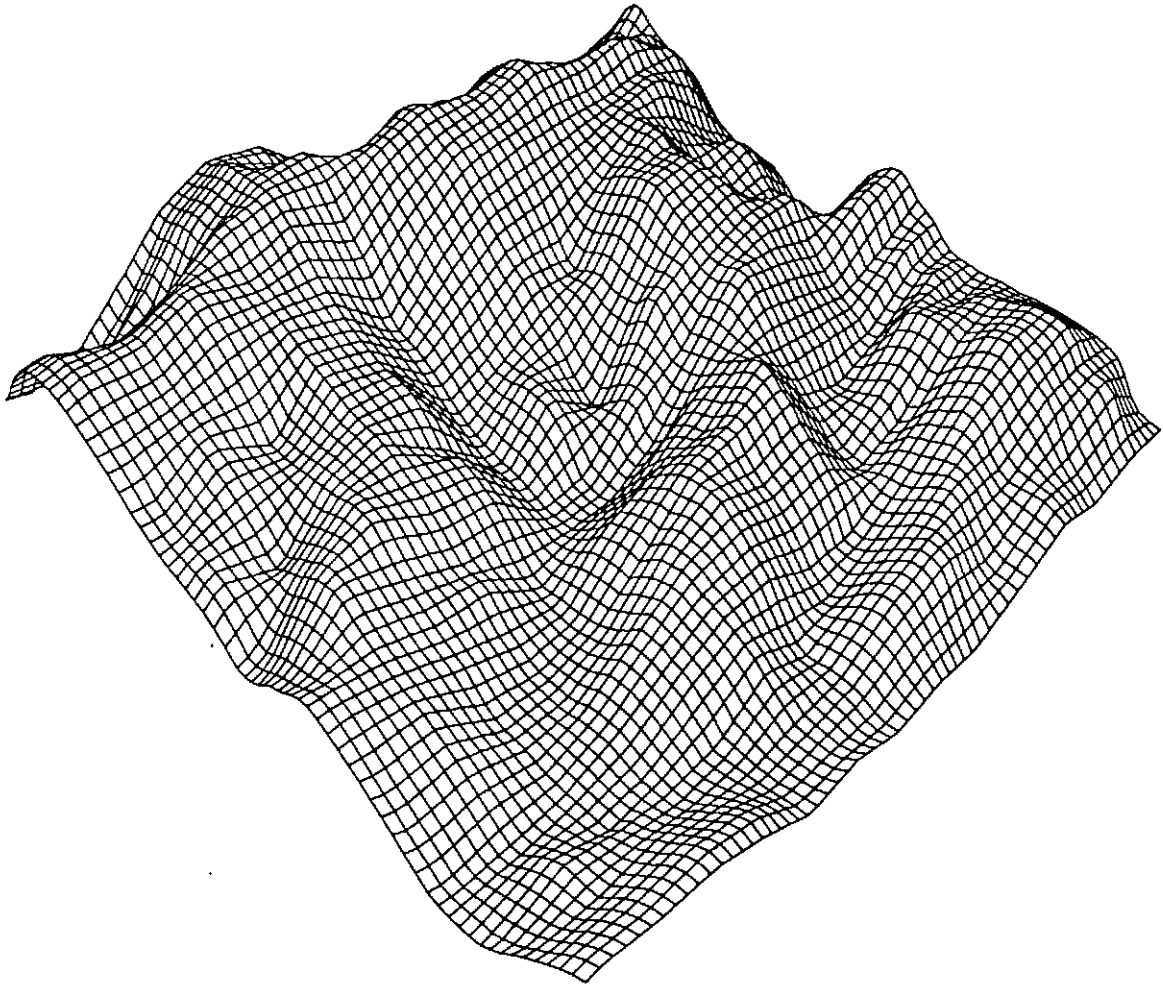
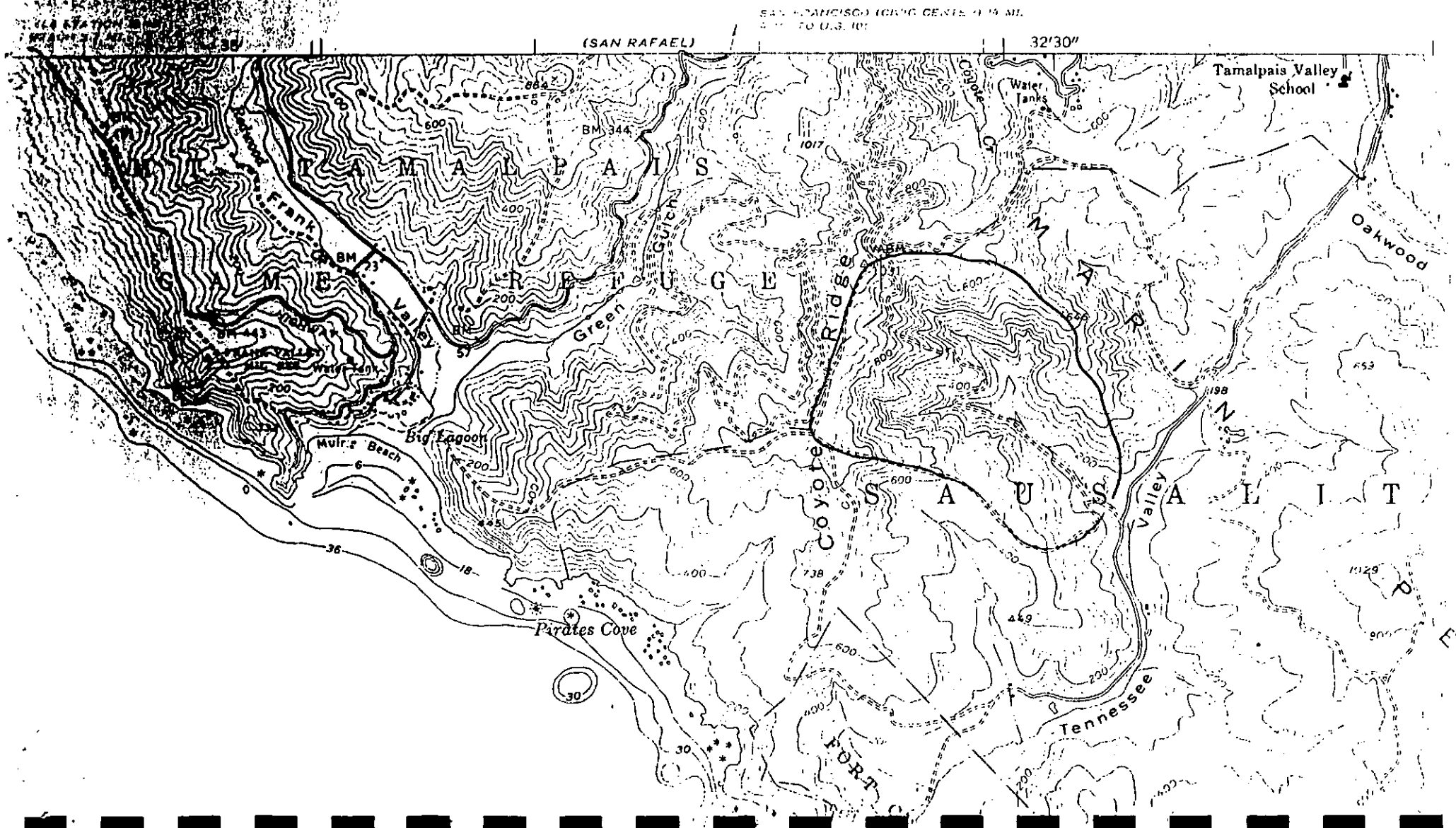


Figure 4: Tennessee Valley from USGS DEM data, 30m grid spacing
3x vertical exaggeration

Figure 5: Tennessee Valley from Point Bonita 7.5' Quadrangle
Contour interval 40 feet



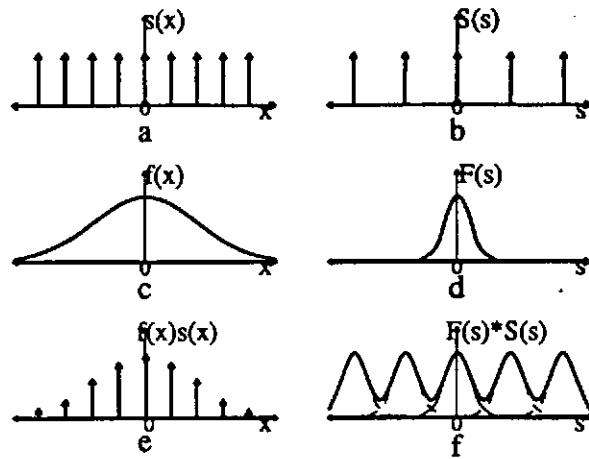


Figure 6: This figure shows the sampling process in the spatial domain on the left and in the frequency domain on the right. a) is the sample function and b) is its Fourier transform. c) is the height function (a Gaussian) and d) is its Fourier transform. e) is the product of the height function and sample function and converts to convolution f) in the frequency domain. $F*S$ (thick line) is the sum of $F(s)$ (thin line) and translations of $F(s)$ (dotted lines) centered at each δ function in $S(s)$.

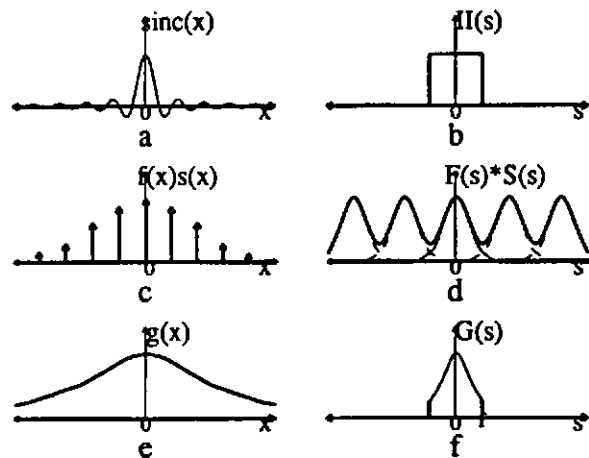


Figure 7: This figure shows the filtering process in the spatial domain on the left and the spectral domain on the right. a) is the filter function, $\text{sinc}(x)$, and b) is its Fourier transform, $\Pi(s)$. c) is the sampled function and d) is its Fourier transform. e) is the new function $g(x) = (f(x)s(x)) * \text{sinc}(x)$ after filtering and f), $G(s) = (F(s)*S(s))\Pi(s)$, is its Fourier transform.

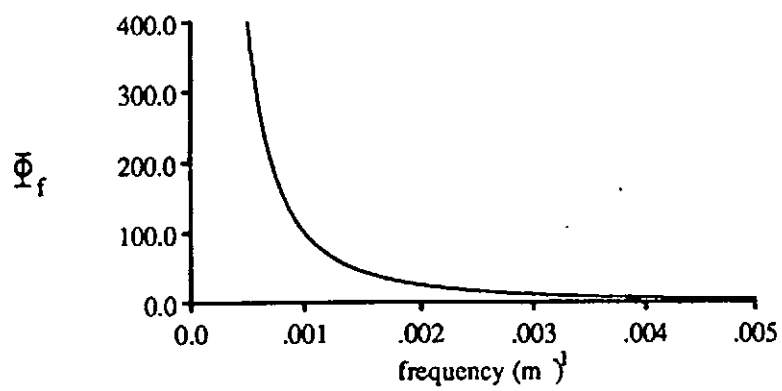


Figure 8: PSD of a fractal curve with $D=1.5$.

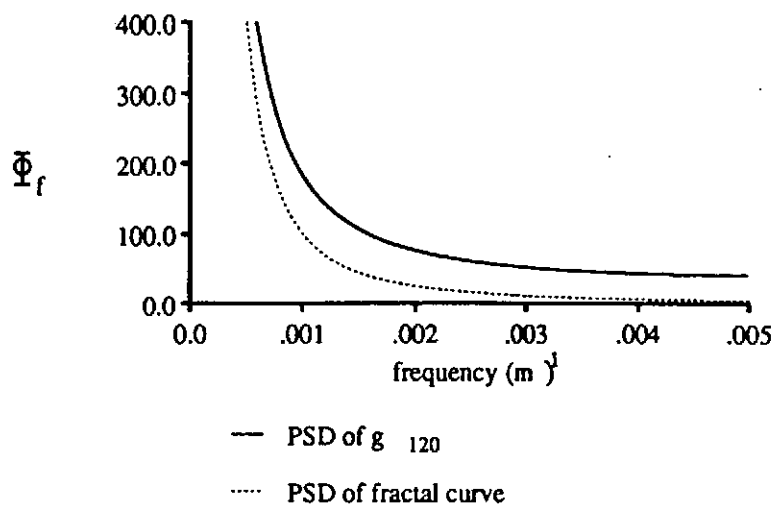


Figure 9a

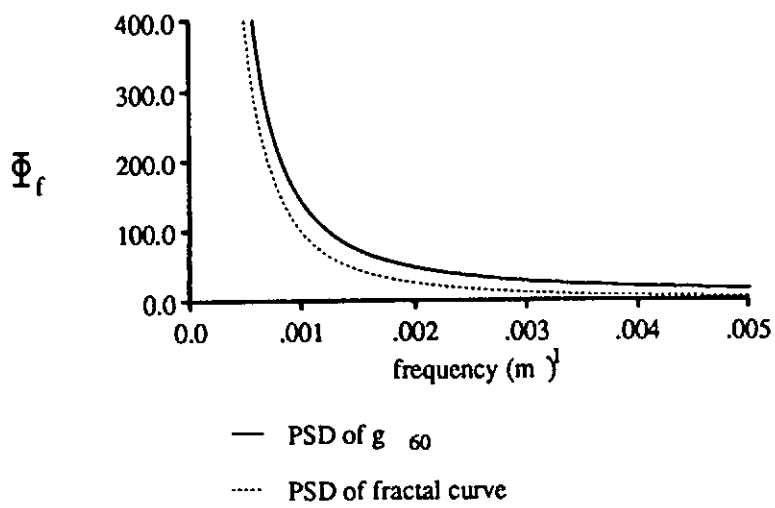


Figure 9b

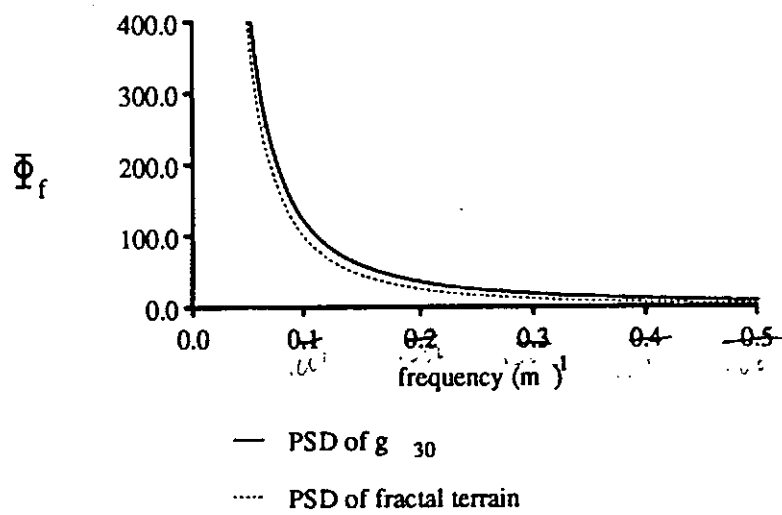


Figure 9c

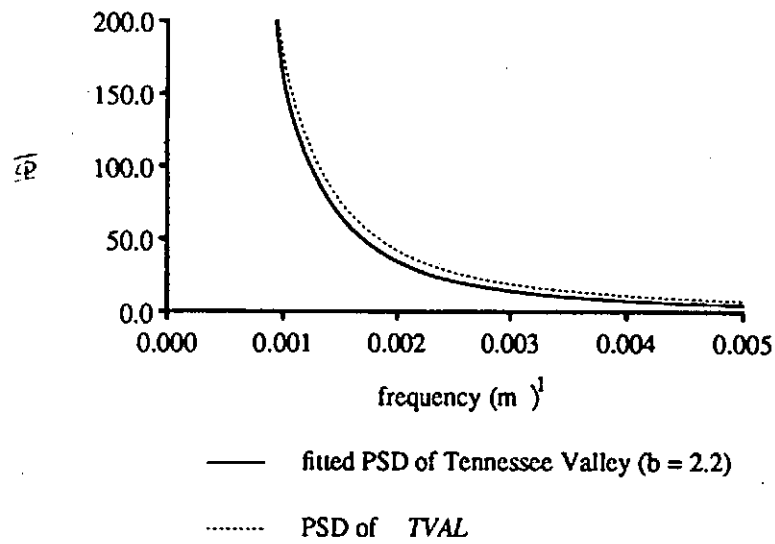


Figure 10 α

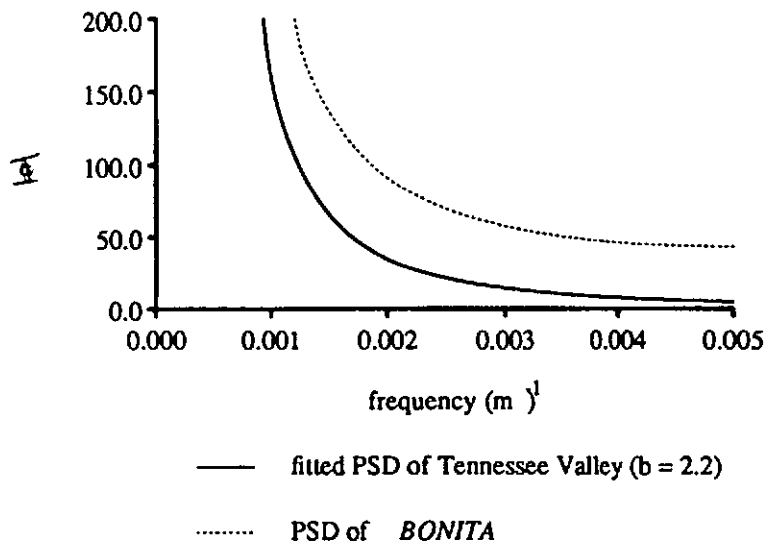


Figure 10b

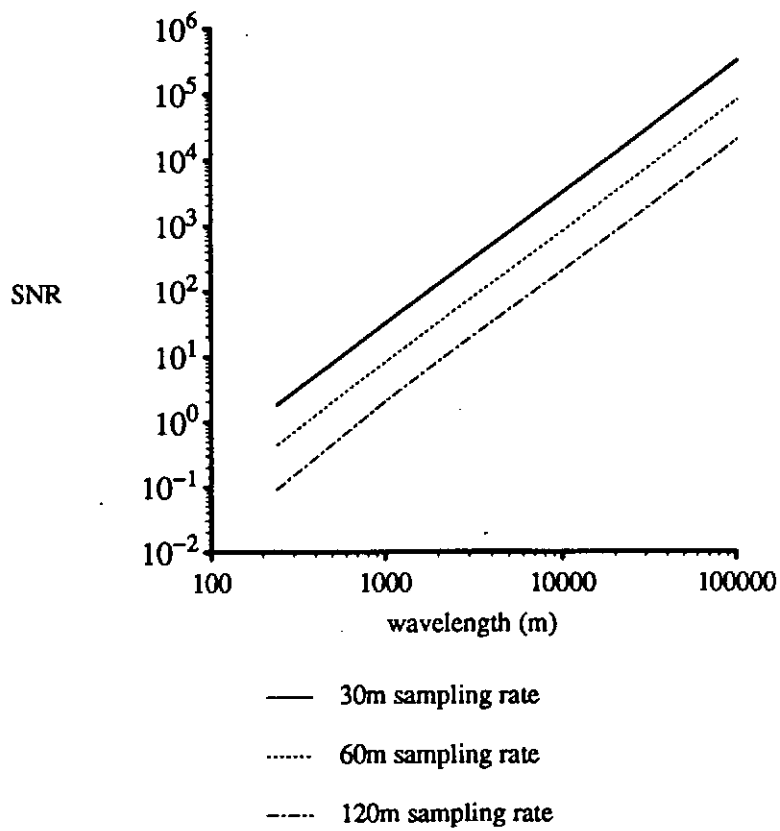


Figure 11: SNRs for a fractal curve ($D = 1.5$)

Appendix 2

Effects of DEM Grid Size on Landscape Representation and Hydrologic Simulations

(to be submitted to Water Resources Research)

Weihoa Zhang and David R. Montgomery
Department of Geological Sciences,
University of Washington, Seattle, WA 98195

Abstract

High resolution digital elevation data from a small catchment in the Oregon Coast Range is used to examine the effect of DEM grid scale on the portrayal of the land surface and on hydrologic simulations based on this representation of the landscape. For comparison purposes, 1:4,800 scale contour map of the catchment is assumed to faithfully represent the land surface. The contour map was vectorized and converted into a set of coordinate and elevation data with an average spacing of 5 meters. These topographic data were then gridded at 1, 2, 4, 10, 30, and 90 meter scales to generate a series of simulated landscapes. Frequency distributions of contributing area per unit contour length (a), slope ($\tan B$), and the topographic index ($a/\tan B$) were calculated for each grid size. The frequency distributions of $a/\tan B$ were then used in O'Loughlin's (1986) criterion for the prediction of surface saturation zone and in TOPMODEL for the simulation of runoff response from a suite of storms. Statistical representations of topographic characteristics change systematically with decreasing grid scale. So does the predicted surface saturation zone using O'Loughlin's criterion for surface saturation. Runoff response, including hydrographs and dynamic variation of surface saturation areas, simulated using TOPMODEL, however, vary non-systematically with DEM grid scale.

These results have fundamental implications for physically-based models of surface processes and hydrologic response.

Introduction

Prediction of catchment runoff processes requires both a hydrologic model and characterization of land surface properties. Among these land surface properties, perhaps the most important one is the characterization of land surface itself. Topography plays a dominant role in controlling both the location and magnitude of surface and subsurface runoff, especially in areas where runoff production is dominated by surface or near surface flow processes [Kirkby and Chorley, 1967; Dunne and Black, 1970a, b]. Many hydrologic simulations rely on physically-based, topographically-driven catchment runoff models [Beven and Kirkby, 1979; O'Loughlin, 1986; Moore and Grayson, 1990]. Most of these topographically-based models rely on preprocessing of topographic data to derive topographic attributes incorporated in the models. Spatially distributed local slopes and upslope contributing areas are the primary topographic attributes used in hydrologic [Beven and Kirkby, 1979; Famiglietti and Wood, 1990], ecologic [Band, 1990], surface processes [Dietrich et al., in press], and hazard assessment [Vertessy, 1990; Montgomery and Dietrich, in prep.] models. These two topographic parameters are the free parameters that essentially dictate the outcome of these simulations. Consequently, it is crucial that the derived topographic attributes faithfully portray the land surface. In spite of the importance of this problem, the degree to which DEM's portray the land surface has not been systematically studied.

Previous Work

Digital elevation data typically are stored in a Digital Elevation Model (DEM) in one of two formats: as point elevation data on a regular grid mesh or as vectorized contour lines stored as Digital Line Graphs (DLG). The resolutions of the available DEMs can vary widely depending on sources of the data and areas of interests, ranging from a few meters for some research catchments to 30 and 90 meters for most DEMs commercially available in the U.S. This raises the question as to how the resolution of a

DEM affects the derived topographic attributes, and ultimately, hydrological simulations based on topographically-driven hydrologic models. Derivation of these topographic attributes by manual methods is extremely tedious. Fortunately, the increasing availability of DEMs allows automatic acquisition of distributions of these topographic attributes for many areas and for even large drainage basins (Jenson, 1991).

Panuska et al. (1990) examined the effects of DEM grid scale on three different derived topographic attributes: slope, upslope contributing area, and maximum flow pathlength using both grid-based and contour-based DEMs. In their study, three different resolutions were used for the two forms of DEMs: a grid spacing of 15, 30 and 90 meters for the grid-based DEM, and a contour interval of 6, 12 and 18 meters for the contour-based DEM. The results show that while the effect of DEM scale on the computed values of slope and maximum flow pathlength was small, the effect on the computed values of upslope contributing area was significant. As the grid spacing increased from 15 meters to 90 meters, the median of the computed contributing area increased by about one order of magnitude. A similar response was also found for the contour-based DEM.

Quinn et al. (1991) computed the distributions of the topographic index ($a/\tan B$) using two different DEM scales, 12.5 and 50 meters, and found that the computed values of this combined topographic attribute increased as the DEM scale increased. Jenson (1991) studied the effects of DEM scale on the calculated local slopes using a grid-based DEM of two different grid spacings: 3 arc-second and 30 arc-second, and found that as the grid spacing of the DEM increases the computed values of local slope decrease. Using two much larger but different scales of a grid-based DEM, 1/40th and 1/20th degree, Hutchinson and Dowling (1991) arrived a similar finding, that is, the computed values of slope decreases with the increase of DEM scale, whereas the computed values of upslope contributing area and topographic index increase with the increase of DEM scale.

Each of these studies showed that the characteristics of the derived topographic attributes depend on the resolution of the DEM and that such a phenomena occurs across a range of scales. None of these studies systematically analyzed the effect of grid scale resolution on the statistical characterization of the land surface. Furthermore, none of these workers

addressed the question of how the derived topographic attributes from different DEM scales affect the computed hydrologic response of a catchment using a topography-based model. As more topography-based models are being developed and applied to practical problems, it is crucial that the effect of DEM grid scale on the hydrologic predictions of topography-based models be studied and understood. This paper examines the effects of DEM scale both on the derived topographic attributes and on the resulting hydrological simulations of a topographically-based hydrologic model.

Study Area and Methods

The study area consists of a 0.4 km² catchment in the Oregon Coast Ranges near Coos Bay, Oregon. The study site is one of the catchments in which previous detailed field mapping documented the extent of the channel network [Montgomery, 1991; Montgomery and Dietrich, 1992]. Channel head locations in this area are controlled primarily by shallow debris flows from small unchanneled valleys [Montgomery and Dietrich, 1988; 1992]. The catchment is highly dissected and hillslopes as steep as 45 degrees are common. Prior to clear cutting in 1986 the catchment supported a forest cover with a canopy estimated to have been on the order of 100 to 200 feet above the ground surface.

A 1:4,800 scale topographic basemap derived from low altitude aerial photographs taken prior to timber clearing was used as the source of digital elevation data. The basemap was scanned and vectorized using an automated vectorizing routine. The vectorized contours were then sampled to yield paired location and elevation points, at an average spacing of about 9 meters. A contour map was generated from these data gridded on a 2 meter spacing (Figure 1). The map is virtually indistinguishable from the original topographic map. During field mapping, however, discrepancies were noted between the original topographic map and the ground surface.

A modified version of the topographic analysis model of Jenson and Domingue [1988] was used to derive topographic attributes from DEM's of the study area gridded at different scales. The subsequent simulations and analysis of catchment hydrologic response were carried out using

TOPMODEL [Beven and Kirkby, 1979]. Both the statistical distribution of topographic attributes and simulated hydrologic response were examined by gridding the original elevation data at scales of 1, 2, 4, 10, 30, and 90 meters.

Topographic Attributes and DEM Scales

The topographic parameters that influence models of surface or hydrologic response are local slope ($\tan B$), upslope contributing area per unit contour length (a), and the topographic or drainage index ($a/\tan B$), as defined by Beven and Kirkby [1979]. These topographic attributes govern models of surface processes and runoff generation and have been widely used in process-based hydrologic models. The effect of DEM grid scale on the distributions of these topographic attributes is examined. In contrast to previous studies, we use the same original elevation data and grid it at several different scales for our comparison.

Slope

Slope is one of the primary topographic attributes controlling hydrologic and surface processes. The computed cumulative distributions of slope for different DEM scales are shown in Figure 2. The result indicates that the percent of the catchment steeper than a given slope decreases as the DEM grid spacing increases. With a 1 meter grid spacing, 50 per cent of the catchment has a computed slope equal or greater than 33 degrees, whereas the same data gridded at a 90 meter spacing reduces the area with a computed slope greater than 33 degree to about 10 percent of the total catchment area. This result is consistent with those of previous studies, however, the effects of different DEM scales on the computed slopes in this case are much stronger than those found in the previous studies. The most likely reason is that the landscape of this area is steeper than those reported in the previous studies. Therefore, as the grid spacing increases, steeper hillslopes are averaged and smoothed out to a greater degree than in gentler landscapes. This effect of DEM scale on the distribution of derived slopes has important implications for geomorphic modeling and land management practices. For example, DEM-based models of potential areas of slope instability are driven primarily by relative saturation and slope. Consequently, predictions of potential slope

instability area will be greatly affected by the resolutions of the available DEM. In essence, more potentially unstable areas would be predicted with a finer resolution DEM than with a coarser resolution DEM.

The effect of DEM grid scale on the slopes simulated should be greatest for a steep landscape where averaging of the slope gradients will have the greatest impact. Consider the distribution of slopes within a single grid cell. The slope associated with the grid cell is the average slope over the entire cell. Consequently, if there are both steep and gentler slopes within a grid cell, then the average slope of the grid cell will be less than the slope of the steeper portion of the area within the grid cell. Consequently, decreasing grid cell size allows resolution of areas with steeper slopes. Thus the convergence of the slope frequency distributions with decreasing grid size reflects the underlying distribution of slopes represented in the original DEM data.

Contributing Area Per Unit Contour Length

The contributing area per unit contour length, a , is defined as the drainage area above a contour line of unit length. The computed upslope contributing area is significantly influenced by the resolution of the DEM. In general, the computed values of the upslope contributing area increase with the increase of the grid spacing, as shown in Figure 3. For example, the mean contributing area per unit length increases from 2.4 meters for 1 meter grid spacing to 4.4 meters for 90 meter grid spacing. However, most of the increases in the contributing area per unit contour length are for the small values. For each case, the smallest possible value of the contributing area per unit length is equal to the grid spacing, which is seen in the frequency distribution curves as the points where the curves make sharp turns into flat lines. Since the locations with small upslope contributing areas are most likely on hillslopes, this suggests that the DEM grid size effectively limits the resolution of hillslope attributes (i.e., hillslope size) from DEM's. Understandably, the magnitude and distribution of the computed upslope contributing area strongly influences the ability of the DEM to resolve hillslopes.

Topographic-Index

The topographic-Index, or drainage index, is the ratio of the upslope contributing area and local slope, $a/\tan B$. The spatial distribution of this index correlates with soil moisture, surface saturation, and runoff generation [e.g., Beven and Kirkby, 1979; O'Loughlin, 1986; Moore et al., 1986]. Accurate estimation of $a/\tan B$ is the first step for hydrological simulations of several topography-based hydrologic models. Moreover, this parameter essentially determines the distribution of simulated soil moisture in steady state simulations and influences the hydrograph in dynamic simulations.

Figure 4 shows distribution maps of $a/\tan B$ computed with four different grid scale resolutions (4 m, 10 m, 30 m and 90 m). As expected, many detailed distribution features of $a/\tan B$ that appear on the finer resolution DEM are smoothed out on the coarser resolution DEM. The cumulative frequency distributions of $a/\tan B$ computed from the DEM of different grid scale are shown in Figure 5. With the increase of DEM grid spacing, the entire cumulative distribution curve shifts toward the higher values of $a/\tan B$, with a greater relative effect on the upper portion of the curve with lower values of $a/\tan B$. The distribution statistics of $a/\tan B$ for different DEM grid spacings are shown in Figure 6. The results show that DEM grid scale affects all three distribution moments: mean, standard deviation and skewness. The mean of the distribution increases monotonically with the increase of the grid spacing. The standard deviation increases initially as the grid spacing increases from 1 meter to 4 meters, and then decreases as the grid spacing increases from 4 meters to 90 meters. The shape of the distribution, in general, become more positively skewed as the grid spacing becomes larger.

Another important effect of DEM grid scale on the derived distribution of $a/\tan B$ is on the distribution tails of higher $a/\tan B$ values. While $(a/\tan B)$ computed from a coarser DEM's has greater percentage of higher values, $(a/\tan B)$ computed from a finer resolution DEM tends to have longer distribution tails. This effect of DEM grid scale on the distribution tail of $a/\tan B$ may have a significant impact for runoff predictions using a topography-based hydrological model, as the areas with higher $a/\tan B$ values are most likely to produce surface saturation during a storm (Beven and Kirkby, 1979).

The results of Figure 5 show that as the grid spacing of the DEM becomes smaller and smaller, the computed frequency distribution curves converge to an apparent underlying distribution function. Whether this trend is a generality is the subject of ongoing investigations. The physical significance of this convergence is unclear. Does it occur at a scale determined by something present in the actual landscape or is the scale of the convergence dictated by the information content in the original gridded topographic information. In either case, the demonstrated effect of DEM scale should not be overlooked when fitting a distribution function to the computed values of $a/\tan B$.

Implications for modelling surface processes

Models of erosional process (e.g., overland flow, seepage erosion, and landsliding) are controlled by discharge (surface and/or subsurface), slope, and physical properties of the soil or bedrock (e.g., hydraulic conductivity, critical shear stress, angle of internal friction). Threshold models for erosion by these processes can be combined with DEM's to predict the spatial dominance of different erosional processes [Dietrich et al., in press; Montgomery and Dietrich, in prep.]. The spatial distributions of drainage area and slope in the simulated landscape essentially dictate the predicted distribution of surface processes. Consequently, the influence of DEM grid size on the distribution of these characteristics has fundamental implications for the coupling of physically-based erosion models with DEM's. Consider the problem of predicting areas prone to shallow slope instability, or debris flows. Models of slope instability involve relations between the slope angle and the angle of internal friction of the soil. In steep landscapes, as the DEM grid size is increased, less and less of the total area is steeper than a given slope. This indicates that the area predicted to be unstable will decrease with increasing grid size, as the modeled slopes will be progressively less steep. This illustrates the importance of using a DEM with a grid size resolution that is appropriate for the processes being modeled. In a steep landscape, it is unreasonable to use a 30 meter grid size to model hillslope processes. Nonetheless, Tarboton and others [1991] attempt to define the "hillslope/channel" transition by an inflection in the relation between drainage area and an averaged link slope from 30 and 90 meter resolution DEM's. Our results indicate, however, that this resolution

is insufficient to resolve hillslopes in steep landscapes. Furthermore, our results indicate that it is crucial to consider the effects of DEM grid scale resolution when translating interpretations from DEM's to actual landscapes.

DEM Scale and Hydrologic Simulations

The effect of DEM grid scale on topographic parameters (a , $\tan B$) will impact models that rely on $a/\tan B$ to simulate topographic control in modeling land surface runoff processes. These models are only as representative of the field case as are the representations of the land surface generated by the DEM. Consequently, the changes in the distribution of these topographic parameters should impact hydrologic simulations based on DEM's. What is the impact of these effects, however, and are there any systematic differences between simulations using different grid scales? These questions are addressed based on hydrologic simulations using the widely-used topography-based hydrologic model TOPMODEL [Beven and Kirkby, 1979] and elements of TOPOG [O'Loughlin, 1986].

Prediction of Surface Saturation Zones

One of the direct consequences of the above analysis is on the prediction of zones where the ground surface is saturated. Since many hydrological, geomorphological and ecological phenomena are closely related to the dynamics and magnitude of the variable saturation area within a catchment, accurate prediction of zones of surface saturation is important for understanding and prediction of these phenomena.

Aside the effects of soil properties, the role of topography in regulating the behavior of zones of surface saturation in a catchment under a prevailing wetness state has been well recognized from field experiments [Dunne and Black, 1970a, b; Anderson and Burt, 1977]. The sufficient condition for the development of local surface saturation in a catchment is that the accumulated water flux from upslope drainage exceeds the capacity of the soil profile to transmit the flux. By assuming a steady state drainage condition, O'Loughlin [1981, 1986] expressed the condition for surface saturation at any location in a catchment as

$$\frac{a}{\tan B} \geq \frac{T A_t}{Q_o} \quad (1)$$

T is the mean soil transmissivity of the catchment, A_t is the total area of the catchment, Q_o is the runoff rate from the catchment. The term on the right hand side of the equation is a ratio of the drainage flux per unit area to the transmissivity of the soil column. This ratio, denoted by O'Loughlin as W, indicates the wetness state of a catchment. The smaller is the W, the wetter is the catchment. For a given wetness condition, W, the total saturation area of a catchment is simply the sum of all the local areas which have the values of $a/\tan B$ so that the above condition for surface saturation is satisfied. Because of the wide availability of DEMs, this model and a similar one by Beven and Kirkby [1979] have been widely used in practice for the prediction or automatic production of zones of surface saturation for catchments [O'Loughlin, 1986, Moore et al., 1986, Phillips, 1990].

To investigate the effect of DEM grid scale on the prediction of surface saturation area, we computed the percentage of saturation areas for the Mettman ridge catchment as the function of the catchment wetness condition using six different DEM resolutions given above (Figure 7). Except for the scale of the horizontal coordinate, the curves for the relationship between percentage of saturation area and wetness conditions are identical to those of the cumulative frequency distribution of $a/\tan B$. This follows directly from the definition of the criterion for surface saturation. The results show that the predicted saturation area is dependent of the resolution of the DEM used. The coarser the grid pacing, the greater the predicted saturation area. For example, the saturation areas predicted with the DEMs of 30 meter and 90 meter grid spacings are about two to six times and three to eight times larger than that predicted with 1 meter grid spacing, respectively.

Prediction of the Catchment Response during a Storm Event

The effect of DEM grid scale on the simulated dynamic response of a catchment, particularly runoff hydrographs and variable saturation area, is

examined using TOPMODEL [Beven and Kirkby, 1979; Beven 1986]. The model predicts the distribution patterns of soil moisture and their associated runoff processes on the basis of surface topography and soils. A critical assumption of the model is that locations with similar topographic and soil properties, defined by $(a/T_0 \cdot \tan B)$ where T_0 is the local soil transmissivity, will respond in a hydrologically similar way to a same input. By assuming a spatially-uniform recharge rate and a quasi-steady subsurface response, Beven and Kirkby [1979] derived a function relating local soil moisture storage to the topographic-index of a basin

$$\bar{S} = S + m \cdot \text{gama} - m \cdot (\ln(a/\tan B) - \ln(T_0)) \quad (2)$$

where, S is the local soil moisture deficit, \bar{S} is the mean soil moisture of the basin, m is a parameter that characterizes decrease in soil conductivity with soil depth, gama is the expected value of $\ln(a/T_0 \cdot \tan B)$, a constant for the catchment. For locations where $S > 0$, the soil moisture store has not been filled, and therefore, there is not surface saturation. For the locations with $S \leq 0$, the soil moisture capacity has been filled, and therefore, surface saturation occurs.

The model computes both the relative amount of subsurface runoff and saturation overland runoff, and the spatial distribution of these runoff processes. During a model simulation, the mean soil moisture deficit for a catchment is calculated at every time step. Then, the updated S at all points in the catchment are computed using equation (2). The areas with soil moisture deficit larger than the incremental precipitation, i.e., ($S > r \cdot dt$), will only have subsurface runoff, while those areas with a soil moisture deficit smaller than the incremental precipitation, i.e., ($S < r \cdot dt$), or those of saturated at the previous time step will have both subsurface and saturation excess runoff. The subsurface flow rate of the catchment is calculated by

$$q = \exp(-\text{gama}) \cdot \exp(-\bar{S}/m) \quad (3)$$

and the saturation excess runoff is the sum of excessive soil moisture and direct precipitation that falls on the saturated areas, and is assumed to reach a channel within one time step.

It is clear from the model that the topographic index, $a/\tan B$, determines both the flow rates and spatial distribution of subsurface and surface runoff. To demonstrate the effect of DEM grid scale on the simulated hydrologic responses, we applied TOPMODEL to the study catchment using the six different grid scale DEM's given above. In the simulation, soil parameters were assumed spatially uniform so that the effect of topography is isolated. The values for m and T_0 are 100 mm and $0.139 \text{ mm}^2/\text{sec}$, respectively. These are the reasonable values for the highly conductive soils (Beven, 1986) of this area. For simplicity, it is also assumed that the percolation rate from the unsaturated zone is equal to the rainfall intensity, and flow routing in the streams is not considered. The model was run for four different rainfall intensities for a duration of 3 hours, and each run started with a same initial mean areal base flow condition of $6 \times 10^{-4} \text{ mm/sec}$. Figure 8 shows the hydrographs simulated from the six different DEM scales for four different rainfall intensities. The results indicate that the computed hydrographs are sensitive to the grid scale of the DEM.

Runoff lag time, peak discharge and the shape of recession limb are considered as the three most important characteristics of a hydrograph. One way to examine the influence of DEM grid scale on the simulated hydrologic hydrographs is to examine the relationship between these hydrograph characteristics and various grid spacings of the DEM under different rainfall intensities. Since we have not considered channel routing in the model simulation, there is no runoff lag time for any of the cases examined. We first discuss the effect of different DEM scales on the simulated peak discharge (Figure 9). For each rainfall intensity, peak discharges are normalized by the corresponding peak discharges simulated from 1 meter grid spacing. The effect of DEM grid spacing on the simulated peak discharge is different for different rainfall intensities. For a rainfall intensity of 5 mm/hr, the antecedent base flow rate is much larger than the recharge rate by rainfall and the simulated peak discharges are

dominated by the antecedent base flow. Consequently, the effect of DEM grid scale is rather small. For this case, the difference in peak discharge rates simulated from different grid spacing is less than 5%. However, as rainfall intensity increases, the peak discharge rate simulated from the DEM of one grid spacing can be significantly different from that simulated from the DEM of a different grid spacing. For example, at a 100 mm/hr rainfall the difference between the peak discharge rate simulated with 1 meter grid spacing and that with 4 meter grid spacing exceeds 35%.

Interestingly, the simulated hydrographs and peak discharges (Figures 8 and 9), in general, do not converge as the resolution of the DEM gets finer. The way in which the DEM scale affects the simulated hydrographs is dependent of the applied rainfall intensities in a rather complicated fashion. For a 100 mm/hr rainfall, the peak discharge decreases initially as the grid spacing decreases from 90 meters to 4 meters; then the peak discharge starts increasing as the grid spacing decreases from 4 meters to 1 meter. The highest peak discharge is for a 1 meter grid spacing, the second highest one is for a 90 meter grid spacing, and the lowest one is for a 4 meter grid spacing. A similar trend can also been seen for the three smaller intensity rainfall simulations although the difference between the peak discharges simulated from different grid spacing become smaller. As the rainfall intensity decreases, the peak discharges from 90 meter grid spacing become greater than those from the smaller grid spacings. Also, as rainfall intensity decreases, the lowest peak discharge gradually shifts from that of the 4 meter grid to that of the 2 meter grid.

To examine the effect of DEM grid scale on runoff recession, we characterized a hydrograph recession limb using a recession coefficient, K_r , as expressed in the following equation (Hall, 1968; Linsley et al., 1982):

$$q_t = q_0 K_r^t \quad (4)$$

where q_0 is the flow discharge at any time, q_t is the flow discharge one unit time later. A small value of K_r indicates a rapid flow recession, and a large value of K_r indicates a slow flow recession.

Figure 10 shows the calculated values for K_r from the DEM of various grid spacings and under different rainfall intensities. As expected, the computed value of K_r generally increases as the rainfall intensity decreases. Clearly, as rainfall intensity decreases, the runoff is increasingly dominated by the initial base flow, therefore, the flow recession will be slow and the value of K_r will be large. Like the peak discharge, the simulated flow recession, or the recession coefficient also exhibits a strong sensitivity to the grid spacing of the DEM. Again, the effect of DEM scale on the values of K_r varies for different rainfall intensities. This may be examined by comparing simulation results for two rainfall intensities of 20 mm/hr and 100 mm/hr. For 100 mm/hr rainfall, the maximum difference in K_r values computed from the different grid spacings is 0.81, with the largest one for 4 meter grid spacing and the lowest one for 1 meter grid spacing. However, for 20 mm/hr rainfall intensity, the maximum difference in K_r is 0.12, and the maximum K_r value is for 2 meter grid spacing and the minimum is for 90 meter grid spacing. Similar to the results shown in Figures 8 and 9, the computed recession coefficients show no systematic convergence as the grid spacing becomes smaller.

Finally, we examine the effect of the DEM scale on the dynamic response of surface saturation area as this is the important indicator of the dominant runoff processes. The simulated dynamic variation of the saturated area is also strongly sensitive to the DEM scale used (Figure 11). The computed saturation area tends to be greater as the grid spacing used becomes larger, except during the hydrograph peak period and a few short periods for the case with 90 meter grid spacing. The computed saturation areas with 30 meter grid spacing for the off peak period can be more than twice those computed with 1 meter grid spacing. The ratio between that computed with 90 meter grid spacing to that computed with 1 meter grid spacing is even higher for some cases. This effect is due to the slope averaging associated with increasing DEM grid spacing, as discussed in the previous section. Everything else being equal, locations with a smaller slope gradients are more likely to be predicted to have surface saturation.

During the hydrograph peak periods, the effect of grid spacing on the computed surface saturation area is different for different rainfall intensities, as shown in Figure 12. Predicted saturated areas for various

grid spacings are normalized with respect to the sizes of those predicted with the 1 meter grid spacing. It can be seen that the effect of DEM scale on the computed saturation area for the peak discharge is significant although the effect reduces as the rainfall intensity increases. For 5 mm/hr rainfall, the saturation area from a 90 meter grid spacing is 2.6 times of that from a 1 meter grid spacing. For 100 mm/hr rainfall, differences between the computed saturation areas become smaller, but the maximum difference still exceeds 30%. As for the case of peak discharge, the size of the computed saturation area at the peak discharge generally does not systematically converge with finer resolution DEMs.

Discussion

These results have two important implications. First, the effect of the DEM scale on the simulated runoff response using a topography-based hydrologic model is significant. Second, the simulated results, of both hydrographs and saturation areas, in general, do not converge to the results simulated from finer scales. These effects are important considerations for interpreting hydrological simulations using a topography-based model.

All hydrological models make certain assumptions about hydrological processes, and they are only approximations of the real hydrologic system. Even if we could build a model that exactly mimics field conditions, then the lack of data and the measurement errors about land surface properties and hydrological variables would still result in an imperfect match between model simulations and field observations. In practice, to obtain an acceptable correspondence between field results and model simulations, hydrologists usually require the calibration of hydrological models with the observed results. The parameters obtained from the model calibrations for a particular catchment are then used for hydrological forecasting either for the same catchment where the physical properties of the catchment are assumed unchanged or for a different catchment whose physical properties are considered the same as the catchment where the parameters were obtained. However, our results suggest that the hydrologic response of a catchment computed with the same set of parameter values, but using a different DEM grid scale, may differ significantly. Consequently,

calibration of hydrologic simulations are not transferable across DEM scales.

These results also have implications for using DEM's in predicting peak discharge in flood forecasting. The magnitude of discharge peaks predicted in response to a given rainfall rate are dependent upon the DEM grid scale used in the simulation. Other important consequences of our results are for using the extent of simulated zones of surface saturation for wetland delineation (steady state case) and on computed runoff processes, and thus on material transport processes (e.g., soil erosion and non-point source pollution). This brings up the question of which grid scale provides the best predictions.

In other words, do the simulation results of a hydrologic model converge with decreasing DEM grid scale? If this were the case, then more detailed DEM data would provide better predictive capability. The topographic parameters do converge with decreasing grid scale, but the simulated hydrologic response does not. Near-surface subsurface runoff processes are not governed by either the finest, or the coarsest, scale topography within a landscape, but rather is governed by some scale between these extremes. This suggests that while there is a lower limit to the distributions of topographic attributes, it is not necessary to use this limit for hydrologic modeling. What then is the proper DEM scale for hydrological modeling? We suggest that this question merits further study.

Conclusions

The grid scale used in creating a digital elevation model strongly effects both the portrayal of the land surface and hydrologic simulations based on this portrayal. While the effect on landscape description is systematic, the effect on hydrologic simulations is not. For models of surface processes, a DEM scale appropriate to the processes of interest should be used. For hydrologic simulations, no clear preferred DEM scale emerges, rather simulation results calibrated using one DEM scale are not directly comparable to those generated using a different DEM scale. These effects need to be considered when applying DEM-based simulations to natural landscapes.

Acknowledgements

This research was supported by NASA grant NAGW-2652A and by Washington State Department of Natural Resources grant TFW FY92-010 from the SHAMW committee of the Timber/Fish/Wildlife agreement. We thank Harvey Greenberg for technical support, Susan Jenson for making her topography analysis model available to us, and Bill Dietrich, Tom Dunne, and Romy Bauer for discussions on subjects related to the study.

References

Anderson, M. G. and T. P. Burt, Automatic monitoring of soil moisture conditions in a hillslope spur and hollow, *J. Hydrol.*, 33, 27-36, 1977.

Band, L. E., D. L. Peterson, S. W. Running, J. Coughlan, R. Lammers, J. Dungan and R. Nemani, Forest ecosystem processes at the watershed scale: basis for distributed simulation, *Ecolog. Modeling*, 56, 171-196, 1991.

Beven, K., and M. J. Kirkby, A physically based, variable contributing area model of basin hydrology, *Hydrol. Sci. Bull.*, 24, 43-69, 1979.

Beven, K., Runoff production and flood frequency in catchment of order n: An alternative approach, in *Scale Problem in Hydrology*, V.K. Gupta et al. (eds.), Reidel Publishing Company, 107-131, 1986.

Burch, G. J., R. K. Batt, I. D. Moore, and E. M. O'Loughlin, Comparative hydrologic behavior of forested and cleared catchments in southeastern Australia, *J. Hydrol.*, 90, 19-42.

Dietrich, W. E., C. J. Wilson, D. R. Montgomery, J. McKean, and R. Bauer, Erosion thresholds and land surface morphology, *Geology*, in press.

- Dunne, T and R. G. Black, An experimental investigation of runoff production in permeable soils, *Water Resour. Res.*, 6(5), 478-490, 1970a.
- Dunne, T and R. G. Black, Partial area contributions to storm runoff in a small New England watershed, *Water Resour. Res.*, 6(5), 1296-1311, 1970b.
- Famiglietti, J.S. and E.F. Wood, Evapotranspiration and runoff from large land areas: Land surface hydrology for atmospheric general circulation models, *Survey in Geophysics*, Vol. 12, 179-204, 1990.
- Hall, F. R. Base-flow recessions - A review, *Water Resour. Res.*, 4(5), 973-983, 1968.
- Hutchinson, M. F. and T. I. Dowling, A continental hydrological assessment of a new grid-based digital elevation model of Australia, *Hydrol. Processes*, 5(1), 45-58, 1991.
- Jenson, S. K. and J. O. Dominique, Extracting topographic structure from digital elevation data for geographic information system analysis, *Photogramm. Eng. Remote Sensing*, 54(11), 1593-1600, 1988.
- Jenson, S. K., Applications of hydrologic information automatically extracted from digital elevation models, *Hydrol. Processes*, 5(1), 31-44, 1991.
- Kirkby, M. J. and R. J. Chorley, Throughflow, overland flow and erosion, *Bull. Int. Assoc. Sci. Hydrol.*, 12, 5-21, 1967.
- Linsley, R. K., M. A. Kohler and J. L. H. Paulhus, *Hydrology for Engineers*, McGraw-Hill Book Company, 206-210, 1982.

- Montgomery, D. R., Channel initiation and landscape evolution (dissert.), University of California, Berkeley, 421p., 1991.
- Montgomery, D. R., and W. E. Dietrich, Where do channels begin?, *Nature*, 336, 232-234, 1988.
- Montgomery, D. R., and W. E. Dietrich, A digital terrain model for predicting debris flow source areas and run out paths, in prep.
- Montgomery, D. R., and W. E. Dietrich, Channel initiation and the problem of landscape scale, *Science*, 255, 826-830, 1992.
- Moore, I. D., S. M. Machay, P. J. Wallbrink, G. J. Burch and E. M. O'Loughlin, Hydrologic characteristics and modeling of a small forested catchment in southeastern New South Wales: Prelogging condition, *J. Hydrol.*, 83, 307-335, 1986.
- Moore, I. D. and R. B. Grayson, Terrain-based catchment partitioning and runoff prediction using vector elevation data, *Water Resour. Res.*, 1990.
- O'Loughlin, E. M., Saturation regions in catchments and their relation to soil and topographic properties, *J. Hydrol.*, 53, 229-246, 1981.
- O'Loughlin, E. M., Prediction of surface saturation zones in natural catchments by topographic analysis, *Water Resour. Res.*, 22(5), 794-804, 1986.
- Panuska, J. C., I. D. Moore, and L. A. Kramer, Terrain analysis: Integration into the agriculture nonpoint source (AGNPS) pollution model, *J. Soil and Water Conserv.*, 46(1), 59-64, 1991.
- Phillips, J., A saturation-based model of relative wetness for wetland identification, *Water Resour. Bull.*, 26(2), 333-342, 1990.

Quinn, P., K. Beven and O. Planchon, The prediction of hillslope flow paths for distributed hydrological modeling using digital terrain models, *Hydrol. Processes*, 5(1), 59-79, 1991.

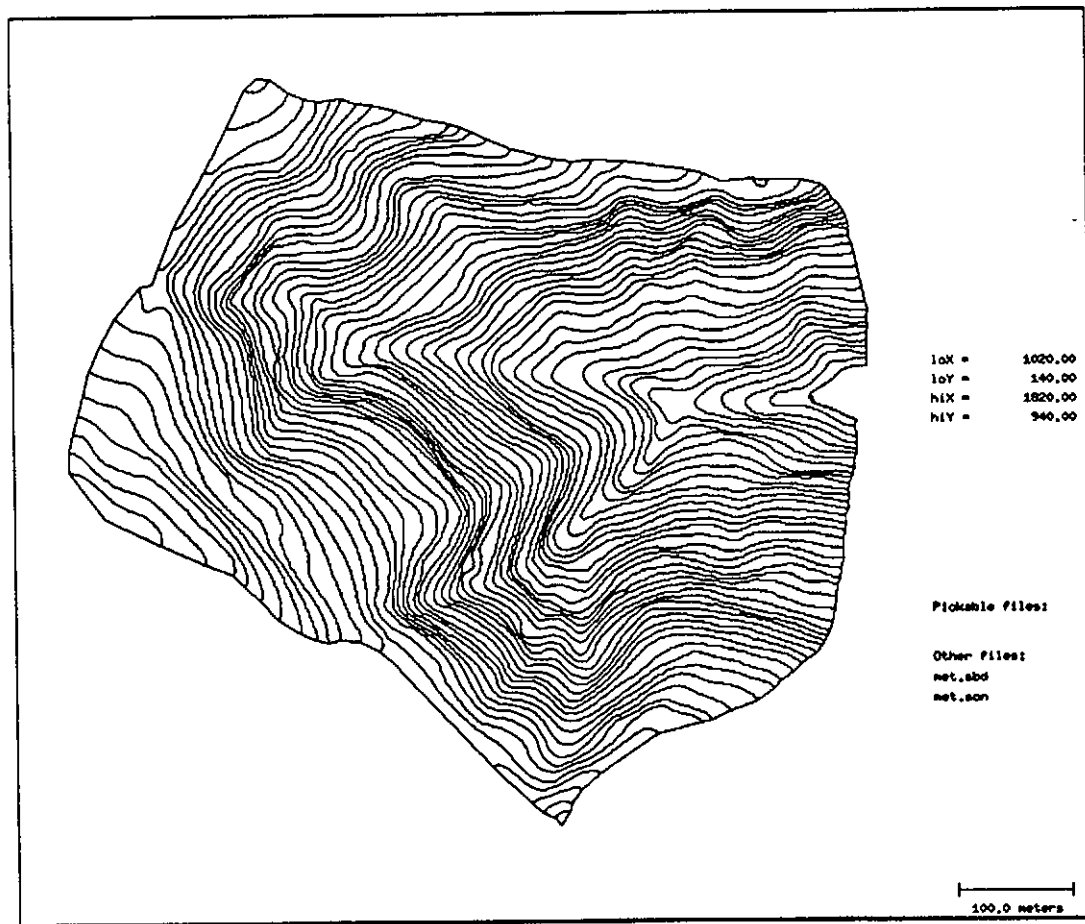
Tarboton, D. G., R. L. Bras and I. Rodriguez-Iturbe, On the extraction of channel networks from digital elevation data, *Hydrol. Processes*, 5(1), 81-100, 1991.

Vertessy, R. A., C.J. Wilson, D.M. Silburn, R. D. Connolly, and C. A., Ciesiolka, Predicting erosion hazard areas using digital terrain analysis, *International Association of Hydrological Sciences, Publication 192*, pp. 298-308, 1990.

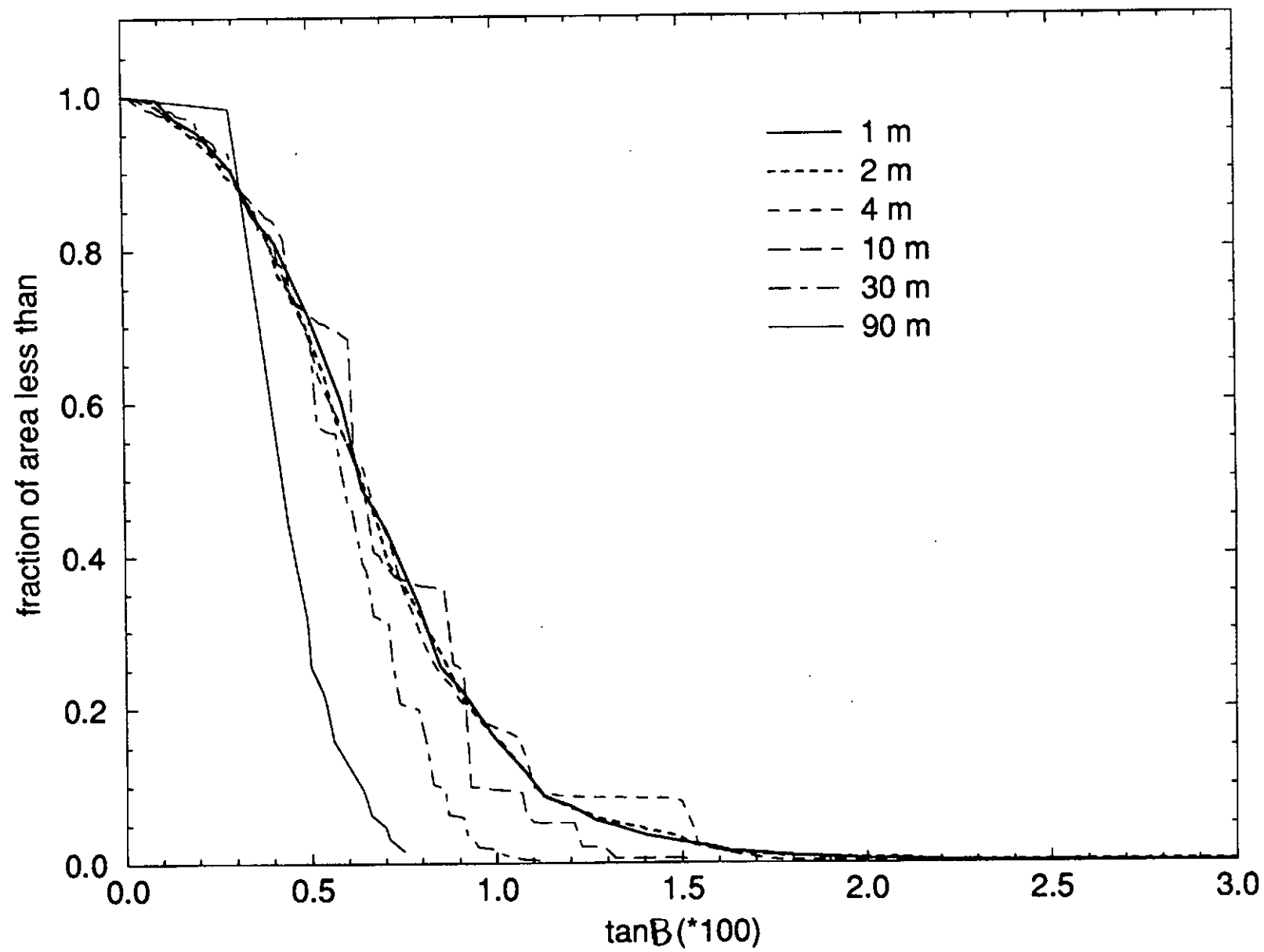
Figure Captions

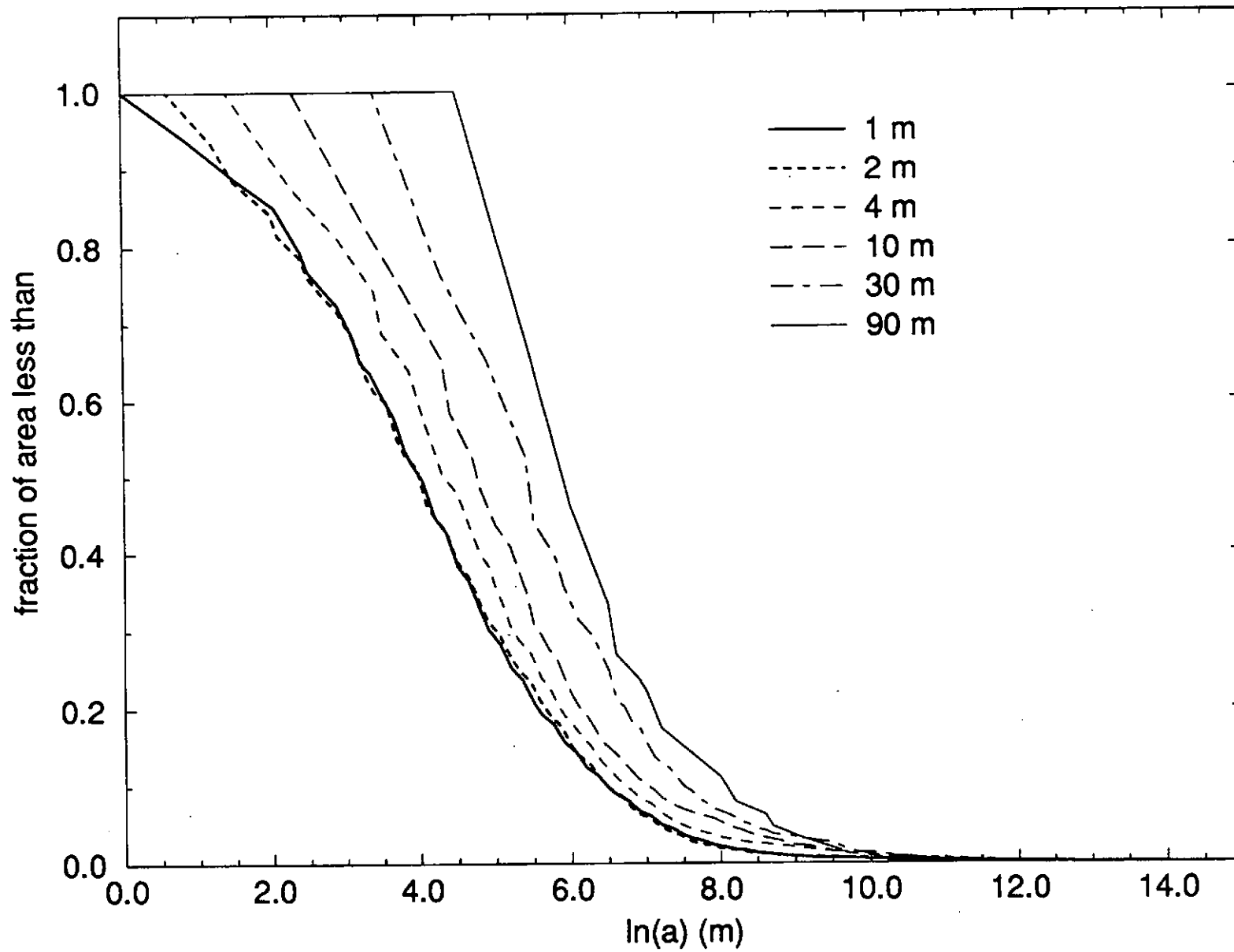
1. Contour map of the Mettman ridge catchment.
2. Cumulative frequency distributions of slope derived for different grid spacings.
3. Cumulative frequency distributions of the contributing areas per unit length for different grid spacings.
4. Maps showing the spatial distribution of the topographic index, $\ln(a/\tan B)$, for four different grid spacings.
5. Cumulative frequency distributions of the topographic index, $\ln(a/\tan B)$, for different grid spacings.
6. Distribution statistics of the topographic index, $\ln(a/\tan B)$, for different grid spacings.

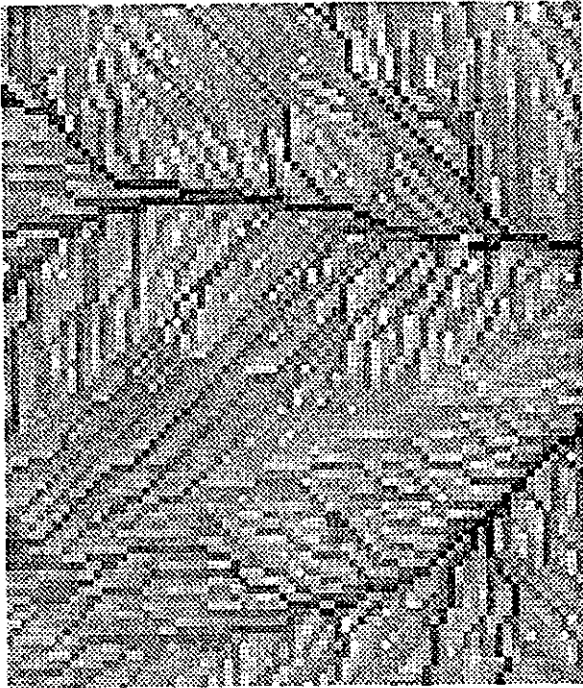
7. Percentage of computed surface saturation area vs. the wetness condition of the catchment.
8. Computed runoff hydrographs from four different DEM scales under four different rainfall intensities: a) 5 mm/hr; b) 20 mm/hr; c) 50 mm/hr; d) 100 mm/hr. For each case, a rainfall starts at $t = 3$ hour and ends at $t = 6$ hour.
9. Peak discharge rates vs. grid spacing for four different rainfall intensities, the peak discharge rates are normalized with those of 1 m grid spacing.
10. Recession coefficient vs. grid spacing for four different rainfall intensities.
11. Dynamic variations of surface saturation area (%) for four different DEM scales under various rainfall intensities: a) 5 mm/hr; b) 20 mm/hr; c) 50 mm/hr; d) 100 mm/hr.
12. Computed surface saturation areas at peak discharges vs. DEM scale for four different rainfall intensities. The values are normalized with those of 1 m grid spacing.



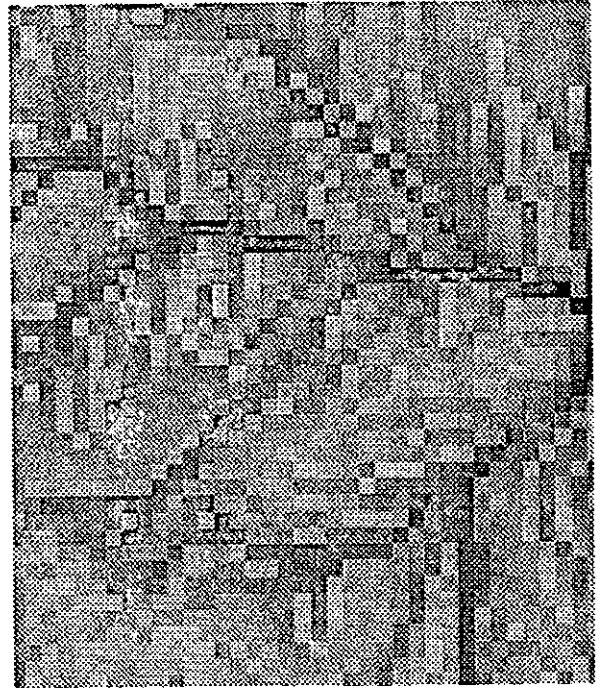
Harveybwtest



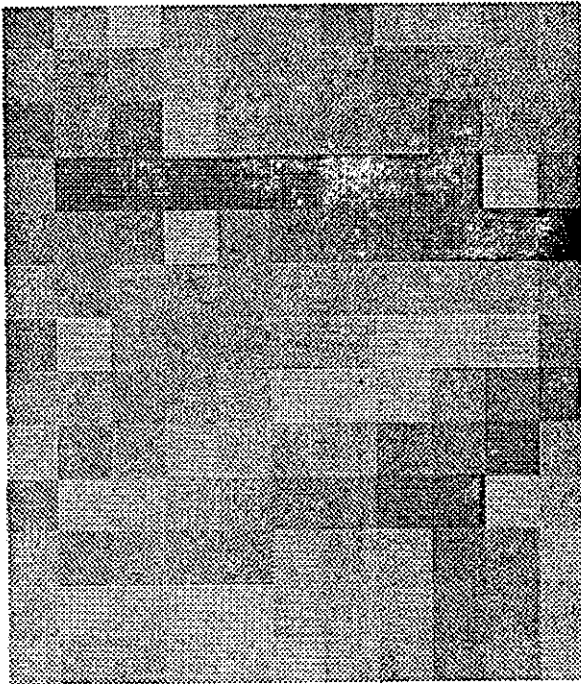




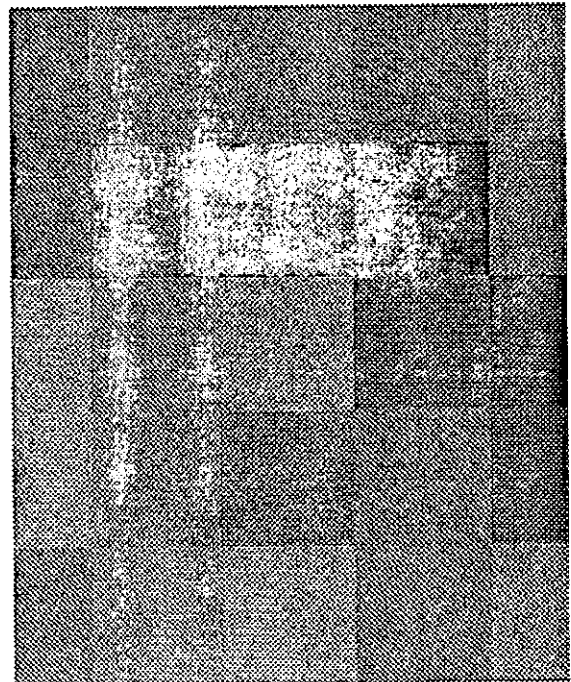
4 meter cells



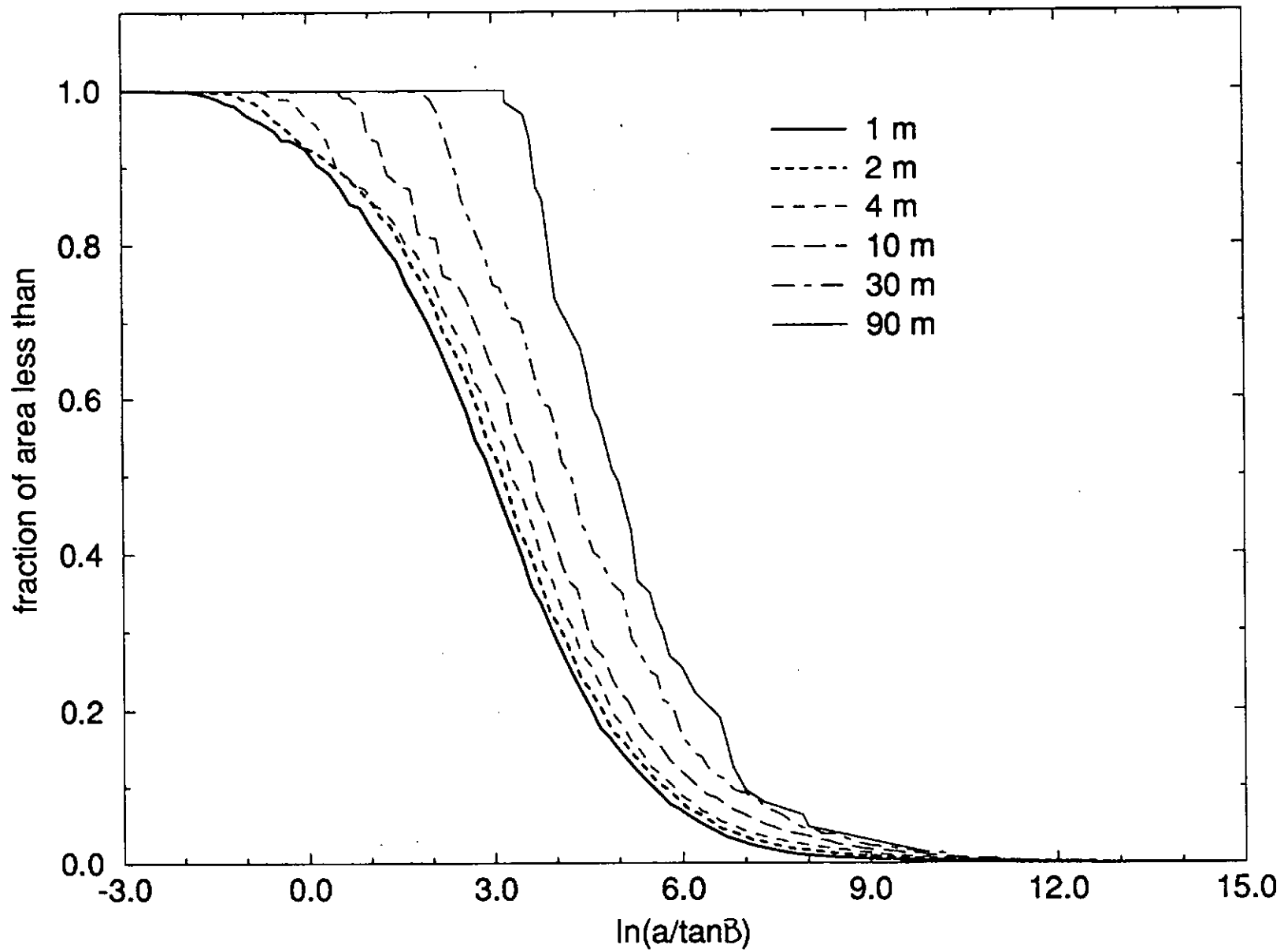
10 meter cells

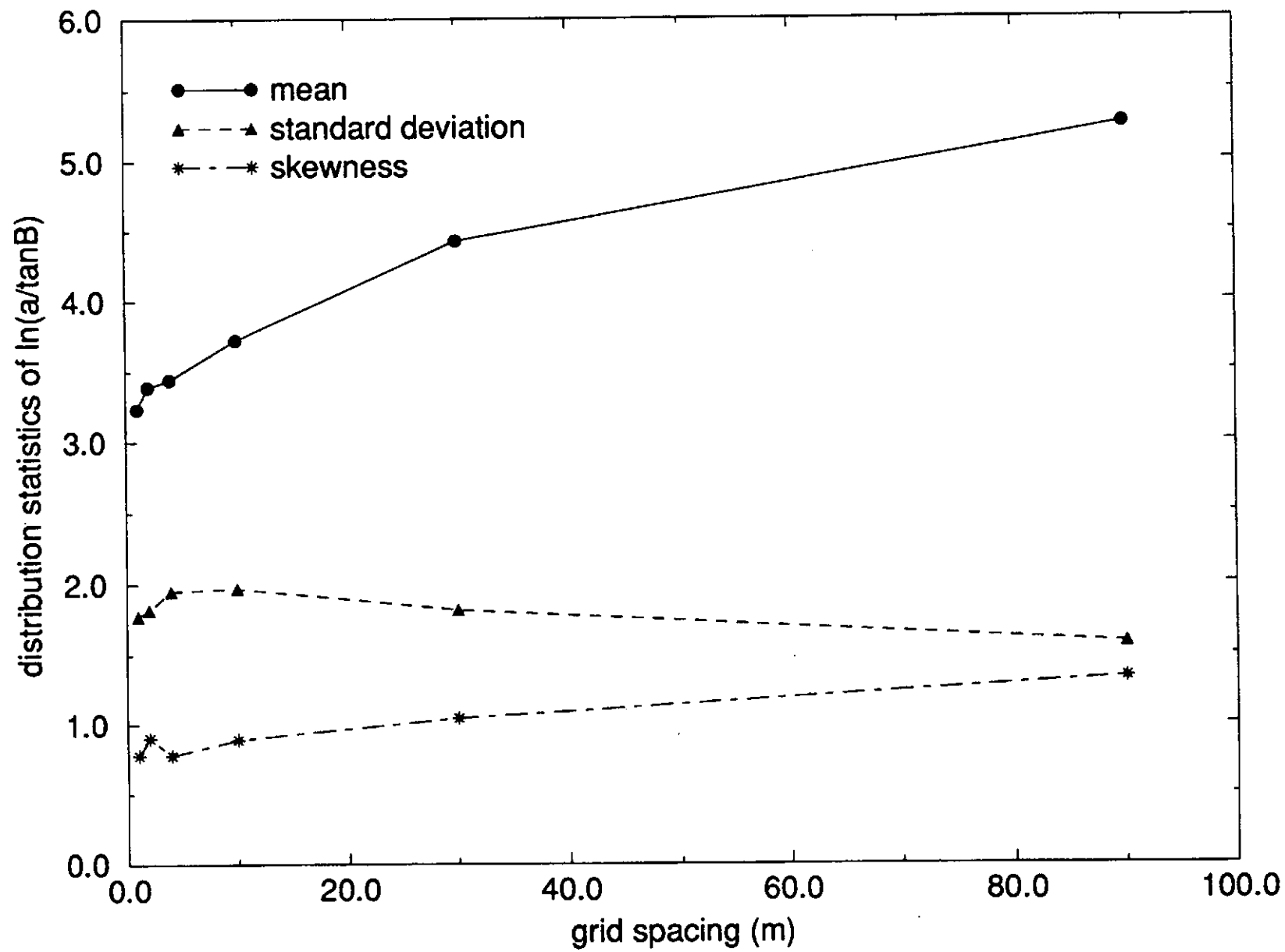


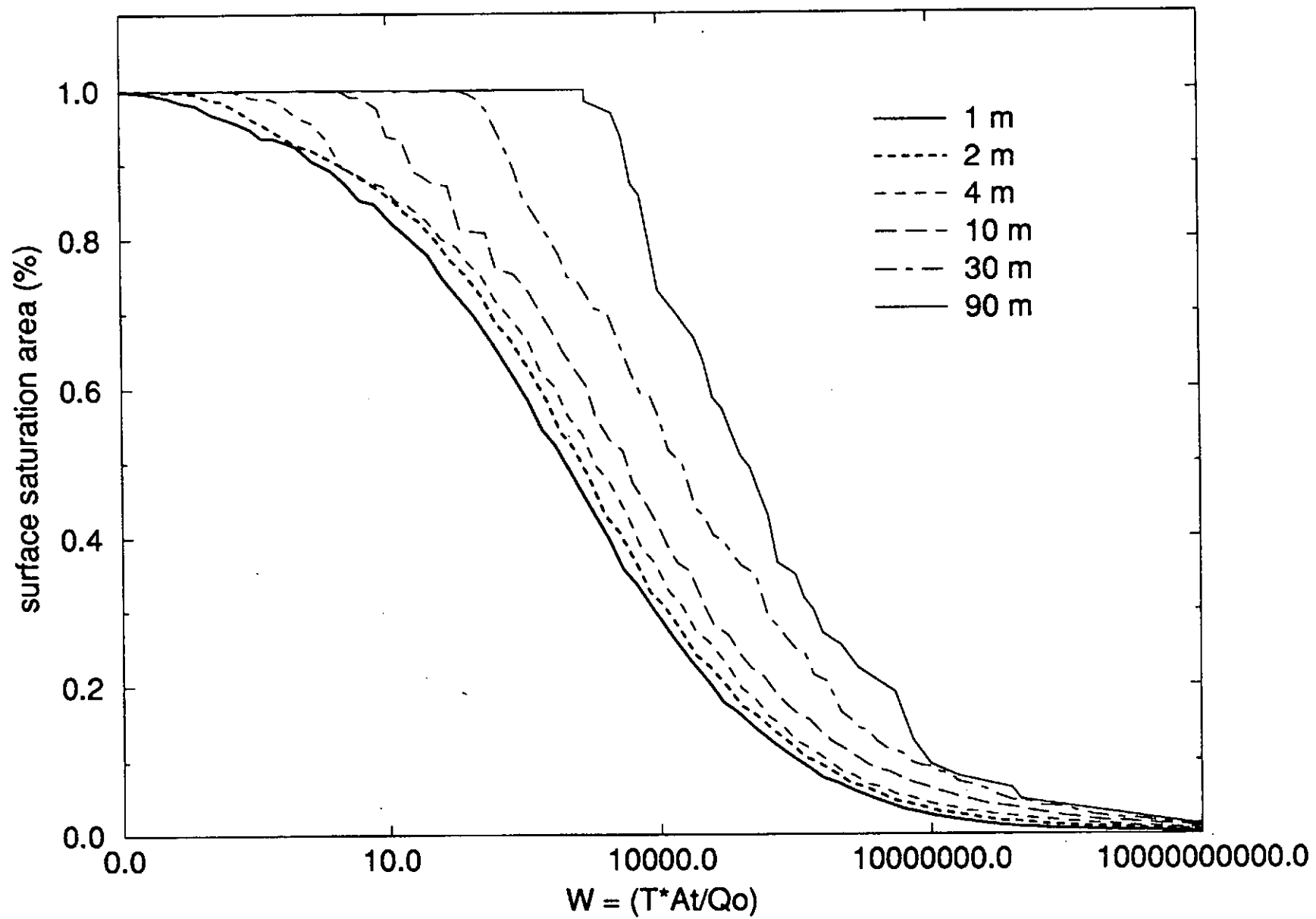
30 meter cells



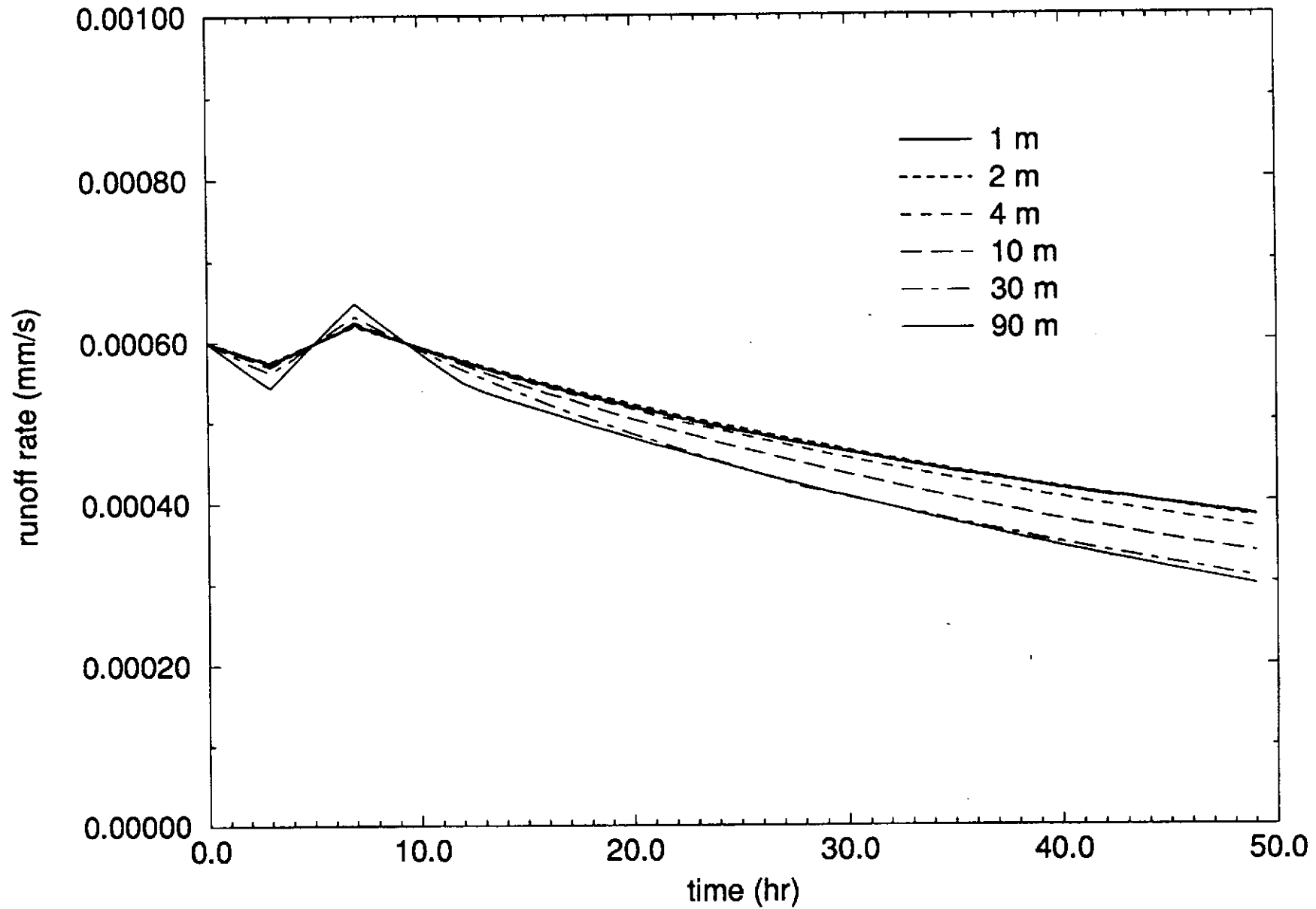
90 meter cells



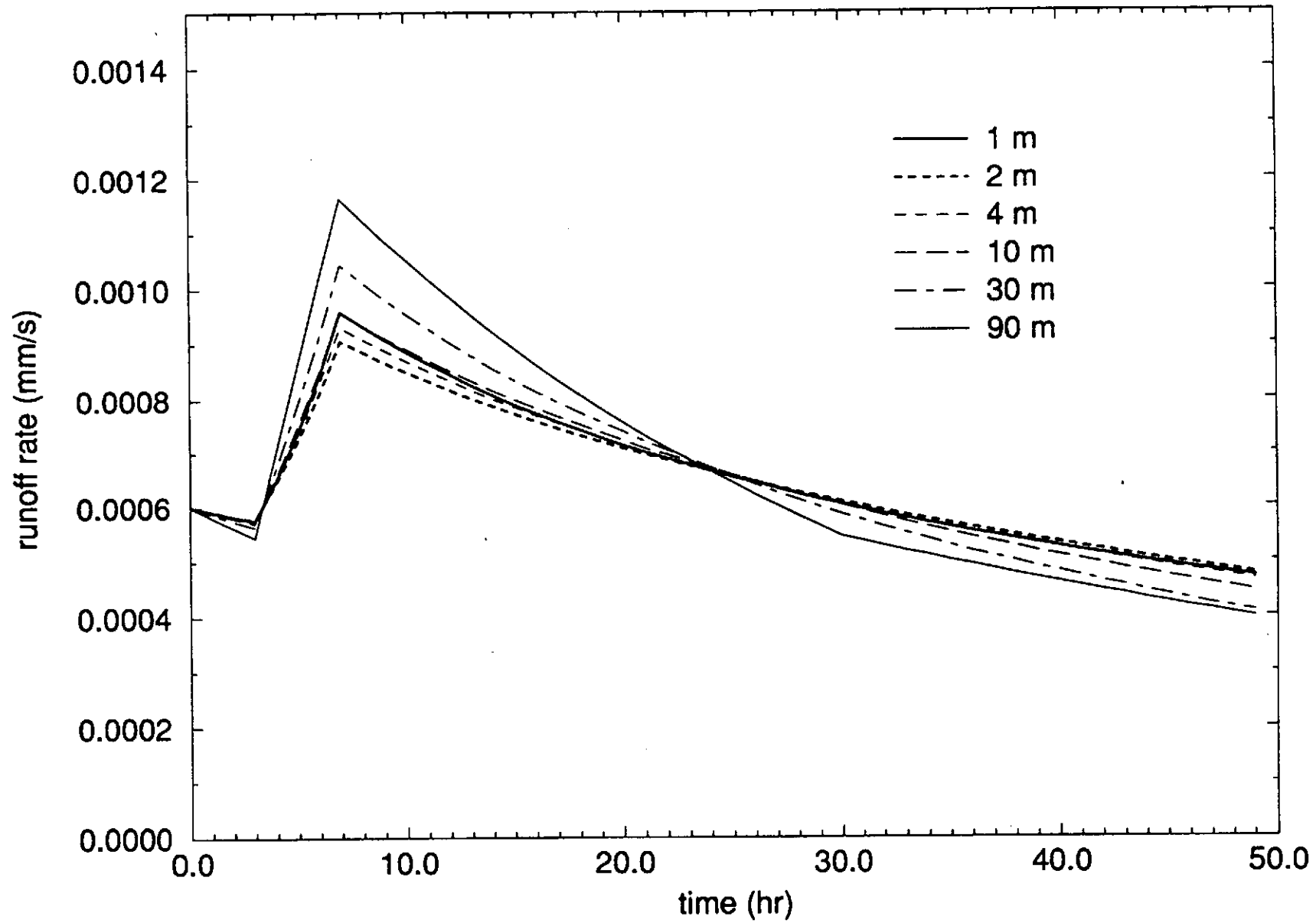




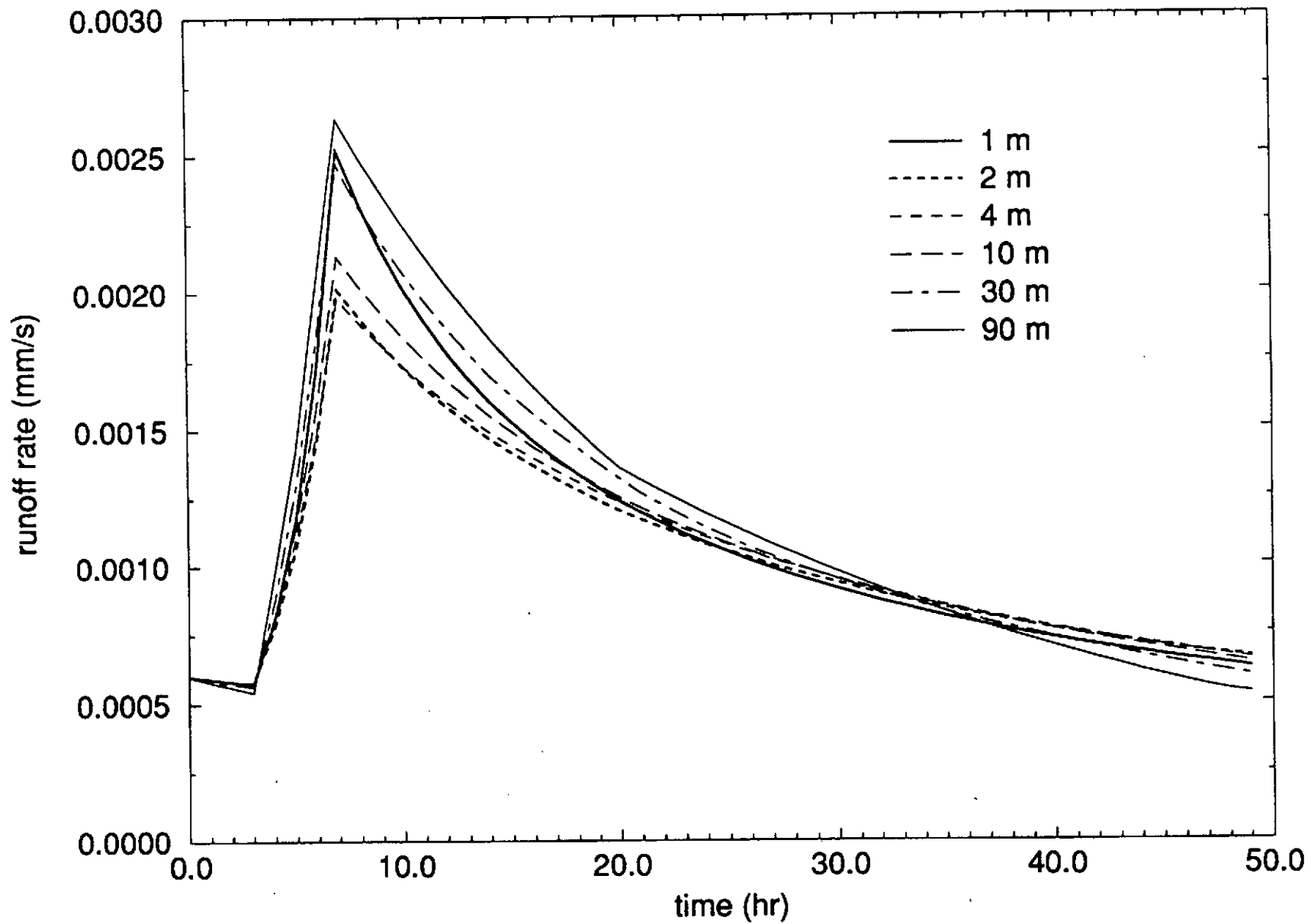
rainfall rate: 5 mm/hr



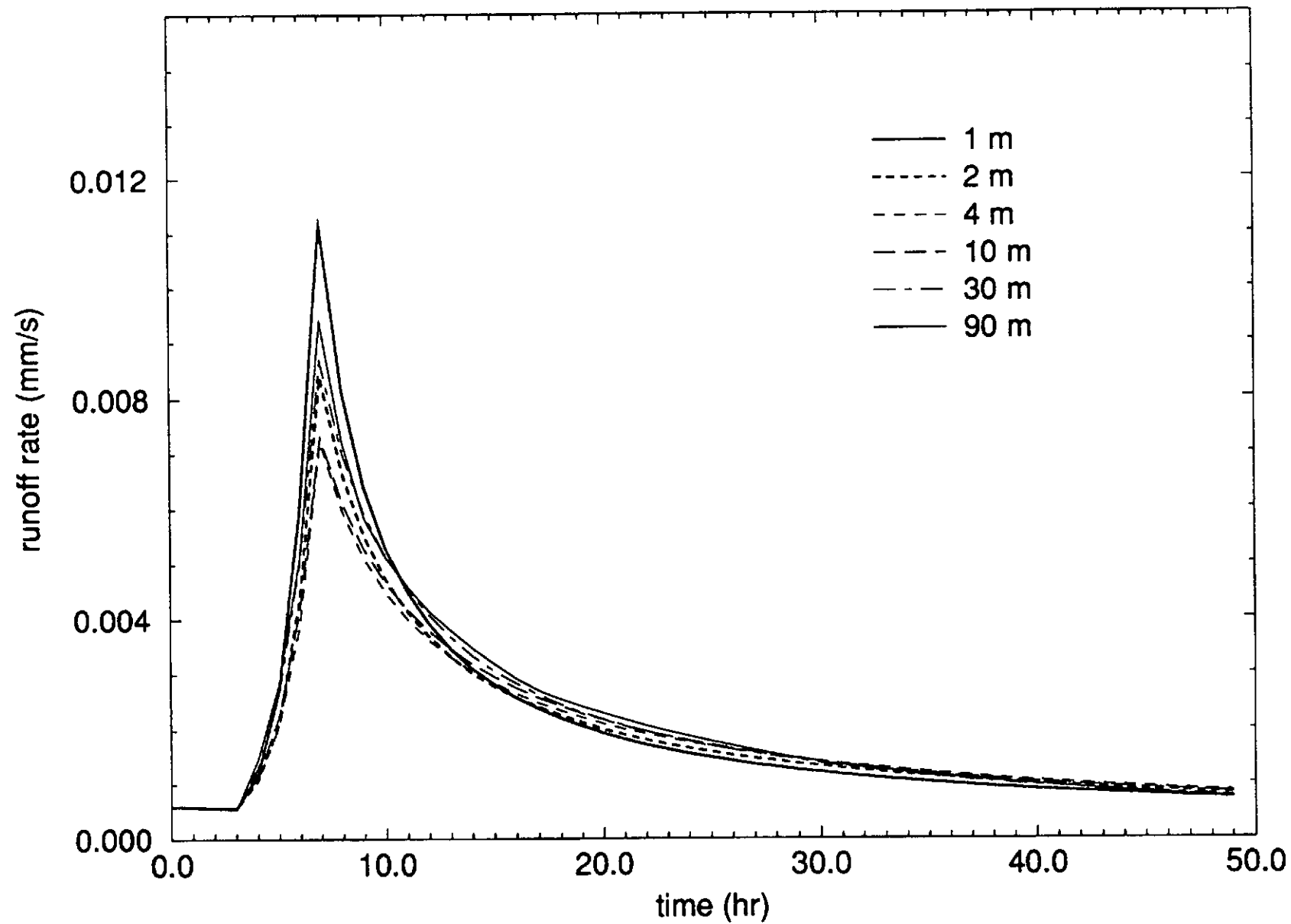
rainfall rate: 20 mm/hr

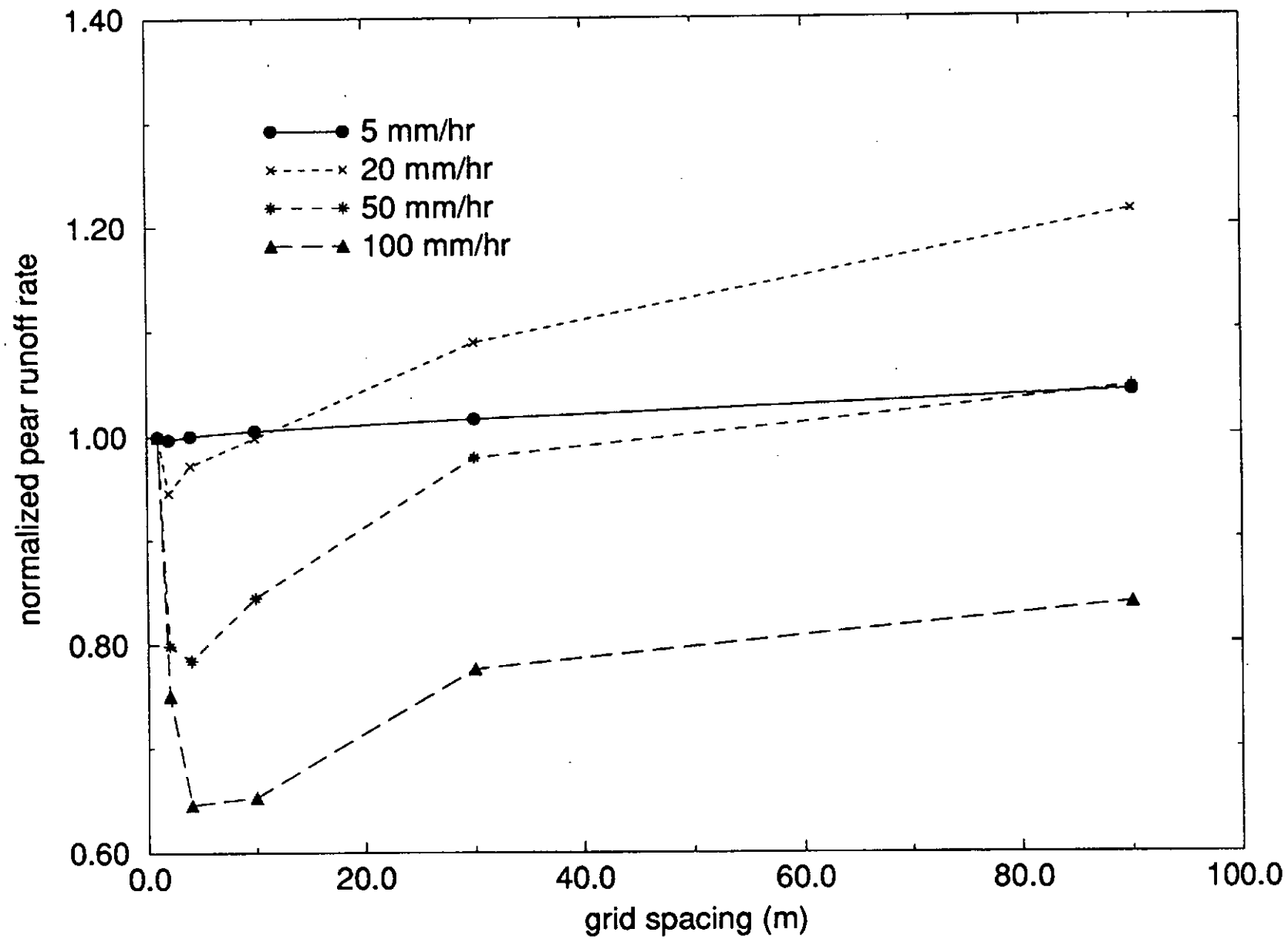


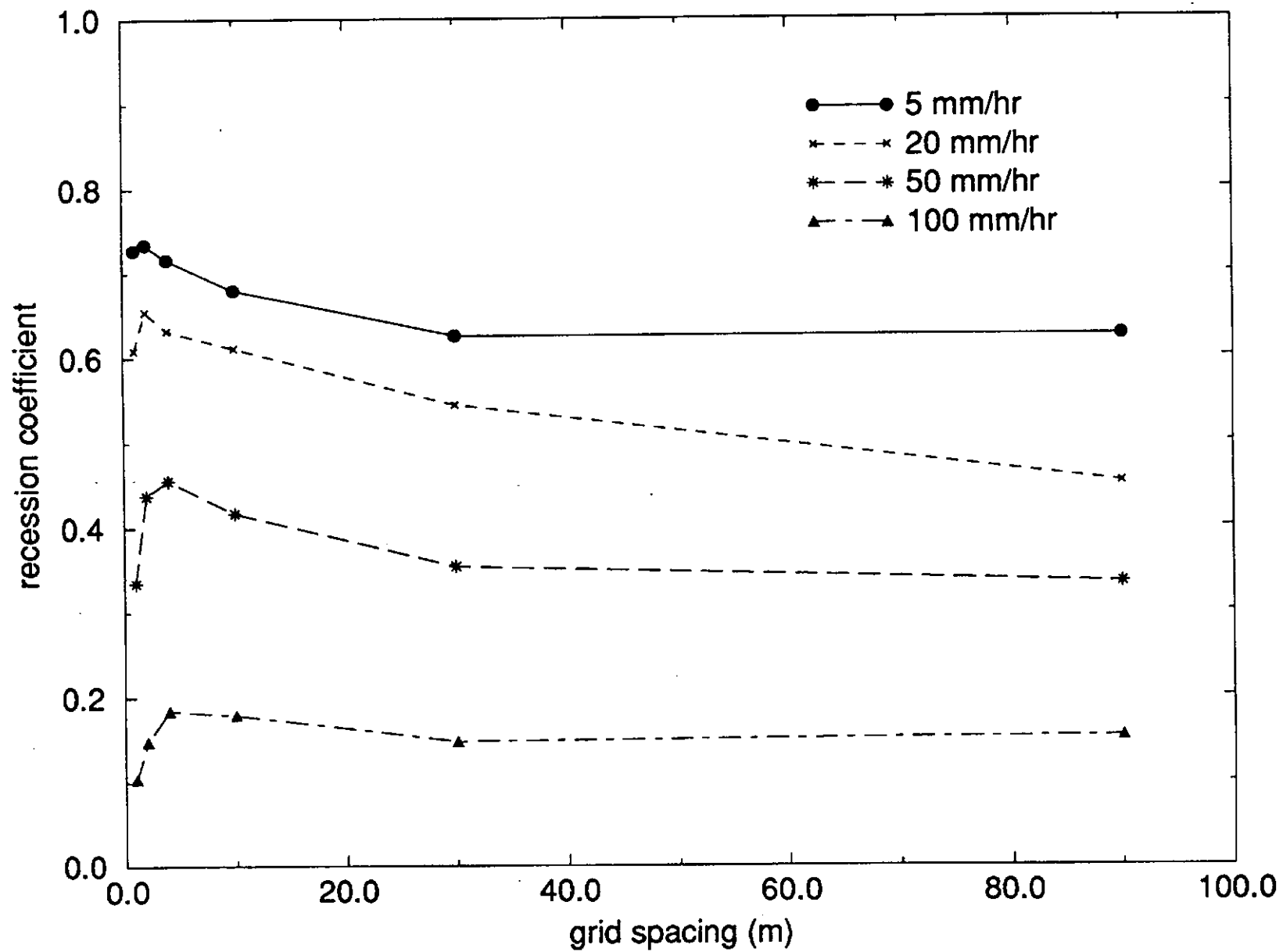
rainfall rate: 50 mm/hr



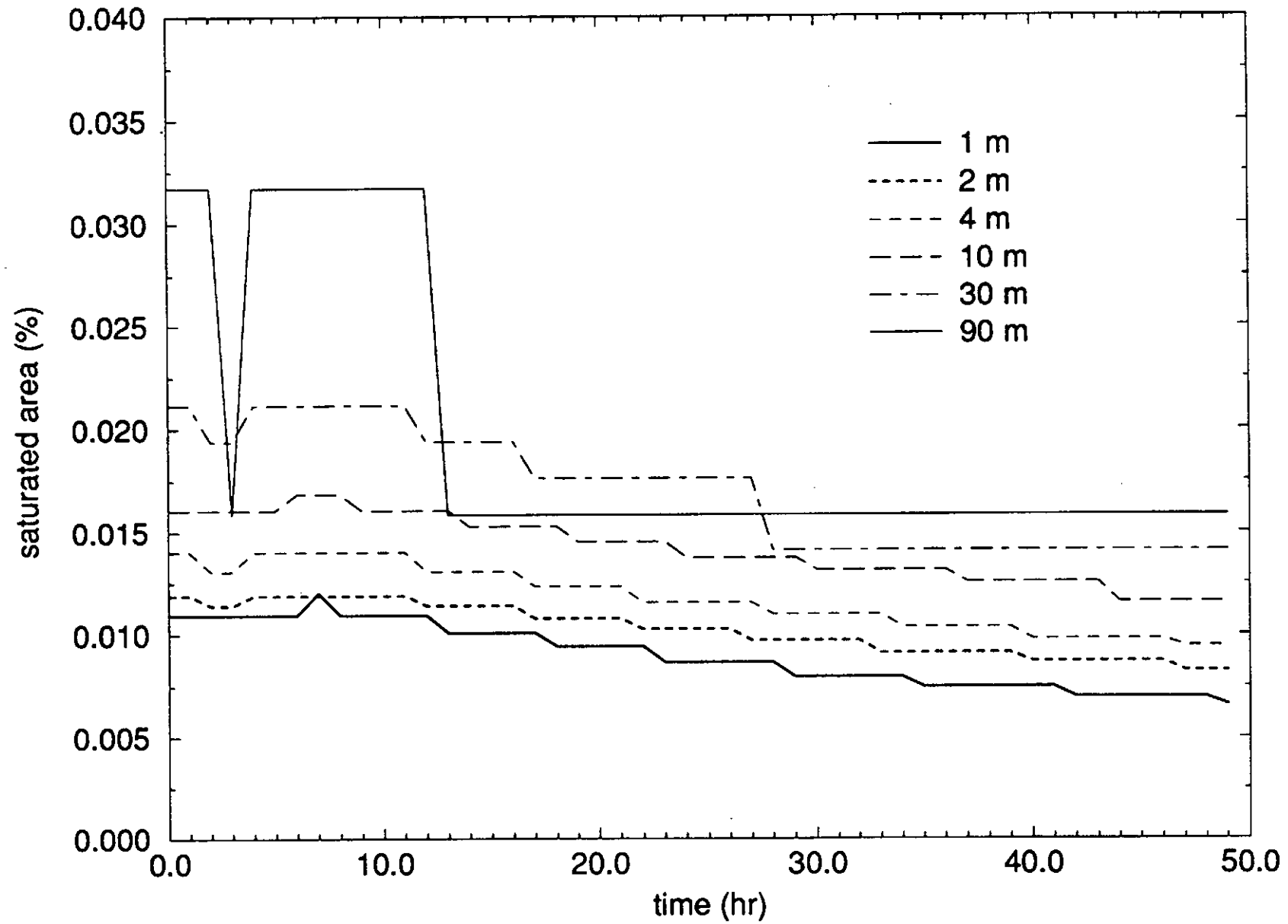
rainfall rate: 100 mm/hr



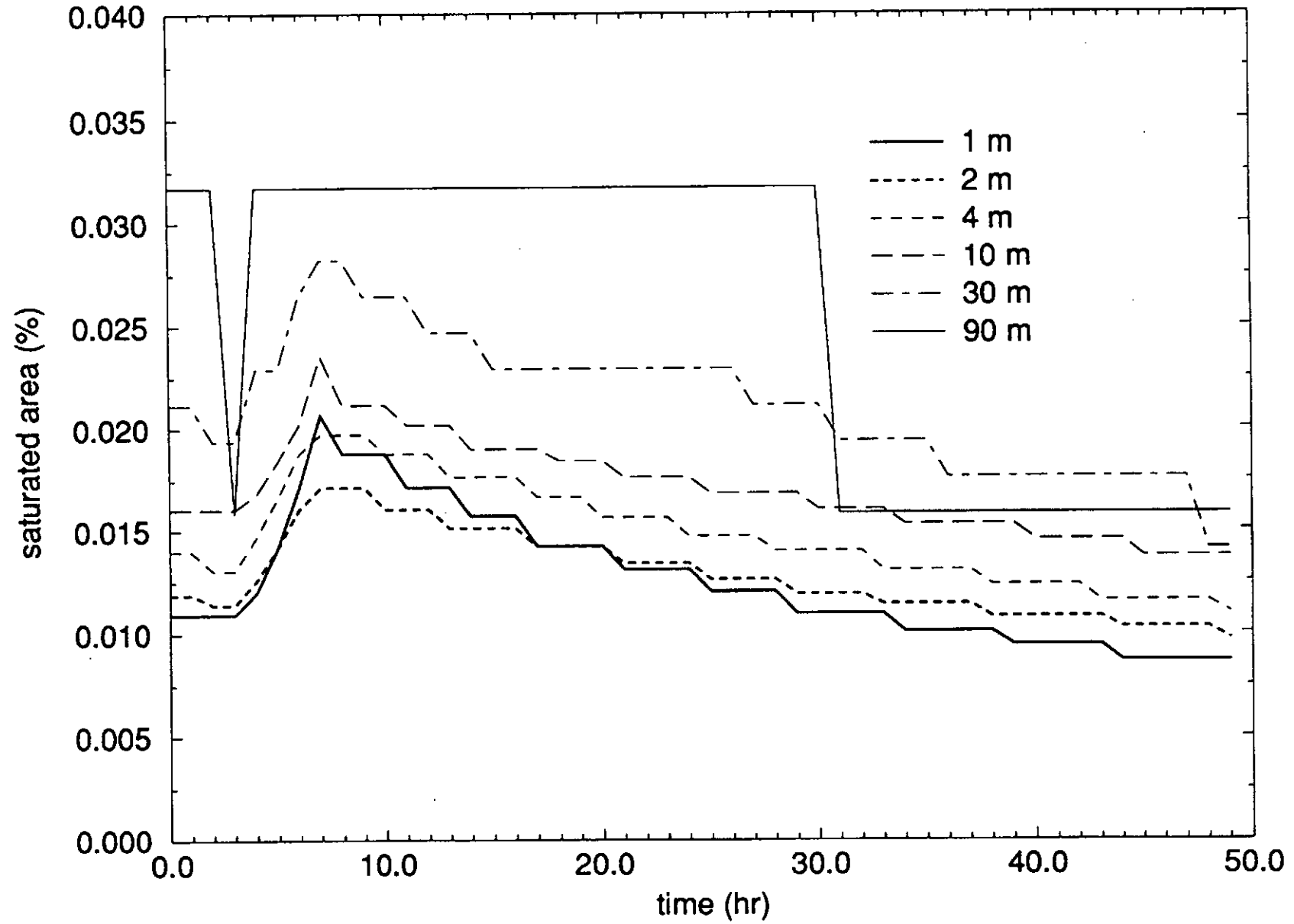




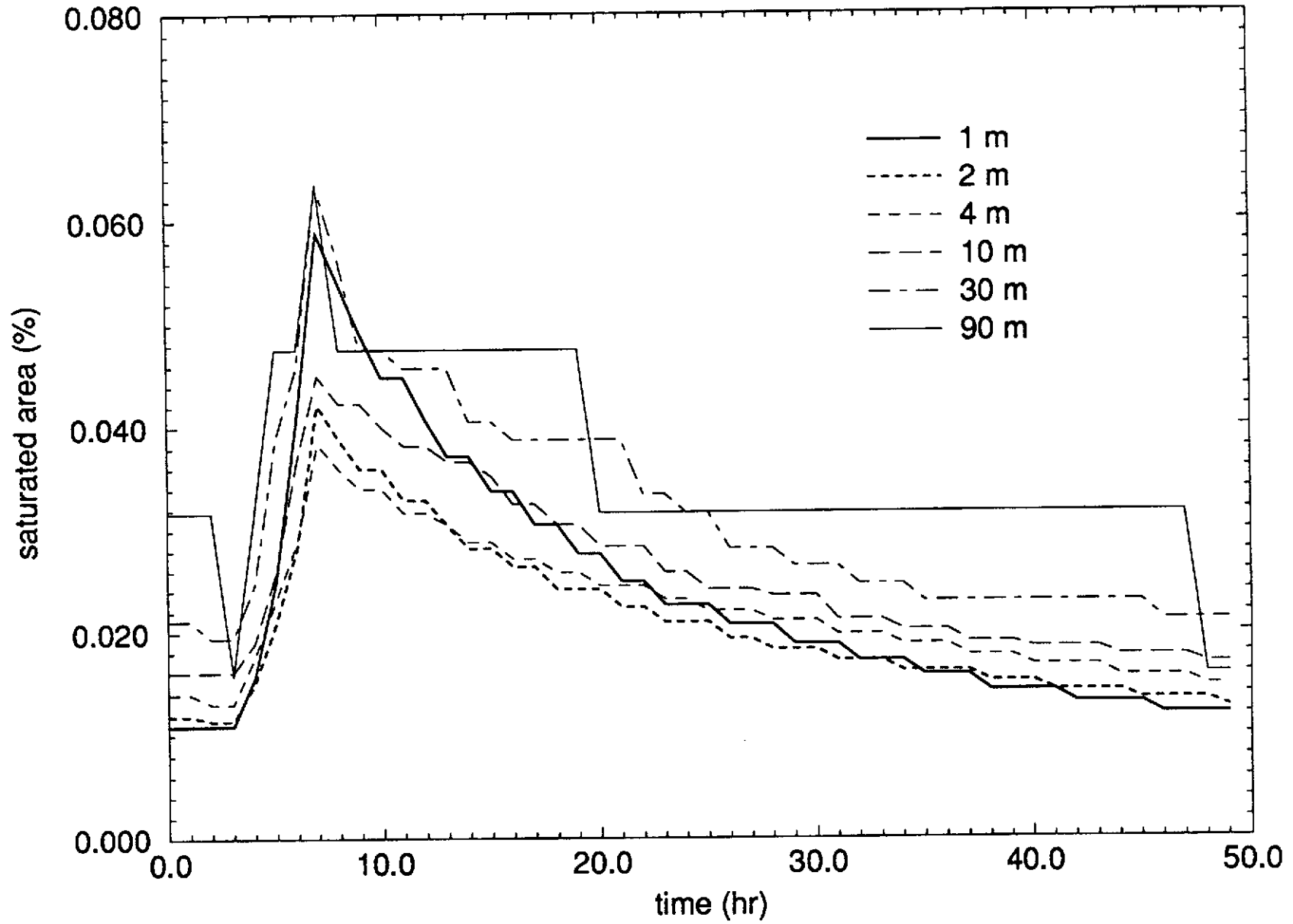
rainfall rate: 5 mm/hr



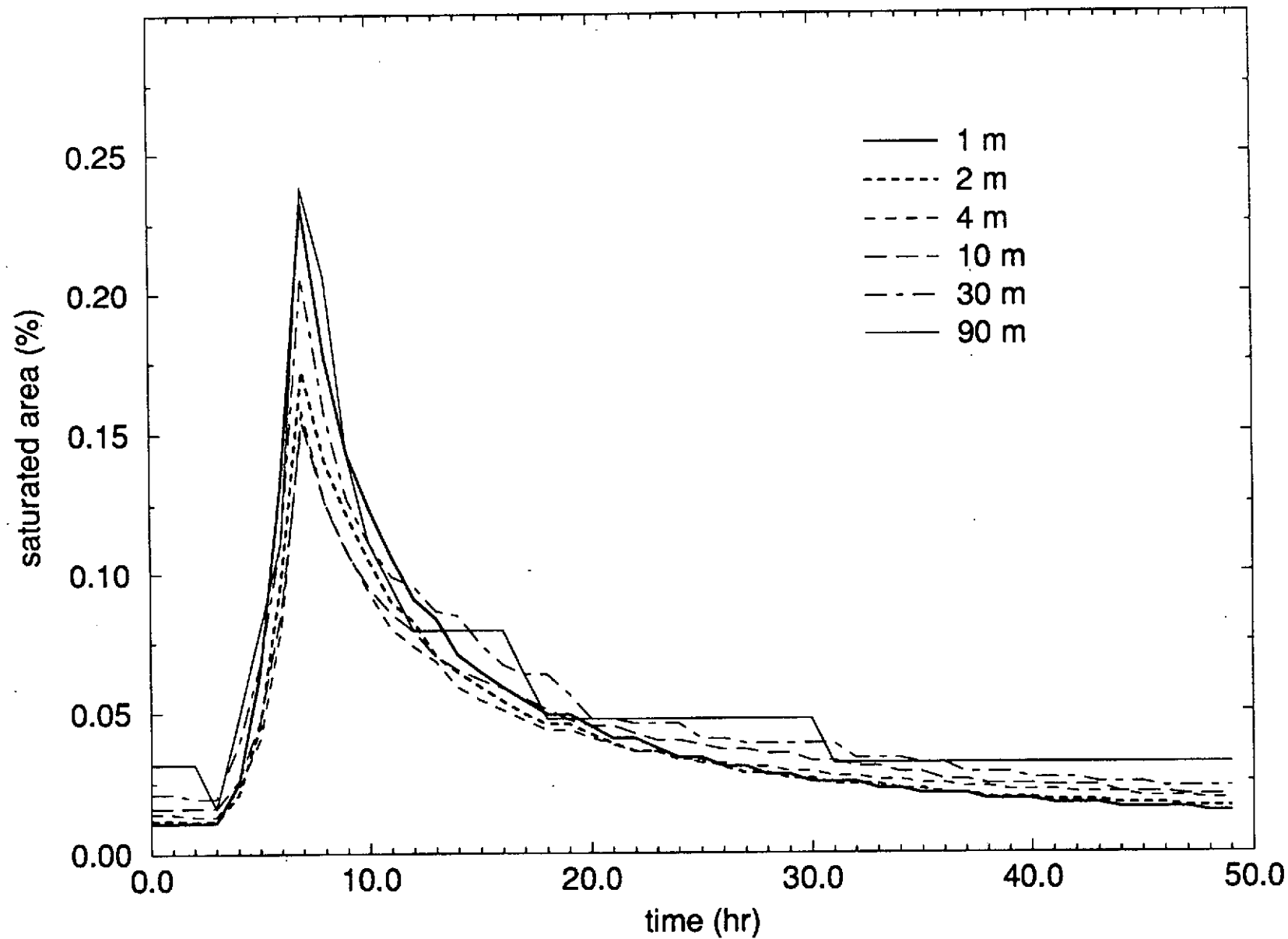
rainfall rate: 20 mm/hr

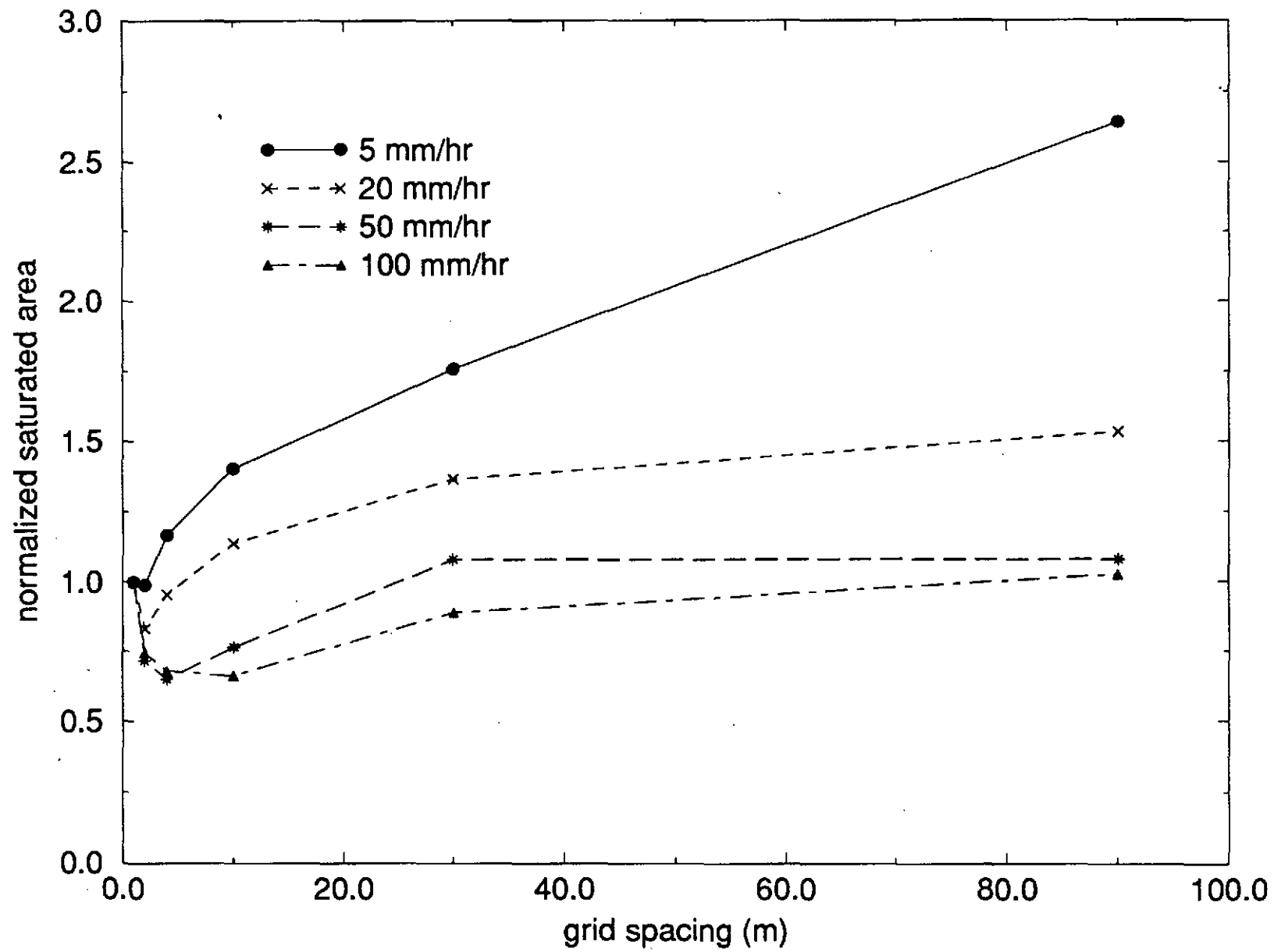


rainfall rate: 50 mm/hr



rainfall rate: 100 mm/hr





Appendix 3

to appear in GEOLOGY in 1992**Erosion thresholds and land surface morphology**

William E. Dietrich

Department of Geology and Geophysics, University of California, Berkeley, California 94720

Cathy J. Wilson

Australian Center for Catchment Hydrology, CSIRO, Canberra, A.C.T. 2601, Australia

David R. Montgomery

Department of Geological Sciences, University of Washington, Seattle, Washington, 98195

James McKean and Romy Bauer

Department of Geology and Geophysics, University of California, Berkeley, California 94720

ABSTRACT

We propose a graphical technique to analyze the entirety of landforms in a catchment to define quantitatively the spatial variation in the dominance of different erosion processes. High resolution digital elevation data of a 1.2 km² hilly area where the channel network had been mapped in the field were used in the digital terrain model, TOPOG, to test threshold theories for erosion. The land surface was divided into ~20 m² elements whose shapes were then classified as convergent, planar, or divergent. The entire landscape plotted on a graph of area per unit contour length against surface gradient shows each plan form plotting as separate fields. A simple steady-state hydrologic model was used to predict zones of saturation and areas of high pore pressure to mimic the extreme hydrologic events responsible for erosive instability of the land surface. The field observation that saturation overland flow is rare outside convergent zones provided a significant constraint on the hydrologic parameter in the model. This model was used in threshold

theories to predict areas of slope instability and areas subject to erosion by saturation overland flow, both of which can contribute to channel initiation. The proportion of convergent elements predicted to exceed the threshold varies greatly with relatively small changes in surface resistance, demonstrating a high sensitivity to land use such as cattle grazing. Overall, the landscape can be divided, using erosion threshold lines, into areas prone to channel instability due to runoff and stable areas where diffusive transport predominates.

INTRODUCTION

Although numerical models can create realistic-looking landscapes by generating ridge and valley topography (e.g., Ahnert, 1976; Kirkby, 1987; Howard, 1990; Willgoose et al., 1991), the three-dimensional form of real landscapes and the processes shaping them are, surprisingly, not well quantified. The recent development of digital terrain models, however, now permits quantitative analysis of actual landscapes and, thus, provides an opportunity to examine the relation between sediment transport processes and landscape form (e.g., Moore et al., 1988a, 1988b; Vertessey et al., 1990; Tarboton et al., 1991).

Here we propose a graphical technique for characterizing real landscapes using digital elevation data to examine the application of erosion theories. We focus on a landscape where previous studies (Montgomery and Dietrich, 1988, 1989, 1992; Montgomery, 1991) have indicated good evidence that threshold-based erosion models are appropriate. Field monitoring and mapping suggest that surface erosion leading to channel initiation occurs where a resistance to saturation overland flow (*sensu*, Dunne, 1980), seepage erosion (*sensu* Dunne, 1990), or shallow landsliding is exceeded. These processes predominate in valleys, whereas on ridges the shallow soil is currently transported primarily by biogenic activity such as burrowing by gophers (Black and Montgomery, 1991), a process that perhaps can be treated as largely slope dependent. Although our analysis focuses on current runoff and erosion processes, our results give insight into how erosion would vary with land use and climate change as well as what erosion laws appear appropriate for modeling long-term landscape evolution.

THRESHOLD THEORIES

Here we use three simple threshold equations to explore the relation between landform and current erosion processes. These equations predict a threshold condition for ground saturation, a threshold to landslide instability of the ground due to high pore pressures, and a threshold of erosion due to saturation overland flow. All three theories have been proposed in various forms by others. Here we write them in a form useful for analysis using a digital terrain model. Several simplifying assumptions are made to reduce the parameters to those that can be crudely estimated from field data and the proposed graphical analysis. These theories, however, are at the same general level of simplicity as those in most numerical models of landscape evolution. Specifically, we use a steady-state, runoff model that assumes that runoff occurs as subsurface flow parallel to the ground surface during significant hydrologic events and that saturated conductivity and transmissivity of the soil mantle are spatially constant. (Despite large differences in soil thickness between ridges and unchanneled valleys, the saturated conductivity and, consequently, the transmissivity are dominated by highly conductive near-surface soil [Wilson, 1988; Montgomery, 1991]). We propose that steady-state runoff for an extreme event will mimic the spatial variation in surface saturation and overland flow that would occur in natural transient storm events responsible for saturation overland flow erosion and landsliding. We also assume that the vegetation and soil properties controlling surface resistance to erosion are spatially constant.

For steady-state, shallow subsurface runoff parallel to the ground surface, the ground will be saturated if the precipitation (minus evaporation and deeper drainage), q , times the area of the upslope catchment, a , equals or exceeds the maximum flux the surface layer can conduct, computed from the product of transmissivity, T , surface slope, M , and unit length of the contour across which the catchment is draining, b (O'Loughlin, 1986). Because of the steep slopes in the study area, M is calculated as the more physically correct sine of the ground surface inclination, θ , rather than $\tan \theta$, as used by O'Loughlin (1986). The threshold of ground saturation can be expressed as

$$\frac{a}{b} \geq \frac{T}{q} M. \quad (1)$$

This simple hydrologic model has been used with good success to predict saturated zones and runoff response in the computer model TOPOG by O'Loughlin (1986) and by Moore et al. (1988a,1988b). It is essentially the same model that underlies the widely used TOPMODEL by Beven and Kirkby (1979).

All parts of the landscape where the area per unit contour length, a/b , equals or exceeds the term on the right hand side of equation 1 will be saturated. Note that if measured values from a landscape of a/b are plotted against M , then equation 1 will be a straight line with a slope given by the hydrologic parameters T/q , and all points above this line will be saturated. This observation suggests that a useful analysis of digital elevation data is to divide the land surface into discrete small catchments for which the physical attributes a/b and M can be determined and plotted on such a graph. Other threshold criteria can be expressed as functions of these two physical characteristics.

A coupled hydrologic and slope stability model proposed by Dietrich et al. (1986) and subsequently modified and tested by Montgomery and Dietrich (1989) can be written as:

$$\frac{a}{b} \geq 2 \left(1 - \frac{\tan \theta}{\tan \Phi} \right) \frac{T}{q} M. \quad (2)$$

Slope instability occurs where a/b equals or exceeds the term on the right hand side which varies with the ratio of ground-surface, $\tan \theta$, to angle of internal friction, $\tan \phi$. It should be noted that the hydrologic component of equation 2 is the same model as that which leads to equation 1 and that equation 2 uses a form of the infinite slope model that ignores strength contribution due to cohesion, i.e. at failure $\tan \theta = [(\rho_s - \rho_w m) / \rho_s] \tan \phi$, where ρ_s and ρ_w are the soil and water bulk densities and m is the proportion of the soil that is saturated. Field data suggests $(\rho_s - \rho_w) / \rho_s$ is ~ 0.5 . The hydrologic model is hydrostatic; hence, excessive pore pressures are not predicted and all slopes less than $0.5 \tan \phi$ are stable even if saturated.

Several authors have suggested that channel initiation by overland flow can be estimated by assuming that incision occurs where some critical boundary shear stress, τ_c , or some other

measure of resistance is exceeded (e.g. Horton, 1945; Schaefer, 1979; Moore et al., 1988b; Vertessey et al., 1990; Montgomery, 1991). In the steady-state model used here, saturation overland flow discharge is simply equal to $qa - TMb$, that is, water which can not be carried as shallow subsurface flow must travel overland. This equation can be solved for the discharge which attains sufficient depth for a given slope to produce a boundary shear stress equal to the critical value for the surface. Letting $qa - TMb = udb$, $\tau_c = \rho_w g d M$, $u = (2gdM)^{0.5} (f)^{-0.5}$, and $f = Kv/ud$, the following threshold of erosion equation can be derived in the desired form :

$$\frac{a}{b} \geq \frac{\alpha}{qM^2} + \frac{T}{q} M . \quad (3)$$

Here $\alpha = 2 \times 10^{-4} \tau_c^3 K^{-1}$ and τ_c is the critical boundary shear stress, K is the roughness intercept for the inverse relation between friction factor, f , and Reynolds number (velocity, u , times depth, d , divided by the kinematic viscosity, ν) that typifies laminar-like flow in grasslands (Dunne and Dietrich, 1980; Wilson, 1988; see review in Reid, 1989), g is the gravitational acceleration, and the numerical constant is for 10 °C water and has units of $(\text{cm} \cdot \text{sec})^5 / \text{gm}^3$.

DIGITAL TERRAIN MODEL ANALYSIS

We selected an area in the hilly grass and chaparral lands north of San Francisco where extensive mapping and hydrologic studies have already been conducted (Wilson and Dietrich, 1987; Montgomery and Dietrich, 1988, 1989; Black and Montgomery, 1991; Montgomery, 1991). These studies have shown that saturation overland flow is common in the lower gradient valleys, and most of the larger debris flow scars originate at channel heads. Digital elevation data were obtained at a density of about every 10 m for the 1.21 km² catchment from stereo digitization of low-level black and white aerial photographs using several mapped ground features to control the registration of digital coordinates. Taking advantage of the clear ground visibility, we selected data points to capture topographic change rather than to follow a regular grid. The digital elevation model component of TOPOG (O'Loughlin, 1986) was then used to construct digital surfaces. A second program in TOPOG divides the surface by drawing the equivalent of flow lines across the

contours from valley bottoms to divides at a user-specified interval (see O'Loughlin, 1986, for examples). The program draws flow lines starting at low elevations and projects upslope, so contour length separating flow lines tend to narrow on topographically divergent slopes.

Individual elements defined by a pair of contour lines on the upslope and downslope sides of the element and a pair of streamlines on the lateral boundaries (Fig. 1) are thus created.

For each element, the total contributing area, a , can be calculated and the ratio a/b determined from the bottom contour length of the element. Local slope between the two contour lines making up the element is also determined. Each element shape was classified as convergent, planar, or divergent according to the difference in length of the upslope, b_1 , and downslope contour length, b_2 , of the element, i.e., whether the ratio $(b_2 - b_1)/(b_2 + b_1)$ exceeded a set percentage change. This percentage is somewhat arbitrary. We chose the smallest values estimated to be relatively free of artifacts of the model (< -0.10 is convergent, > 0.10 is divergent, otherwise planar). These values clearly delineated the convergent valley axes in the landscape (Figure 1). In addition we used detailed field mapping of the current extent of the channel network to classify those elements (always convergent) that contained a channel.

Figure 2 shows the data field for each element type as a function of specific catchment (a/b) and local slope ($\tan \theta$) for the case of 5 m contour interval and 20 m interval between flow lines. For a given slope, the channel elements drain the largest specific catchment whereas the divergent elements drain the smallest. There is very little overlap between divergent and convergent element data fields and essentially none between divergent and channel elements. These differences are much larger than that which might be created by the definition of element types. Comparison of the data fields for different contour intervals and flow-line spacing shows that there are some artifacts in Figure 2. The apparent log-linear line of data in the divergent elements are a portion of the triangular-shaped elements created at divides by diverging flow lines. They have no physical relation to each other, and, while they are purely an artifact of the analysis, they still describe aspects of the divergent topography and so were retained. For planar elements, the minimum size of the elements varies with slope as controlled by the contour spacing (5 m in this case), hence a/b

(minimum) = $5/\tan \theta$, and no points plot below this value in Figure 2. Reducing the contour spacing and the flow line spacing, however, had negligible effect on the general distribution of the data. Furthermore, we found that a grid-based digital terrain model developed by one of us (Bauer) also produced very similar results.

LANDFORM AND PROCESS THRESHOLDS

In order to apply the threshold equations 1-3, the parameters controlling their predictions must be estimated. This problem is more constrained than may at first be apparent. We know from field work in this area during major runoff events (Wilson and Dietrich, 1987; Montgomery, 1991) that extensive saturation overland flow does not occur on divergent and planar slopes. We have seen exceptions, but they are of local extent only. This allows us to vary the hydrologic ratio, T/q , and note where the line of saturation crosses the various topographic elements (see thresholds box and then comparison with data in other boxes, Fig. 2). Note that T/q of 350 m clips just the top of the divergent and planar elements. Conversely, we would expect most of the channel elements to be saturated during an extreme event, and, as expected, the line with T/q of 350 m lies below most of the elements; halving this value adds few more channel elements but cuts deeply across the divergent element field. We have observed saturation overland flow extend up to nearly the divide in this area in relatively common storms; hence, it is realistic to predict that nearly all of the convergent elements will saturate in a major storm. On the basis of previous studies (Wilson, 1988), the transmissivity is largely controlled at saturation by the high conductivity of the near-surface soils, apparently differing little between nose and hollow. We estimate this value to be $17 \text{ m}^2/\text{d}$, which indicates that for a T/q of 350 m the q is equal to 5 cm/d of precipitation or runoff. According to the analytical procedure of Iida (1984), it would take about 9 d for a 59-m-long planar slope to reach steady state with this estimated transmissivity and rainfall; a storm of about this magnitude (45 cm) and duration occurred here in 1986 (Wilson, 1988).

With T/q defined, the only remaining parameter in equation 2 is the angle of internal friction; previous studies indicate this value may commonly be as high as 45° (Reneau et al.,

1984). This stability analysis ignores the contribution of apparent cohesion from root strength. In Figure 2, the slope stability threshold line is plotted for values of ϕ equal to 35° and 45° . The number of elements predicted to fail is greatly increased with the diminished friction angle, including many divergent elements. This is inconsistent with field observations in which shallow soil landslides are mostly in convergent zones. Decreasing T/q tends to overpredict the number of planar elements in which failure might be expected. Preliminary field mapping indicates that all but five of the 39 shallow landslide scars currently visible in the study area lie above the predicted threshold line for a T/q of 350 m and $\phi = 40^\circ$. Hence, the position of the slope stability curve is reasonably well-defined. This curve lies on the outer edge of the data fields, suggesting that this stability criterion imposes a physical limit on hillslope morphology, as traditionally argued from simpler analyses (i.e., Strahler, 1950). Consistent with field observations, the steeper channel and convergent elements lie above the threshold line of slope stability.

The saturation overland flow erosion threshold given in equation 3 requires estimates of K , τ_c , and q for a specified T/q and water temperature (which sets the value of ν). Measurements at times of significant overland flow at a nearby grassland site document that K is about 10,000 for well-vegetated surfaces (Wilson, 1988, p.109) and that shear stresses in excess of 200 dyne/cm² generated by this flow did not cause measurable incision into the vegetated areas. High runoff events, however, have caused scour in the unvegetated tips of the channel networks. Reid (1989), in a thorough review of critical shear stress values, showed that τ_c must exceed 1000 dyne/cm² to incise a well-vegetated mat, whereas values of 250 to 500 dyne/cm² are sufficient to incise the underlying soils. If τ_c were 1000 dyne/cm², for a threshold line defined by equation 3 to separate channeled from unchanneled elements, q would have to be ~ 1.5 m/d, clearly an impossibility. As argued by Reid (1989), channel initiation in grasslands is likely to occur where local barren areas caused by fire, trampling, or other effects reduce the critical shear stress to the underlying value of the soil.

Figure 2 shows the position of threshold lines for a τ_c of 160 dyne/cm² and 320 dyne/cm² for q of 5 cm/d (appropriate for $T/q = 350$ m and $T = 17.5$ m²/d). Given the observed roughness

value, τ_c and q are constrained by the threshold relation required to separate channeled from unchanneled elements. The critical shear stress can not be significantly different from 160 to 320 dyne/cm² without requiring either too great or too small a precipitation rate. It is worth noting that, as indicated in equation 3, a doubling of critical boundary shear stress is equivalent to decreasing precipitation or K by a factor of 8. Such a doubling greatly alters the location of this erosion threshold line and raises questions concerning the worth of trying to measure a parameter in the field whose value is so difficult to estimate but that so greatly affects the pattern of channelization. This analysis also shows, however, how land use practices or climate change that only modestly alters surface resistance (τ_c) could lead to a great expansion of the channel network into previously unchanneled elements. Such an expansion due to the introduction of cattle grazing and presumed reduction in surface resistance has been proposed for this area by Montgomery and Dietrich (1989) and Montgomery (1991). The inverse dependency of the erosion threshold on precipitation is also consistent with the proposal by Reneau et al. (1986) and Montgomery (1991) that drying and warming of this area from the Pleistocene into the Holocene caused channel heads to retreat downslope.

In Figure 3, stability fields generated by the combination of equations 1 through 3 are labeled with the dominant hydrologic and erosion processes. Simple field observations constrain the threshold of saturation and slope stability lines and lead to the interpretation that a significant proportion of the landscape, nearly all the divergent elements, most of the planar, and some of the convergent ones, are presently stable or resistant to surface erosion due to runoff. In this region below the erosion threshold lines (shaded region in Fig. 3), surface transport is currently dominated by the slope-driven (diffusive) processes of soil creep, rain splash, and biogenic disturbance. The area labeled "SOF (saturation overland flow) without erosion " mostly includes elements lying in unchanneled valleys currently collecting colluvium (but which in the long term experience periodic erosion apparently driven by climatic change [Reneau et al., 1986]). Hence, this graph shows a new way to analyze the entirety of landscapes to define quantitatively the spatial variation in the dominance of different erosion processes in a catchment. An analysis of this kind

should also be a useful tool in constructing sediment budgets for catchments, when the spatial distribution of dominant transport processes must be ascertained (i.e., Dietrich and Dunne, 1978; Dietrich et al., 1982; Reid, 1989).

CONCLUSION

The plotting of discrete elements of landscapes separated by planform on a graph of the two topographic variables that control runoff and erosion (area per unit contour width and surface gradient) provides a powerful means to evaluate hydrologic and erosional hypotheses about real landscapes. This analysis and the parallel study reported by Montgomery and Dietrich (1992) on the relation between position of the channel head and landscape scale add considerable support to the Horton hypothesis of a threshold control on surface instability leading to channel development (Horton, 1945). The simple, steady-state, hydrologic models employed here could be made more realistic by using a transient model, but this introduces more parameters, and at least for the problem of examining the relationships between form and erosion thresholds, it is not clear that the transient model is essential to the outcome. The threshold theories are similar to those used to model landscape evolution; the analysis performed here suggests a procedure to evaluate transport laws used in numerical models. The plotting of threshold lines on a data field of a/b vs. M is an instructive procedure for examining the possible effects of land use and climatic change.

REFERENCES CITED

- Ahnert, F., 1976, Brief description of a comprehensive three-dimensional process-response model of landform development: *Zeitschrift fur Geomorphologie, Supplement Band 25*, p. 25-49.
- Beven, K., and Kirkby, M.J., 1979, A physically based variable contributing area model of basin hydrology: *Hydrological Sciences Bulletin*, v. 24, p. 43-69.
- Black, T. and Montgomery, D.R., 1991, Sediment transport by burrowing mammals, Marin County, California: *Earth Surface Processes and Landforms*, v. 16, p. 163-172.
- Dietrich, W.E., and Dunne, T., 1978, Sediment budget for a small catchment in mountainous terrain: *Zeitschrift fur Geomorphologie Supplement Band*, v. 29, p. 191-206.
- Dietrich, W.E., Dunne T., Humphrey, N.F., and Reid, L.M., 1982, Construction of sediment budgets for drainage basins, *in* Swanson, F.J., et al., eds., *Sediment budgets and routing in forested drainage basins: USDA Forest Service General Technical Report PNW-141*, Pacific Northwest Forest and Range Experiment Station, Portland, Oregon, p. 5-23.
- Dietrich, W.E., Wilson, C.J., and Reneau, S.L., 1986, Hollows, colluvium, and landslides in soil-mantled landscapes, *in* Abrahams, A.D., ed., *Hillslope processes: London, Allen and Unwin*, p. 361-388.
- Dunne, T., 1980, Formation and controls of channel networks: *Progress in Physical Geography*, v. 4, p.211-239.
- , 1990, Hydrology, mechanics and geomorphic implications of erosion by subsurface flow, *in* Higgins, C.G., and Coates, D.R., eds., *Groundwater geomorphology: The role of subsurface water in Earth-surface processes and landforms: Geological Society of America Special Paper 252*, p. 1-28.
- Dunne, T. and Dietrich, W.E., 1980, Experimental study of Horton overland flow on tropical hillslopes; 1. Soil conditions, infiltration and frequency of runoff; 2. Hydraulic characteristics and hillslope hydrographs: *Zeitschrift fur Geomorphologie, Supplement Band 35*, p.40-80.

- Howard, A., 1990, Prospects for simulation modelling of valley networks on Mars:
Planetary Geology and Geophysics Program Report , NASA TM 4210, p. 348-350.
- Horton, R.E., 1945, Erosional development of streams and their drainage basins; hydrophysical approach to quantitative morphology, *Geological Society of America Bulletin*, v. 56, p. 275-370.
- Iida, T., 1984, A hydrological method of estimation of the topographic effect on the saturated throughflow: *Japanese Geomorphological Union Transactions*, v. 5, p. 1-12.
- Kirkby, M.J., 1987, Modelling some influences of soil erosion, landslides and valley gradient on drainage density and hollow development, *in* Ahnert, F., ed., *Geomorphological models*, Catena, Supplement 10, p. 1-11.
- Montgomery, D.R., 1991, Channel initiation and landscape evolution [Ph.D. thesis]:
Berkeley, University of California, 421p.
- Montgomery, D.R., and Dietrich, W.E., 1988, Where do channels begin?: *Nature*, v. 336, p. 232-234.
- , 1989, Source areas, drainage density and channel initiation: *Water Resources Research*, v. 25, p. 1907-1918.
- , 1992, Channel initiation and the problem of landscape scale: *Science*, v. 255, p. 826-830.
- Moore, I.D., O'Loughlin, E.M., and Burch, G.J., 1988a, A contour-based topographic model for hydrological and ecological applications: *Earth Surface Processes and Landforms*, v. 13, p. 305-320.
- Moore, I.D. , Burch, G.J., and Mackenzie, D.H., 1988b, Topographic effects on the distribution of surface soil water and location of ephemeral gullies: *American Society of Agricultural Engineers Transactions*, v. 31, p. 1098-1107.
- O'Loughlin, E.M., 1986, Prediction of surface saturation zones in natural catchments by topographic analysis: *Water Resources Research*, v. 22, p. 794-804.

- Reid, L.M., 1989, Channel incision by surface runoff in grassland catchments [Ph.D. thesis]: Seattle, University of Washington, 135 p.
- Reneau, S.L., Dietrich, W.E., Wilson, C.J., and Rogers, J.D., 1984, Colluvial deposits and associated landslides in the northern S.F. Bay Area, California, USA: Proceedings of the Fourth International Symposium on Landslides, Toronto, 1984, pp. 425-430.
- Reneau, S.L., Dietrich, W.E., Dorn, R.I., Berger, C.R., and Rubin, M., 1986, Geomorphic and paleoclimatic implications of latest Pleistocene radiocarbon dates from colluvium-mantled hollows, California: *Geology*, v. 14, p. 655-661.
- Schaefer, M.G., 1979, The zero order watershed [Ph.D. dissertation]: Rolla, University of Missouri, 69 p.
- Strahler, A.N., 1950, Equilibrium theory of erosional slopes approached by frequency distribution analysis, *American Journal of Science*, v. 248, p. 673-96, 800-814.
- Tarboton, D.G., Bras, R.L., and Rodriguez-Iturbe, I., 1991, On the extraction of channel networks from digital elevation data: *Hydrological Processes*, v. 5, p. 81-100.
- Vertessy, R.A., Wilson, C.J., Silburn, D.M., Connolly, R.D., and Ciesiolka, C.A., 1990, Predicting erosion hazard areas using digital terrain analysis: *International Association of Hydrological Sciences*, v. 192, p. 298-308.
- Wilson, C.J., 1988, Runoff and pore pressure development in hollows [Ph.D. dissertation]: Berkeley, University of California, 284 p.
- Willgoose, G.R., Bras, R.L., and Rodriguez-Iturbe, I., 1991, A coupled channel network growth and hillslope evolution model: *Water Resources Research*, v. 27, p. 1671-1702.
- Wilson, C.J., and Dietrich, W.E., 1987, The contribution of bedrock groundwater flow to storm runoff and high pore pressure development in hollows: *International Association of Hydrological Sciences*, v. 165, p. 49-59.

ACKNOWLEDGMENTS

Supported by National Science Foundation grant EAR-8917467, by Washington State Department of Natural Resources grant TFW-FY92-010, and by the Australian Center for Catchment

Hydrology (for Wilson). We thank the USDA Forest Service, Pacific Southwest Region, engineering staff for providing access to an analytical stereo plotter for generating the digital elevation data. Rob Reiss played a crucial role in running TOPOG and generating plots. Keith Loague and Bob Anderson provided useful reviews of the manuscript.

FIGURE CAPTIONS

Figure 1. Planform analysis of a 1.2 km^2 catchment in Marin County, California, studied by Montgomery and Dietrich (1989, 1992). Topographic contours and flow lines were generated by TOPOG (O'Loughlin, 1986), which in this case gives contour interval of 5 m and flow lines ~20 m apart. Element types are divergent (white), planar (shaded), and convergent (black).

Figure 2. Plot of element topographic properties and comparison of threshold lines with data fields. Channeled elements were identified on the basis of field observations. Solid line represents threshold of saturation consistent with field data.

Figure 3. Definition of stability fields using threshold lines for case of $T/q = 350 \text{ m}$, $\phi = 35^\circ$, $K = 10,000$, critical shear stress = 160 dyne/cm^2 and $q = 0.05 \text{ m/d}$. SOF is saturation overland flow and SOF erosion means erosion by saturation overland flow. Shaded region is below the threshold of erosion by either saturation overland flow or landsliding

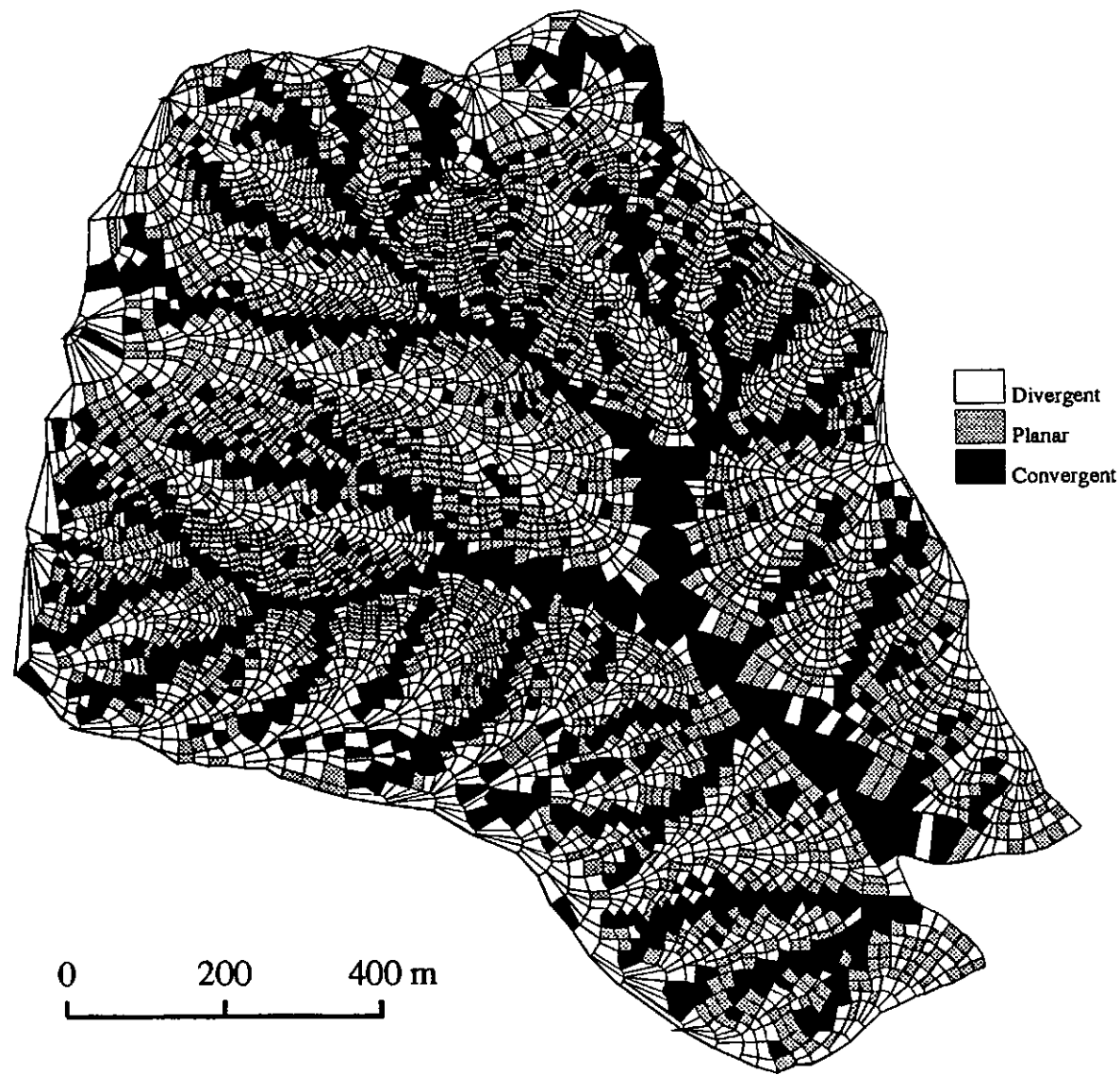


Figure 1.

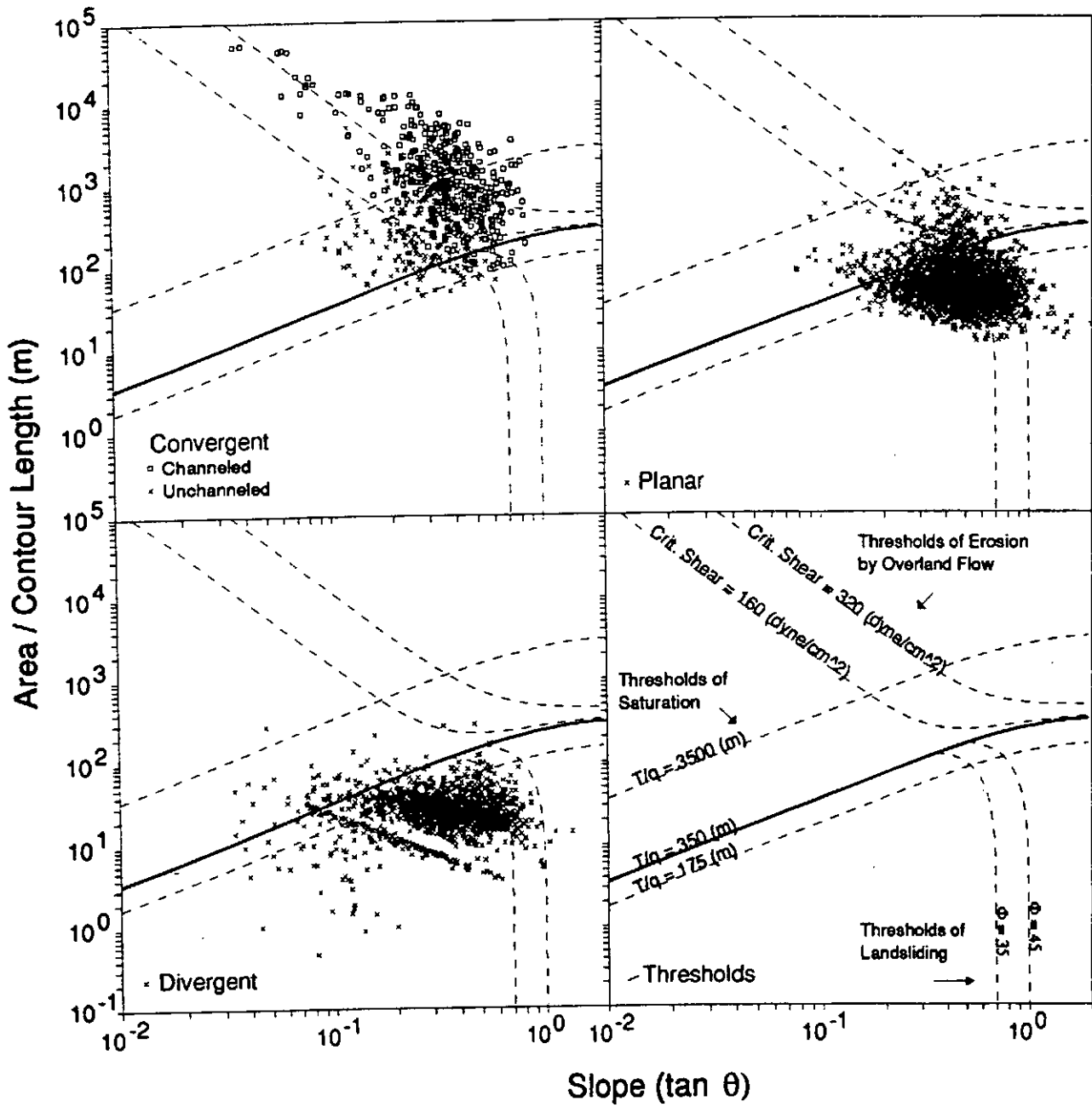


Figure 2.

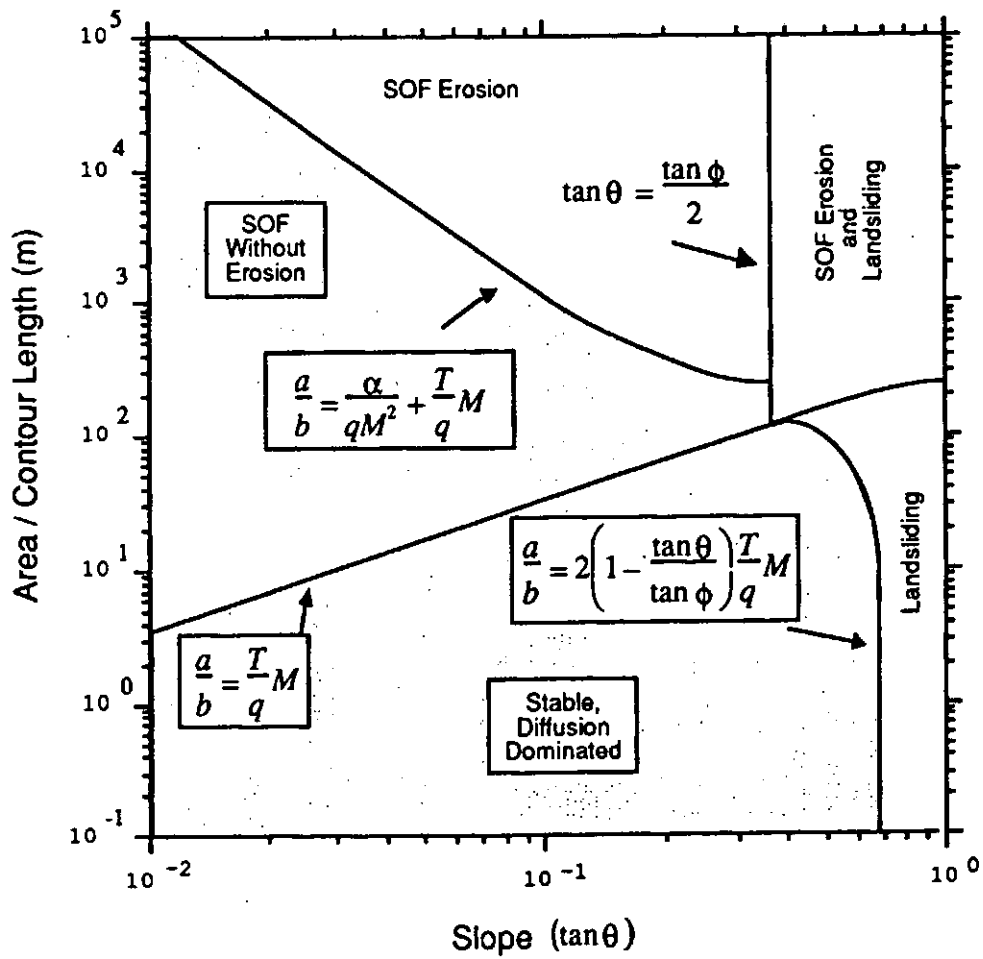


Figure 3.

Appendix 4

A Digital Terrain Model for Predicting
Debris Flow Source Areas and Run Out Paths

David R. Montgomery
Dept. of Geological Sciences and Quaternary Research Center
University of Washington
Seattle, WA 98195

and

William E. Dietrich
Dept. of Geology and Geophysics
University of California
Berkeley, California 94720

For submission to Water Resources Research

Abstract

A digital terrain model for predicting the potential for shallow debris flow initiation throughout a catchment is developed by coupling near-surface throughflow and slope stability models. The hydrologic model determines the proportion of the soil thickness that is saturated in response to a steady-state rainfall for topographic elements defined by the intersection of contours and flow tube boundaries. The slope stability component uses this relative soil saturation to analyze the stability of each topographic element for the case of cohesionless soils. Model sensitivity is examined with respect to the physical parameters incorporated in the model [soil thickness, conductivity, bulk density, and angle of internal friction, and simulated rainfall rate]. Simulations are performed for two study basins where detailed digital elevation data are available, one in Tennessee Valley in Marin County, California, and the other in a steep catchment along Mettman Ridge in the Coast Range near Coos Bay, Oregon. The pattern of relative debris flow initiation potential for each of these basins is consistent with the spatial patterns of observed debris flow scarps. Independent estimates of the steady-

state rainfall necessary to cause debris flows in these areas constrain model simulations that identify as unstable the locations of 87 and 92% of the observed debris flow scarps in the study catchments. Unfailed locations predicted to be unstable probably represent likely locations for future instability, but local hydrologic complexities not accounted for in the model preclude unique prediction of specific sites of debris flow initiation.

Introduction

Debris flows are an important sediment transport linkage between hillslopes and stream channels in steep, soil-mantled landscapes. In such terrain, infrequent debris flows are an important hillslope evolution process [e.g., Okunishi and Iida, 1983; Tsukamoto et al., 1982; Dietrich et al., 1986; Crozier et al., 1990], may control low-order channel morphology [e.g., Benda and Dunne, 1987], and have disastrous consequences where they interfere with human activities [e.g., Smith and Hart, 1982; Ellen and Wieczorek, 1988; Brabb and Harrod, 1989]. Accelerated sediment delivery to stream channels from increased debris flow frequency caused by land management also may impact channel morphology and adversely impact aquatic resources [c.f., Salo and Cundy, 1987]. Increased pressure to develop and intensively manage upland landscapes and concurrently minimize impacts on downstream facilities and ecosystems necessitate development of a method for objectively assessing potential debris flow source areas.

The episodic nature of debris flow occurrence makes it difficult to predict debris flow frequency and thus rates of sediment delivery from debris flow activity. Many workers, however, report that the majority of debris flows originate in areas of topographic convergence (see reviews in Reneau and Dietrich [1987], Smith [1988], and Montgomery and others [1991]). Several workers use qualitative topographic analyses to delineate potential debris flow source areas [e.g., Fowler, 1984; Smith, 1988; Montgomery et al., 1991]. More detailed, quantitative analyses may be employed for evaluation of potential instability at specific locations [e.g., Burroughs, 1985], but such techniques require labor-intensive field measurements. Consequently, there is a need for an objective, quantitative method for predicting areas of a landscape most likely to generate shallow slope instability leading to rapidly moving debris flows.

The development of digital terrain models offers opportunities to advance both the modelling of surficial processes and natural hazards assessments. A digital terrain model can rapidly calculate, for any point in a catchment, the two topographic attributes that dominate sediment transport, the contributing drainage area (a surrogate for the convergence of runoff) and the local slope. If the processes of interest can be related to drainage area, local slope, and physical parameters, such as soil properties, then a digital terrain model may be used to analyze spatial patterns of processes or sediment transport [see Dietrich et al., in press]. Several hydrologic models may be used to simulate runoff generation and relate relative soil saturation to contributing drainage areas [e.g., Beven and Kirkby, 1979; O'Loughlin, 1986; Moore et al., 1988]. Slope stability models are governed by the ground slope, physical properties of the soil or hillslope forming material, and the degree of soil saturation. Consequently, digital terrain models may be used to combine hydrologic models with models of slope stability to objectively predict portions of the landscape susceptible to slope failure under a variety of conditions. This paper presents a combined hydrologic and slope stability model for predicting areas susceptible to debris flow generation and tests the model against observed distributions of debris flows in two catchments in the western United States.

Model

Coupled models for the generation of soil saturation and slope instability are needed in order to predict the spatial distribution of potential debris flow source areas. Our approach combines the hydrologic and digital terrain model TOPOG [O'Loughlin, 1986] with the infinite-slope stability model [e.g., Selby, 1982]. Each of the components of this hybrid model involves assumptions that constrain this approach. The relative simplicity of each of these models, however, is attractive for the typical case where little is known about the spatial variability of the other important, naturally variable factors that affect both runoff generation and slope stability.

The hydrologic model assumes a steady-state rainfall and maps the spatial pattern of equilibrium soil moisture based on analysis of the upslope contributing areas, soil transmissivity, and local slope. Flow is modeled only through a shallow soil layer and flow in the deeper bedrock groundwater system is not considered. The steady-state assumption compromises the

ability of the model to predict instability in response to specific storms, but it does not influence estimates of relative susceptibility to failure. Flow through near-surface bedrock strongly influences the piezometric response, and thus, the stability of colluvial soils [e.g., Wilson and Dietrich, 1987; Montgomery, 1991; Montgomery et al., in prep.]. The discrete nature of bedrock fracture patterns, however, complicates inclusion of bedrock flow. Although the program may be modified in the future to accommodate both a dynamic rainfall signal and bedrock flow [Wilson, pers. comm.], the present model is appropriate for use in relative hazard assessments.

A brief review of TOPOG and its potential applications can be found in Vertessy and others [1990]. The model consists of three integrated programs. One generates a digital elevation model from a file of original location and elevation data. A second program discretizes the modeled land surface into a series of elements defined by contour lines on the upper and lower boundaries and flow lines defined orthogonal to contours. The program does this by projecting flow lines upslope along the shortest distance between adjacent contours at a spacing that maintains an average element size predetermined by the user (Figure 1). This routine has the effect of dividing a catchment into a series of flow tubes defined by adjacent flow lines, effectively reducing a complex two dimensional problem into a series of linked one dimensional problems. The final program simulates steady-state soil saturation resulting from shallow subsurface flow.

This final program calculates the ratio of the subsurface flux to the discharge that would occur at saturation for each element generated by the intersection of contour lines and flow lines. This dimensionless ratio, the wetness index (W) varies from 1.0 at saturation to 0 when dry (values of wetness greater than 1.0 are possible and represent saturation overland flow) and can be expressed as

$$W = \frac{\int q da}{b \sin\theta T} \quad (1)$$

where q is the effective steady-state rainfall or catchment discharge, b is the contour length across which the upslope catchment area (a) drains, θ is the slope of the ground surface and T is the transmissivity of the soil, which also

may vary with position in the catchment. The transmissivity is equal to the soil conductivity (K) integrated over the depth of the soil (z)

$$T = \int K dz \quad (2).$$

The discharge equivalent at the catchment outlet reflects the steady-state rainfall R, evaporation E, and leakage to the deeper bedrock groundwater table D,

$$q = R - E - D \quad (3).$$

The wetness index defined by equation (1) can be calculated for each element in a catchment. For the case of spatially uniform transmissivity, equation (1) can be simplified to the product of two ratios

$$W = (q/T) [(a/b) / \sin\theta] \quad (4)$$

in which q/T characterizes the hydrologic control on runoff generation and $(a/b)/\sin\theta$ characterizes the topographic control on throughflow routing. The spatial distribution of the wetness index can be used to investigate the relative pattern of soil moisture in a catchment for either a given rainfall rate.

The wetness parameter is defined as the ratio of the subsurface discharge to profile transmissivity, which allows incorporation of the wetness parameter into slope stability models. Hydrostatic flow in an inclined soil of uniform thickness may be expressed as

$$K h \sin\theta \cos\theta \quad (5)$$

where h is the thickness of the saturated zone. At saturation, the transmissivity of the soil is equal to

$$K z \sin\theta \cos\theta \quad (6)$$

where z is the soil thickness. Consequently, the wetness parameter may be expressed as the ratio of equations (5) and (6)

$$W = h/z \quad (7)$$

which implies that the wetness index represents the proportion of the soil column that is saturated. This expression for soil wetness allows coupling with a simple slope stability model for an inclined soil of uniform thickness over bedrock.

The infinite-slope stability model assumes that, at failure, the forces acting on a slab-like section of soil are balanced between resisting forces and gravitational forces. This model does not consider the effect of upslope, downslope, and lateral boundaries. For the case of cohesionless soil, this model predicts that at failure

$$\rho_s z \tan\theta \geq (\rho_s z - \rho_w h) \tan\phi \quad (8)$$

where ρ_s and ρ_w are the bulk densities of soil and water, respectively, and ϕ is the angle of internal friction of the soil. Rearranging equation (8) and substituting in equation (7) allows an expression for the soil wetness required to cause slope failure as a function of the soil bulk density, angle of internal friction, and the local slope

$$W \geq \rho_s [1 - (\tan\theta / \tan\phi)] \quad (9)$$

for the case where water is the fluid. Note that equation (9) is valid only up to values of $h/z = 1.0$, as there is no mechanism for generating pore pressures greater than hydrostatic in the model. Thus the combined hydrologic and stability model does not apply for the case where a pore pressure greater than hydrostatic is required for failure. This condition may be expressed as

$$\tan\theta \leq [(\rho_s - 1) / \rho_s] \tan\phi \quad (10)$$

and equation (9) does not apply for slopes gentler than indicated by equation (10) with a wetness greater than 1.0. For the case of no cohesion, soil will not be stable even when dry where the slope angle exceeds the angle of internal friction of the soil. Thus areas where

$$\tan\theta > \tan\phi \quad (11)$$

define areas of chronic instability where only shallow soils or bedrock outcrops are to be expected. Consequently, we may use the calculated wetness index and slope for each topographic element with equations (9), (10), and (11) to define the predicted stability of any point within a catchment under a variety of steady state discharges, transmissivities, and soil properties (Figure 2). For discussion and general amusement purposes, we call this combined hydrologic and stability model TOPSLOP.

We define four stability classes for the elements in a catchment in a particular simulation: chronically unstable, unstable, stable, and not steep enough to fail even if saturated. Chronically unstable elements are those predicted to be unstable when dry. Stable elements are those in which the wetness index is less than the value necessary for failure indicated by equation (9). In effect, elements classified as stable are those that are steep enough to fail, but have insufficient drainage area for a given simulation. Unstable elements are those with a wetness index value greater than indicated by equation (9). However, equation (9) is not applicable for elements with a wetness index greater than 1.0 and a slope less than that indicated by equation (10). In effect, these areas have sufficient drainage area, but insufficient slope to cause instability. Consequently, these elements are labeled as having too low a slope for failure to occur.

These stability categories are easily defined on a plot of wetness versus slope (Figure 2). The stability criterion defined by equation (9) intersects the slope axis at the angle of internal friction and the wetness axis at a value equal to the bulk density of the soil. The boundary of model applicability is indicated by a box defined by a wetness of 1.0 and equation (10). The stability of each element may be determined by plotting its position on this graph relative to these thresholds or boundaries. The seepage gradient necessary to destabilize a slope depends on the flow orientation [Iverson and Major, 1986], but this effect is not included in the model. Neither are the effects of seepage from the underlying bedrock or pore pressures greater than hydrostatic resulting from topographic convergence. Although these effects influence debris flow initiation, they are difficult to include in a model without knowledge of either bedrock fracture density and distribution or soil depths

The model is intended to simulate the topographic control on debris flow initiation.

Different steady state rainfall rates (q) will alter the wetness value for each element. Those elements steeper than the angle of internal friction of the soil will be unstable even when dry (wetness = 0). For other elements, the wetness will increase with increasing q until the stability threshold is crossed. Once this threshold is crossed, an element will remain unstable at all greater rainfall rates. Thus we may determine the minimum steady-state rainfall required to cause instability (q_f) in each element by combining equations (4) and (9)

$$q_f \geq [T \sin\theta \rho_s / (a/b)] [1 - (\tan\theta / \tan\phi)] \quad (12).$$

This corresponds to the q value required for the wetness in an element to exceed the criterion of equation (9).

Study Areas

We test this model in two catchments on the west coast of the United States (Figure 3). The study areas were selected on the basis of the availability of high-resolution digital elevation data in debris-flow-prone terrain. Previous field work in these areas allows estimation of both the soil property and hydrologic parameters involved in the model. In addition, these two areas allow testing of the model under significantly different conditions. The sensitivity of the model is investigated by comparing model predictions for a range in values of soil properties and hydrologic conditions. Model performance using independently constrained parameter values is then examined by comparing observed and predicted distributions of debris flows within the study areas.

The Marin County catchment (Figure 4a) occupies 1.2 km² in the Tennessee Valley area of the Marin Headlands just north of San Francisco, California. The area has broad convex hilltops and deeply alluviated major valleys. The catchment is underlain by stacked thrust sheets composed of Cretaceous greenstone, greywacke, and chert of the Franciscan Complex [Warhaftig, 1984]. Vegetation is composed of coastal scrub and grasslands communities. The area has a mediterranean climate with a mean annual rainfall of about 760 mm. Landsliding is an important sediment transport

process on the steeper slopes in this area, whereas overland flow and seepage erosion dominate on lower-gradient slopes [Montgomery and Dietrich, 1988; 1989]. Further description of geomorphic processes in this catchment and response to climate and land use changes are presented elsewhere [Montgomery, 1991].

Dietrich and others [in press] generated high resolution digital elevation data for this catchment from low-altitude, stereo aerial photographs. They also used the program TOPOG to map topographic attributes associated with threshold process theories and divided the catchment into areas dominated by diffusive sediment transport, overland flow, non-erosive overland flow, and landsliding. We use the same digital elevation data set contoured at a 5 m interval in our analysis of this catchment.

Field work in this and neighboring catchments provides the basis for estimating values for the soil thickness, conductivity, and bulk density. Soil thickness on the hillslopes in this area varies from 0.1 to 0.5 m on topographic noses to depths of up to 4.0 m in topographic hollows [Wilson and Dietrich, 1987; Montgomery, 1991]. The saturated conductivity of the soil, however, varies from 10^{-1} to 10^{-2} cm/s at soil depths less than 1 meter to from 10^{-7} to 10^{-8} cm/s for soil depths between 3 and 4 meters [Montgomery, 1991]. The transmissivity of the soil profile is dominated by highly-conductive, near-surface soils due to an exponential decay of conductivity with increasing soil depth. Based on these data, Dietrich and others (in press) estimate the transmissivity of soils in this catchment to be 17 m²/day. Based on data presented by Reneau and others (1984) we estimate that saturated bulk densities are on the order of 2.0 gm/cm³ and friction angles of roughly 45° for colluvial soils at the Marin County study site. We will use these values as representative for the study catchment.

The coastal Oregon study site consists of a 0.3 km² drainage basin along Mettman Ridge in the Oregon Coast Range just north of Coos Bay, Oregon (Figure 4B). As is typical in the Oregon Coast Range, the area is highly dissected and characterized by narrow ridgetops and steep slopes. Bedrock consists of gently dipping Eocene sandstones [Beaulieu and Hughes, 1975]. The study area was recently (1986) clear cut and replanted with Douglas fir, has a maritime climate, and receives approximately 1500 mm of precipitation annually. Landsliding is a major sediment transport process in this basin.

Shallow debris flows deliver the colluvial soils that accumulate within topographic hollows to the downslope channel system. Flow in a system of shallow bedrock fractures strongly influences the piezometric response in, and thus the stability of, the overlying colluvial soils [Montgomery, 1991]. Further descriptions of the geomorphic processes active in this and adjacent catchments are given elsewhere [Montgomery, 1991; Anderson et al., in prep; Montgomery et al., in prep; Torres et al., in prep.].

Digital terrain data was generated by scanning and vectorizing a 1:4800 scale topographic basemap of the catchment. The original basemap was constructed from low altitude aerial photographs obtained prior to forest clearance. During field work in the catchment, significant discrepancies were noted between the land form and that portrayed on the basemap. The discretized data were gridded at a 2 m spacing and then contoured at the same contour interval as the original base map using the program TOPOG. The two maps are essentially identical. Analysis was conducted using a map with a 5 m contour interval constructed from this data set.

Field work in these catchments and similar areas of the Oregon Coast Range provides constraints on the soil bulk density, thickness, and conductivity. The colluvial soil in the study area ranges in thickness from roughly 0.1 to 0.5 m on topographic noses to greater than 2 m in topographic hollows [Montgomery, 1991]. Saturated hydraulic conductivity of the colluvial soil declines from about 10^{-1} cm/s at the ground surface to about 10^{-2} cm/s at a depth of 2 meters [Montgomery, 1991]. Based on these data, we estimate that an appropriate transmissivity for use in this catchment is 64.8 m²/day. Saturated soil bulk density is about 1.6 gm/cm³ [Torres et al., in prep.]. Reported values of the angle of internal friction for soils developed on sandstones in the Oregon Coast Range vary from about 35° to 45° [Yee and Harr, 1977; Schroeder and Alto, 1983; Burroughs et al., 1985], with substantially lower values for saturated soils due to disaggregation upon wetting [Yee and Harr, 1977]. Although the colluvial soils may be cohesionless, the vegetation in the area provides significant apparent cohesion to the soil. Montgomery [1991] discusses the influence of root strength on slope stability in this and adjacent catchments. This effect will be pursued further elsewhere.

These observations provide the basis for the parameter values adopted in our test of the model. The spatial variability of each of these parameters

could be included in model simulations. They are treated as spatially uniform, however, because more detailed information on soil properties is unlikely to be available in most applications. Moreover, the goal of the present exercise is to develop a method for predicting those portions of a catchment that are most likely to be unstable, rather than predicting specific sites of instability.

Model Sensitivity

We ran model simulations on both catchments for a variety of steady-state rainfall conditions and for bulk densities of 1.6 and 2.0 gm/cm³ and angles of internal friction of 35° and 45°. In each simulation, relatively few elements are classified as unstable at low steady-state rainfall rates (Figure 5). With increasing rainfall, the wetness in each topographic element increases and progressively more elements are predicted to be unstable.

Figures 6 and 7 illustrate the patterns of predicted instability for a number of these simulations for the Mettman Ridge study site. In the case of a 35° friction angle, a large portion of the basin is predicted to be exposed bedrock and a substantial number of elements are predicted to be unstable even with a steady-state rainfall of 10 mm/day (Figure 6). Virtually the entire catchment is predicted to be unstable at a steady-state rainfall rate of 250 mm/day (Figure 6C), which in this area would correspond to about a 40 to 100 year 24-hr rainfall total. This pattern of extensive predicted instability reflects the low angle of internal friction assumed for the soil in the simulation relative to that measured by previous workers for the colluvial soils in this area. More reasonable predictions result from incorporation of the friction angles at the high end of the observed range. This may also reflect the neglect of effective cohesion due to trees and undergrowth vegetation, which may play a significant role in stabilizing these hillslopes [Montgomery, 1991].

For simulations using a 45° friction angle and a minimal rainfall of 10 mm/day, bands of predicted chronic instability reflect local steps in the ground surface (Figure 7A). The trend of these bands mirrors the low dips of the underlying bedrock. In the field, these steep bedrock steps typically are covered, if at all, by only a thin veneer of sediment and moss. These zones are areas where slopes are too steep to allow the accumulation of significant soil. Consequently, they pose little risk of generating debris flows. Increasing

the rainfall rate to 100 mm/day (Figure 7B), the zones of predicted instability spread to steep, low-order channels, topographic hollows, and the base of steep side slopes bordering channels. These areas are locations where debris flows are observed to occur in response to moderate storms in this area [Montgomery, 1991]. Further increasing the simulated rainfall to 250 mm/day (Figure 7C) expands the zones of predicted instability away from channels, toward drainage divides, and into the hillslopes where debris flows are uncommon.

These simulations indicate that the zones of predicted instability are quite sensitive to the assumed friction angle of the soil and the simulated rainfall rate. The sensitivity of the model for each catchment was analyzed by determining the percentage of the total catchment area predicted to be unstable for a variety of conditions (Figures 8 & 9). In each case, the proportion of the catchment predicted to be unstable smoothly increases with increasing discharge and asymptotically approaches the total catchment area for which equations (10) and (11) are satisfied, and the model is applicable. For the Mettman Ridge study area, the proportion of the catchment classified as unstable is more sensitive to the angle of internal friction than to the bulk density of the soil (Figure 8), while model predictions are sensitive to estimates of both soil bulk density and friction angle for the Tennessee Valley study area (Figure 9). Estimation of these soil properties is not difficult and should not limit the usefulness of the model. The spatial variability of these parameters, however, should be considered when interpreting model results. Selection of the simulated rainfall rate, however, involves some judgement.

The steady-state rainfall required for failure can be calculated from equation (12) for each element in a catchment. Elements requiring a greater rainfall for instability are interpreted to be more stable, as a less frequent rainfall event would be required to cause instability. Conversely, those elements requiring the least rainfall are interpreted to be the most susceptible to debris flow initiation. The spatial pattern of the rainfall required for instability consequently defines a map of the relative potential for debris flow initiation.

Figures 10 and 11 compares the distribution of the steady-state rainfall required for instability for the Tennessee Valley and Mettman Ridge catchments. Most of the Tennessee Valley catchment has slopes that are too gentle for failure from the criterion of equation (10) (Figure 10). Only the

steeper slopes along valley margins and at the head of hollows are susceptible to debris flow initiation. These areas define the general areas in which debris flow scarps were observed in the field. Overland flow and seepage processes dominate sediment transport in the lower-gradient portions of this catchment [Montgomery and Dietrich, 1989; Montgomery, 1991]. In contrast, most of the Mettman Ridge catchment is predicted to be unstable at some rainfall rate (Figure 11). The pattern of predicted instability, however, changes systematically with increasing rainfall in a manner consistent with field observations. Initially, only steep bands corresponding to bedrock steps exposed at the ground surface are predicted to be unstable. These areas represent sites of chronic instability and do not present a great debris flow hazard, as significant material does not accumulate on these slopes. As rainfall increases to 100 mm/day the zones of predicted instability extend to low-order channels and unchanneled hollows and onto the base of some steeper hillsides. These are the general locations where debris flow scarps are observed both within and around this study basin. At even greater rainfall rates, the zones of predicted instability expand further into hillslopes and up to the heads of valleys until they virtually enclose the valley network. The ridgelines and hillslopes between valleys are unstable only at extreme steady-state rainfall rates. Debris flow processes are the dominant sediment transport process on these slopes and this pattern is consistent with a threshold control on landscape dissection (Montgomery and Dietrich, 1992). The general correlations of these patterns with the locations of observed debris flows in these study areas indicates that equation (12) can be used to map the relative potential for debris flow generation within a catchment.

Prediction of Response to Specific Rainfall

Use of the model for other than relative hazard assessment purposes requires determination of an appropriate steady state rainfall. Although a wide range of rainfall intensities will impact any field site, it is possible to constrain the rainfall associated with debris flow initiation. We compare landslide distributions for the Tennessee Valley and Mettman Ridge study sites with zones of predicted instability for a steady-state rainfall simulation determined from rainfall characteristics associated with observed landslides in these basins.

Debris flows in the grasslands of Marin County typically occur during runoff producing storms in which the hollow axes upslope of channel heads are saturated. The steady-state rainfall necessary to generate saturation of valley axes in TOPOG is about 50 mm/day [Dietrich et al., in press]. Using the estimated soil transmissivity of 17 m²/day and saturated bulk density of 2 gm/cm³, 34 out of the 39 landslide scars (87%) presently visible in the study area occupy elements predicted to be unstable (Figure 12).

The Mettman Ridge catchment has seventeen debris flow scars presently visible. Five of these failures involve failure of road fill or side-cast material from logging landings. Selection of an appropriate steady-state rainfall for testing model predictions against the remaining twelve failures is somewhat problematic. Over the period 1990-1992, six debris flows were observed to occur in this basin during 24-hr rainfall of less than 100 mm. Eight out of twelve debris flows (67%) occurred in locations predicted to be unstable in a 100 mm/day rainfall simulation. The piezometric response in the hillslopes and hollows of this area, however, is strongly related to the one- to two-hour rainfall intensity [Montgomery, 1991]. Maximum observed one-hour rainfall intensity associated with debris flow initiation in the winter of 1989-1990 was 8 to 10 mm/hr [Montgomery, 1991], which translates into a steady-state rate of about 200 to 250 mm/day. Eleven out of twelve debris flow scars (92%) are in locations predicted to be unstable for a 200 mm/day rainfall simulation (Figure 13). The unexplained debris flow scarp is located at the downslope end of a colluvium-filled hollow that is not portrayed on the topographic basemap.

These examples indicate that 87 to 92% of the observed debris flow scars occur in locations predicted by the model to be unstable for cases with independent controls on the steady-state rainfall rate associated with debris flow initiation. This concordance of observation and prediction indicates that, with appropriate constraints, the model may serve to identify likely sites of failure initiation and relative hazard assessment. However, the accuracy and resolution level of the original topographic information is important in steep, finely dissected terrain and model results are only as accurate as the topographic information on which they are based. See Bauer (in prep.) and Zhang and Montgomery (in prep.) for further discussion of DEM representation of the landscape surface and implications for modelling geomorphic and hydrologic processes.

Run Out Paths

The flow-tube architecture of TOPOG facilitates determination of debris flow runout paths. The farthest upslope element predicted to be unstable in each flow tube is determined for a given rainfall simulation. The potential debris flow path is then traced down the flow tube until a depositional criteria is exceeded. A number of workers have reported that debris flows tend to deposit on slopes of roughly 3° to 6° [e.g., Campbell, 1975; Ikeya, 1981; Takehashi et al., 1981; Benda and Cundy, 1990]. Consequently, we define a zone of likely debris flow deposition as the first set of consecutive topographic elements with slopes between 3° and 6° downslope of an element predicted to be unstable. Zones of potential debris flow scour are delineated as the topographic elements along the flow tube between initiation and deposition points.

Figure 14 illustrates the predicted pattern of debris flow scour and deposition for the Tennessee Valley study area using steady-state rainfall simulation of 100 mm/day. For this catchment, the steep channels in the basin headwaters are predicted to be subject to scour while the lower-gradient channels in the major valleys are predicted to be within zones of debris accumulation. These patterns of predicted instability correlate well with the observed distribution of bedrock channels and Holocene valley fills. Furthermore, exposures of the valley fill along incised channel banks indicate that they are composed of interstratified debris flow and alluvial deposits.

Figure 15 illustrates the predicted runout paths for the Mettman Ridge study area for a steady-state rainfall of 100 mm/day. In this case, the entire channel network is too steep to allow deposition. Although the channels in this catchment are bedrock floored, there are several debris flow deposits located along the channels. These deposits are located at channel confluences, are associated with major accumulations of large woody debris, and probably represent transient channel blockages that will be remobilized during subsequent scouring events. In this regard, the zone of scour predicted by the model does not apply to individual debris flows, but to the cumulative action of many debris flows within a catchment.

Discussion

Several important caveats apply to DTM-based models of geomorphic processes. These caveats concern the quality of the DEM data, the relevance of the model to specific field applications, and methods employed to evaluate, constrain, or calibrate the model.

Digital terrain models are only as accurate as the digital elevation data upon which they are based. Unfortunately, many digital elevation models bear little resemblance to the landscapes from which they are derived [see Bauer, in prep; Zhang and Montgomery, in prep.]. Consequently, high-resolution DEM data is required to analyze spatial patterns of erosional processes through analysis of drainage area and slope. Without high-quality data, any DEM-based model may yield inaccurate, if not misleading, results.

The model developed here only applies to shallow mass wasting in cohesionless material resulting from topographically-induced convergence of shallow subsurface flow. This is most appropriate for modelling topographically-induced debris flow generation common in hollow-and-nose topography. The model is not intended to reproduce the behavior of large-scale bedrock landslides. Furthermore, since the root strength of vegetation may provide an apparent cohesion to even cohesionless soils, the present model best approximates either grasslands environments where root strength is minimal or post-forest clearance conditions when root strength decreases dramatically.

With these caveats in mind for the cases discussed above, both observed landslides and zones with bedrock exposed at the ground surface correspond to locations predicted by the model to be unstable. However, more areas are predicted to be unstable than have failed in the field. Are these locations predicted to be unstable, but lacking landslide scars, places where the model has been unsuccessful, or can these sites be considered as likely sites for slope failures in future storms? We maintain that treating these sites as potential failure sites is most consistent with both theory and observation.

Flow in near-surface bedrock strongly influences the piezometric response in the overlying colluvium, and thus debris flow initiation, in both the Tennessee Valley and Mettman Ridge study areas. Wilson and Dietrich [1987] reported that low conductivity zones in the underlying bedrock may influence colluvium saturation at another study site in Marin County

approximately 10 km north of the Tennessee Valley study site. Montgomery and co-workers [Montgomery et al., 1990; in prep.; Montgomery, 1991] reported evidence indicating that local flow exfiltrating from a shallow bedrock fracture system controls the location of debris flows in the Mettman Ridge study area in coastal Oregon. Consequently, neglect of bedrock flow in the model requires that the zone of predicted instability be considered as encompassing areas most susceptible to slope failure, rather than as specific locations where instability will occur for a given simulated rainfall.

The spatial variability of bedrock properties would be virtually impossible to assess on a reconnaissance level and extremely difficult to map at any confidence level. Consequently, successful prediction of specific locations of debris flow initiation in response to a given storm would be difficult in areas with a strong bedrock control on near-surface hydrologic response. This suggests that zones of predicted instability be interpreted as defining those portions of the landscape that are likely to be susceptible to debris flow initiation. The role of bedrock properties in determining sites of specific failure initiation further suggests that more detailed site-specific analyses may yield unwarranted confidence.

Coupled hydrologic, slope stability, and digital terrain models provide a powerful tool for debris flow hazard assessments and predictions of runout paths and travel distances. In particular, the model described above provides an objective methodology for identifying debris-flow-prone locations in a catchment. Portions of the landscape predicted by the model to be the most sensitive to debris flow initiation (low-order channels, topographic hollows, and steep side slopes) correspond to locations where debris flows are observed to occur and which have been described subjectively as debris flow source areas [see review in Montgomery et al., 1991].

The simulated rainfall necessary to generate slope instability provides an objective method for determining relative debris flow hazard potential. Several methods are possible for evaluating the hydrologic parameter T/q without field measurements of soil conductivity and thickness. This parameter may be set so as to include all of the observed landslide scarps in a basin within the zone predicted to be unstable. This approach has the disadvantage of relying on the present distribution of failures to define the expected distribution. An alternative approach is to use topographic constraints on T/q [see Dietrich et al., in press] through the observation that

divergent hillslopes only rarely saturate. Finally, there also is the problem of flow leakage to bedrock. Some landscapes are well-drained with most of the rainfall infiltrating to the groundwater table. Such landscapes will be more stable than this model predicts. Consequently, the model discussed above should be analyzed by a geomorphologist familiar with landslide and runoff generation processes within the catchment of interest.

While the model provides a useful relative hazard assessment methodology, a number of improvements may be desirable. Soil cohesion and the effect of root strength can be incorporated, but requires further soil depth information. Often this is not available. However, a model currently under development for predicting soil depth may provide a method for adding cohesion to the analysis. Inclusion of a dynamic hydrologic response would greatly expand the utility of the model and could be used to model rates of erosion and sediment delivery to downslope channels in response to simulated stream events. Development of these capabilities is being pursued.

Conclusions

A simple, physically-based digital terrain model allows objective determination of relative slope stability from estimates of the soil conductivity, thickness, bulk density, and friction angle. Spatial variability of these properties and temporal variability of rainfall may be accommodated in future versions of the model, but are unnecessary for relative hazard assessments. Given independent constraints on soil properties and the steady-state rainfall associated with debris flow initiation the model predicts slopes to be unstable in the location of approximately 90% of the observed debris flow scarps in two study catchments. Modelled debris flow run out paths and depositional areas correspond to those observed in the field.

Acknowledgements

This work was supported by grant TFW FY92-010 from the Washington State Department of Natural Resources through the CMER and SHAMW committees of the Timber/Fish/Wildlife agreement and NSF grant 89-17467. Harvey Greenberg and Rob Reiss provided analysis, programming, and graphics support.

References Cited

- Beaulieu, J. D., and P. N. Hughes, Environmental Geology of Western Coos and Douglas Counties, Oregon, *Oregon Dept. of Geol. and Min. Ind. Bull.* 87, 148p.
- Benda, L., and Cundy, T. W., Predicting deposition of debris flows in mountain channels, *Can. Geotech. Jour.*, 27, 409-417, 1990.
- Benda, L., and Dunne, T., Sediment routing by debris flow: in *Erosion and Sedimentation in the Pacific Rim*, edited by R. L. Beschta, T. Blinn, G. E. Grant, F. J. Swanson, and G. G. Ice, International Association of Hydrological Sciences Publication 165, 213-223, 1987.
- Beven, K. J., and M. J. Kirkby, A physically based variable contributing area model of basin hydrology, *Hyd. Sci. Bull.*, 24, 43-69, 1979.
- Brabb, E. E., and B. L. Harrod (editors), *Landslides: Extent and Economic Significance*, A. A. Belkema, Rotterdam, 385p, 1989.
- Burroughs, E. R., Jr., C. J. Hammond, and G. D. Booth, Relative stability estimation for potential debris avalanche sites using field data, in *Proceedings of the International Symposium on Erosion, Debris Flow and Disaster Prevention*, Tsukuba, Japan, pp. 335-339, 1985.
- Campbell, R. H., Soil Slips, Debris Flows and Rainstorms in the Santa Monica Mountains and Vicinity, Southern California, *U.S. Geol. Surv. Prof. Pap.* 851, 51p, 1975.
- Crozier, M. J., E. E. Vaughn, and J. M. Tippett, Relative instability of colluvium-filled bedrock depressions, *Earth Surface Processes and Landforms*, 15, 329-339, 1990.
- Dietrich, W. E., C. J. Wilson, and S. L. Reneau, Hollows, colluvium, and landslides in soil-mantled landscapes, in *Hillslope Processes*, edited by A. D. Abrahams, pp. 361-388, Allen and Unwin, London, 1986.
- Dietrich, W. E., C. J. Wilson, D. R. Montgomery, J. McKean, and R. Bauer, in press, Erosion thresholds and land surface morphology, *Geology*.
- Ellen, S. D., and Wiczorek, G. F., editors, *Landslides, Floods and Marine Effects of the Storm of January 3-5, 1982, in the San Francisco Bay region, California*, U.S. Geological Survey Professional Paper 1434, 310p, 1988.

- Fowler, W. L., Potential Debris Flow Hazards of the Big Bend Drive Drainage Basin, Pacifica, California, Unpublished Masters Thesis, Department of Applied Earth Sciences, Stanford University, Stanford, CA, 101p, 1984.
- Ikeya, H., A method for designation for areas in danger of debris flow, in *Erosion and Sediment Transport in Pacific Rim Steeplands*, IAHS Spec. Pub. 132, 576-588, 1981.
- Iverson, R. M., and J. J. Major, Ground-water seepage vectors and the potential for hillslope failure and debris flow mobilization, *Wat. Resour. Res.*, 22, 1543-1548, 1986.
- Montgomery, D. R., *Channel Initiation and Landscape Evolution*, Ph.D. dissertation, Dept. of Geology and Geophysics, University of California, Berkeley, California, 421p.
- Montgomery, D. R. and W. E. Dietrich, Where do channels begin?, *Nature*, 336, 232-234, 1988.
- Montgomery, D. R., and W. E. Dietrich, Source areas, drainage density, and channel initiation, *Wat. Resour. Res.*, 25, p. 1907-1918, 1989.
- Montgomery, D. R., R. H. Wright, and T. Booth, Debris flow hazard mitigation for colluvium-filled swales: *Bull. Assoc. of Eng. Geol.*, 28, 303-323, 1991.
- Moore I. D., E. M. O'Loughlin, and G. J. Burch, A contour-based topographic model for hydrological and ecological applications, *Earth Surf. Proc. Land.*, 13, 305-320.
- Okunishi, K., and Iida, T., Evolution of hillslopes including landslides, *Trans. Jap. Geom. Un.*, 2, 191-200, 1983.
- O'Loughlin, E. M., Prediction of surface saturation zones in natural catchments by topographic analysis, *Wat. Resour. Res.*, 22, 794-804, 1986.
- Reneau, S. L., W. E. Dietrich, C. J. Wilson, and J. D. Rogers, Colluvial deposits and associated landslides in the northern San Francisco Bay area, California, USA, in *Proceedings of IVth International Symposium on Landslides*, pp. 425-430, International Society of Soil Mechanics and Foundation Engineering, Toronto, Ontario, Canada, 1984.
- Reneau, S. L., and W. E. Dietrich, The importance of hollows in debris flow studies; examples from Marin County, California, in *Debris Flows/Avalanches: Process, Recognition and Mitigation*, edited by J. E.

- Costa, and G. F. Wieczorek, Geological Society of America Reviews in Engineering Geology, 7, 165-180, 1987.
- Salo, E. O., and T. W. Cundy (editors), Streamside Management: Forestry and Fishery Interactions, University of Washington Institute of Forest Resources Contribution No. 57, 471p.
- Schroeder, W. L., and J. V. Alto, Soil properties for slope stability analysis; Oregon and Washington coastal mountains, *Forest Science*, 29, 823-833.
- Selby, M. J., Hillslope Materials & Processes, Oxford University Press, 264p., 1982.
- Smith, T. C., A method for mapping relative susceptibility to debris flows, with an example from San Mateo County, in *Landslides, Floods, and Marine Effects of the Storm of January 3-5, 1982, in the San Francisco Bay Region, California*, edited by S. D. Ellen and G. F. Wieczorek, U.S. Geol. Surv. Prof. Pap. 1434, p. 185-194, 1988.
- Smith, T. C., and Hart, E. W., Landslides and related storm damage, January 1982, San Francisco Bay Region, *California Geology*, 35, 139-152, 1982.
- Takahashi, T., Ashida, K., and Sawai, K., Delineation of debris flow hazard areas, in *Erosion and Sediment Transport in Pacific Rim Steeplands*, IAHS Spec. Pub. 132, 589-603, 1981.
- Tsukamoto, Y., T. Ohta, and H. Noguchi, Hydrological and geomorphological studies of debris slides on forested hillslopes in Japan, in *Recent Developments in the Explanation and Prediction of Erosion and Sediment Yield*, edited by D. E. Walling, International Association of Hydrological Sciences Publication 137, p. 89-98, 1982.
- Vertessy, R. A., C. J. Wilson, D. M. Silburn, R. D. Connolly, and C. A. Ciesiolka, Predicting erosion hazard areas using digital terrain analysis, International Association of Hydrological Sciences Publication 192, pp. 298-308, 1990.
- Warhaftig, C., Structure of the Marin Headlands Block, California: A progress report, in *Franciscan Geology of Northern California*, edited by M. C. Blake, Jr., vol. 43, pp. 31-50, Society of Economic Paleontologists and Mineralogists, Pacific Coast Section, Bakersfield, Calif., 1984.
- Wilson, C. J., and W. E. Dietrich, The contribution of bedrock groundwater flow to storm runoff and high pore pressure development in hollows, *IAHS Publ.*, 165, 49-59, 1987.

Yee, C. S. and Harr, R. D., Influence of soil aggregation on slope stability in the Oregon Coast Ranges, *Environmental Geology*, 1, 367-377, 1977.

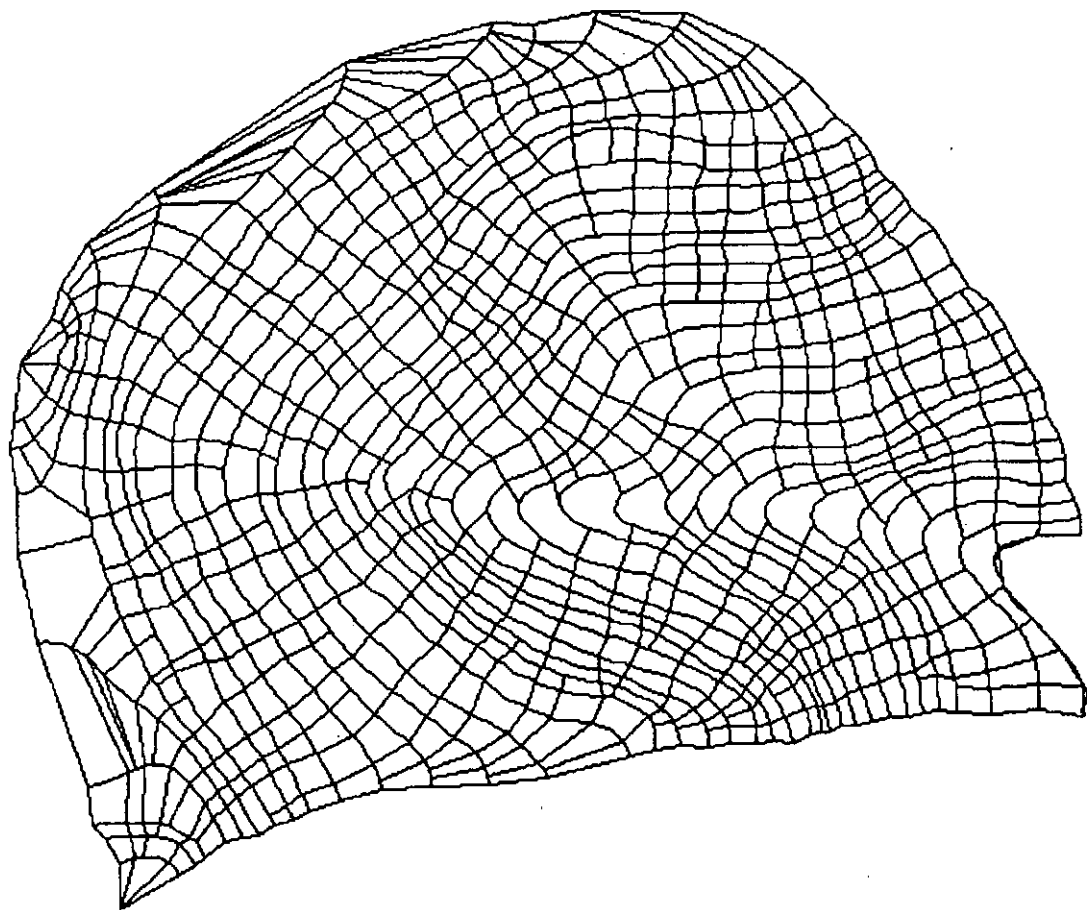
Figure Captions

- Figure 1 Illustration of the definition of flow tubes in the program TOPOG [O'Loughlin, 1986].
- Figure 2 Definition of stability fields on a plot of the wetness index versus slope.
- Figure 3 Location map for the Mettman Ridge and Tennessee Valley study areas.
- Figure 4 Topographic maps of the A) Tennessee Valley and B) Mettman Ridge study catchments.
- Figure 5 Plots of wetness versus slope for each topographic element in the Mettman Ridge study catchment for $T=64.8 \text{ m}^2/\text{day}$, $\tan\phi = 45^\circ$, and $\rho_s = 1.6 \text{ gm/cm}^3$, for A) $q = 10 \text{ mm/day}$; B) $q = 100 \text{ mm/day}$; and C) $q = 250 \text{ mm/day}$.
- Figure 6 Maps of predicted element stability for the Mettman Ridge study catchment for the case of $\tan\phi = 35^\circ$, $T=64.8 \text{ m}^2/\text{day}$, and $\rho_s = 1.6 \text{ gm/cm}^3$ for A) $q = 10 \text{ mm/day}$; B) $q = 100 \text{ mm/day}$; and C) $q = 250 \text{ mm/day}$.
- Figure 7 Maps of predicted element stability for the Mettman Ridge study catchment for the case of $\tan\phi = 45^\circ$, $T=64.8 \text{ m}^2/\text{day}$, and $\rho_s = 1.6 \text{ gm/cm}^3$ for A) $q = 10 \text{ mm/day}$; B) $q = 100 \text{ mm/day}$; and C) $q = 250 \text{ mm/day}$.
- Figure 8 Plots showing the percent of the total catchment area predicted to be unstable for the Mettman Ridge study

catchment for the case of A) $\tan\phi = 35^\circ$ and 45° , $T=64.8$ m^2/day , and $\rho_s = 1.6$ gm/cm^3 and for B) $\tan\phi = 45^\circ$, $T=64.8$ m^2/day , and $\rho_s = 1.6$ and 2.0 gm/cm^3 .

- Figure 9 Plots showing the percent of the total catchment area predicted to be unstable for the Tennessee Valley study catchment for the case of A) $\tan\phi = 35^\circ$ and 45° , $T=17$ m^2/day , and $\rho_s = 1.6$ gm/cm^3 [note that the cross-over of the two trends is due to the greater area predicted to be bedrock outcrops for the case of $\tan\phi = 35^\circ$] and for B) $\tan\phi = 45^\circ$, $T=17$ m^2/day , and $\rho_s = 1.6$ and 2.0 gm/cm^3 .
- Figure 10 Map showing the rainfall intensity necessary for slope instability for the Tennessee Valley study catchment.
- Figure 11 Map showing the rainfall intensity necessary for slope instability for the Mettman Ridge study catchment.
- Figure 12 Map of the Tennessee Valley study catchment showing the channel network, areas of predicted instability [$q=50$ mm/day ; $\tan\phi = 45^\circ$, $T=17$ m^2/day , and $\rho_s = 2.0$ gm/cm^3], and observed debris flow scarps (●).
- Figure 13 Map of the Mettman Ridge study catchment showing the channel network, areas of predicted instability [$q=200$ mm/day ; $\tan\phi = 45^\circ$, $T=64.8$ m^2/day , and $\rho_s = 1.6$ gm/cm^3], and observed debris flow scarps (●).
- Figure 14 Map of the Tennessee Valley study catchment showing farthest upslope most sites of debris flow initiation within a flow tube (black areas), areas of downslope scour (dark gray areas), and zones of predicted debris flow deposition (light gray areas). [$q=100$ mm/day ; $\tan\phi = 45^\circ$, $T=17$ m^2/day , and $\rho_s = 2.0$ gm/cm^3]

Figure 15 Map of the Mettman Ridge study catchment showing upslope most sites of debris flow initiation within a flow tube (black areas), areas of downslope scour (dark gray areas), and zones of predicted debris flow deposition (light gray areas). [$q=100$ mm/day; $\tan\phi = 45^\circ$, $T=64.8$ m²/day, and $\rho_s = 1.6$ gm/cm³].



loX = 1400.00
loY = 0.00
hiX = 1780.00
hiY = 400.00

Pickable files:

Other files:
met2.sbd
met2.scn
met2.stj

50.0 meters

Figure 1

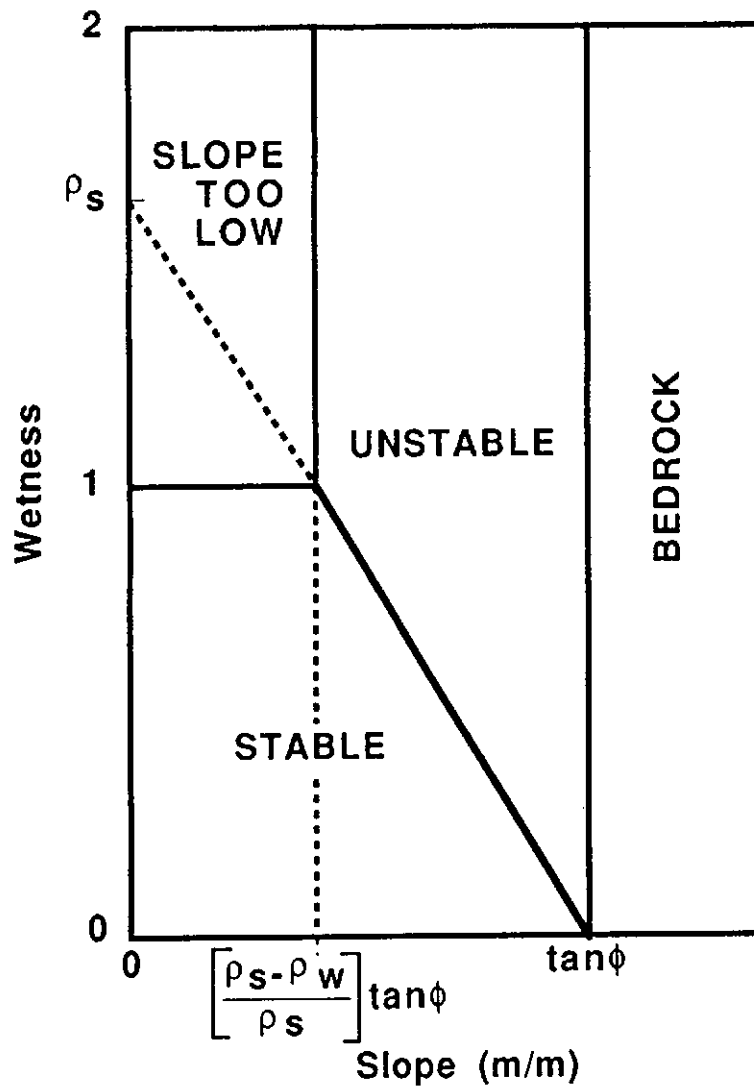


Figure 2

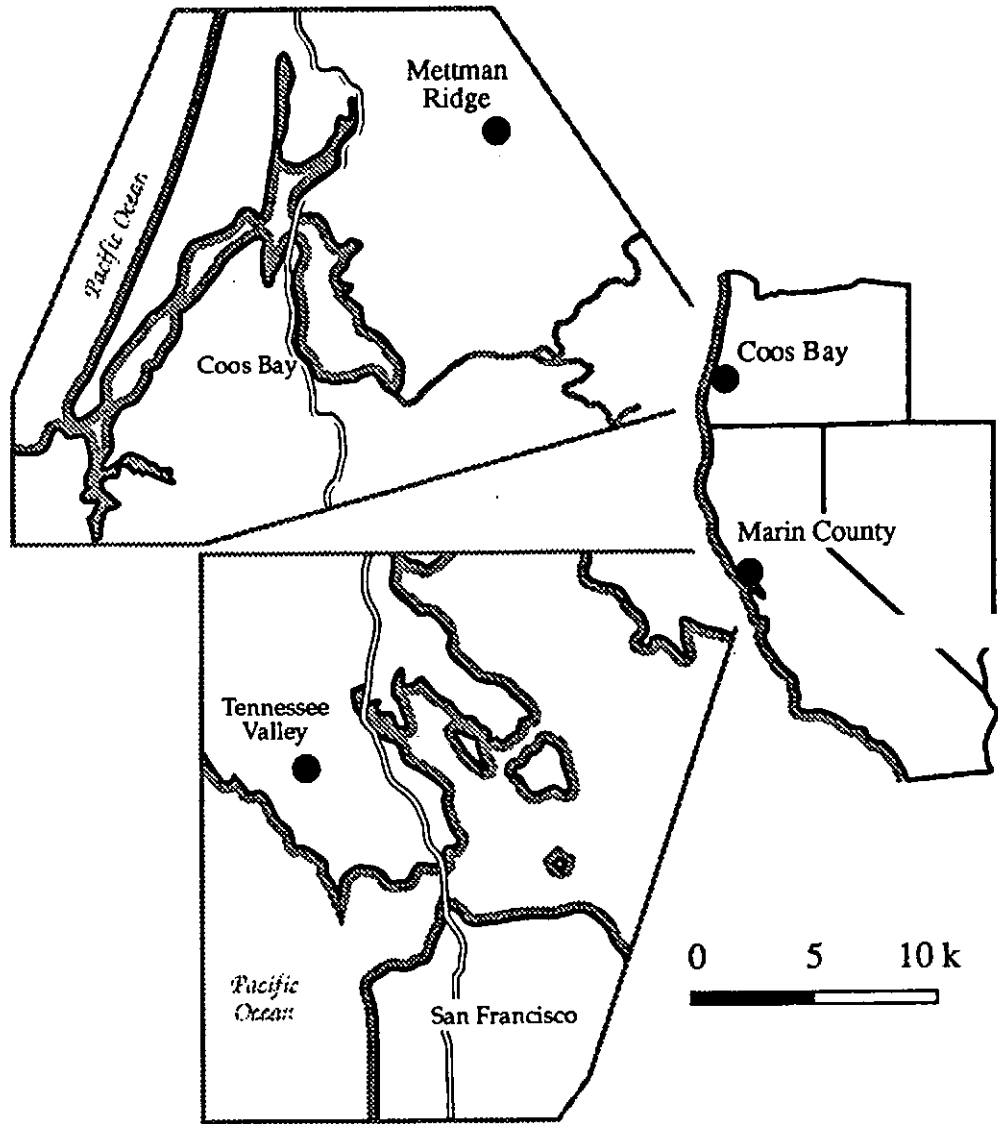


Figure 3

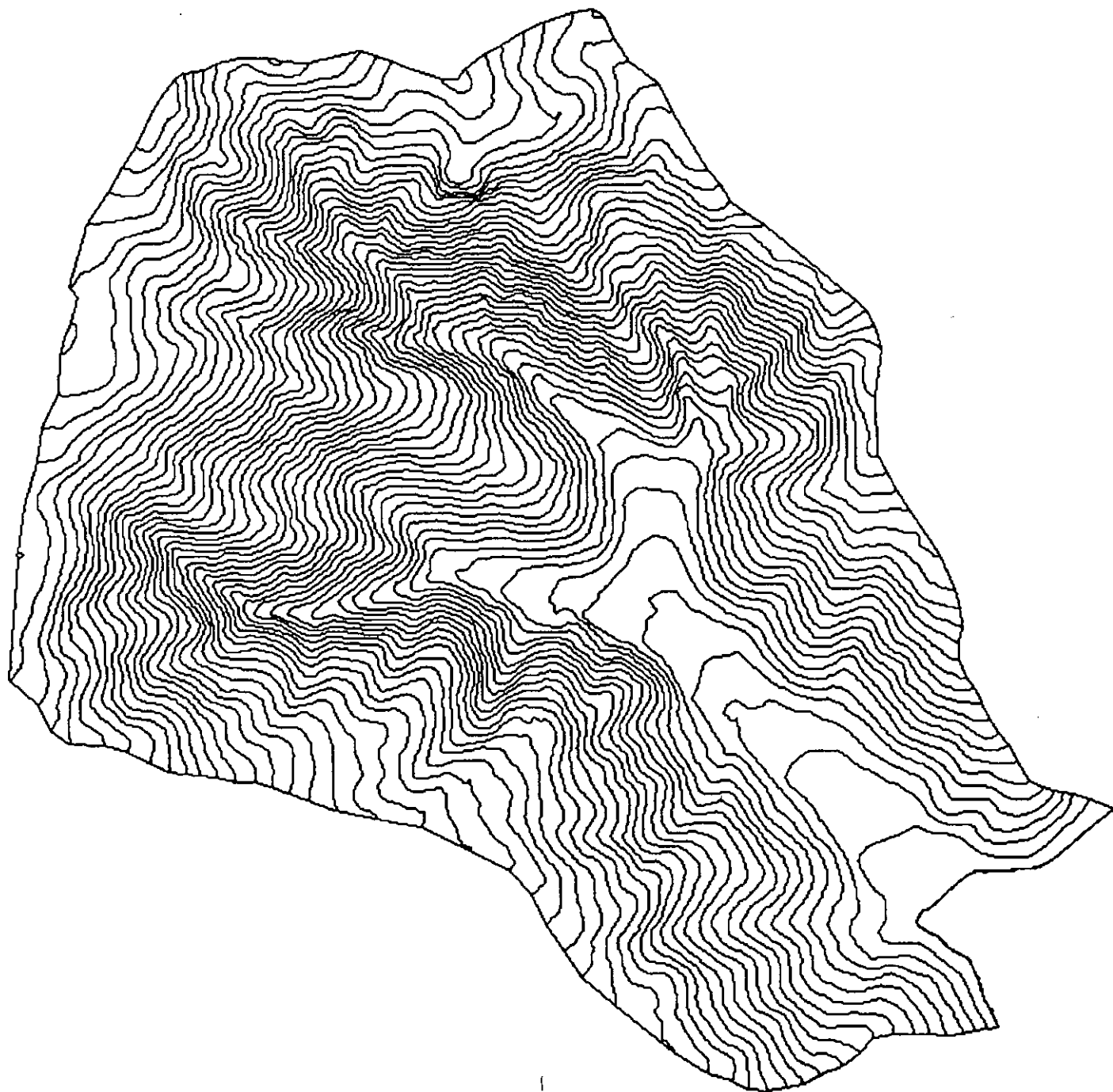
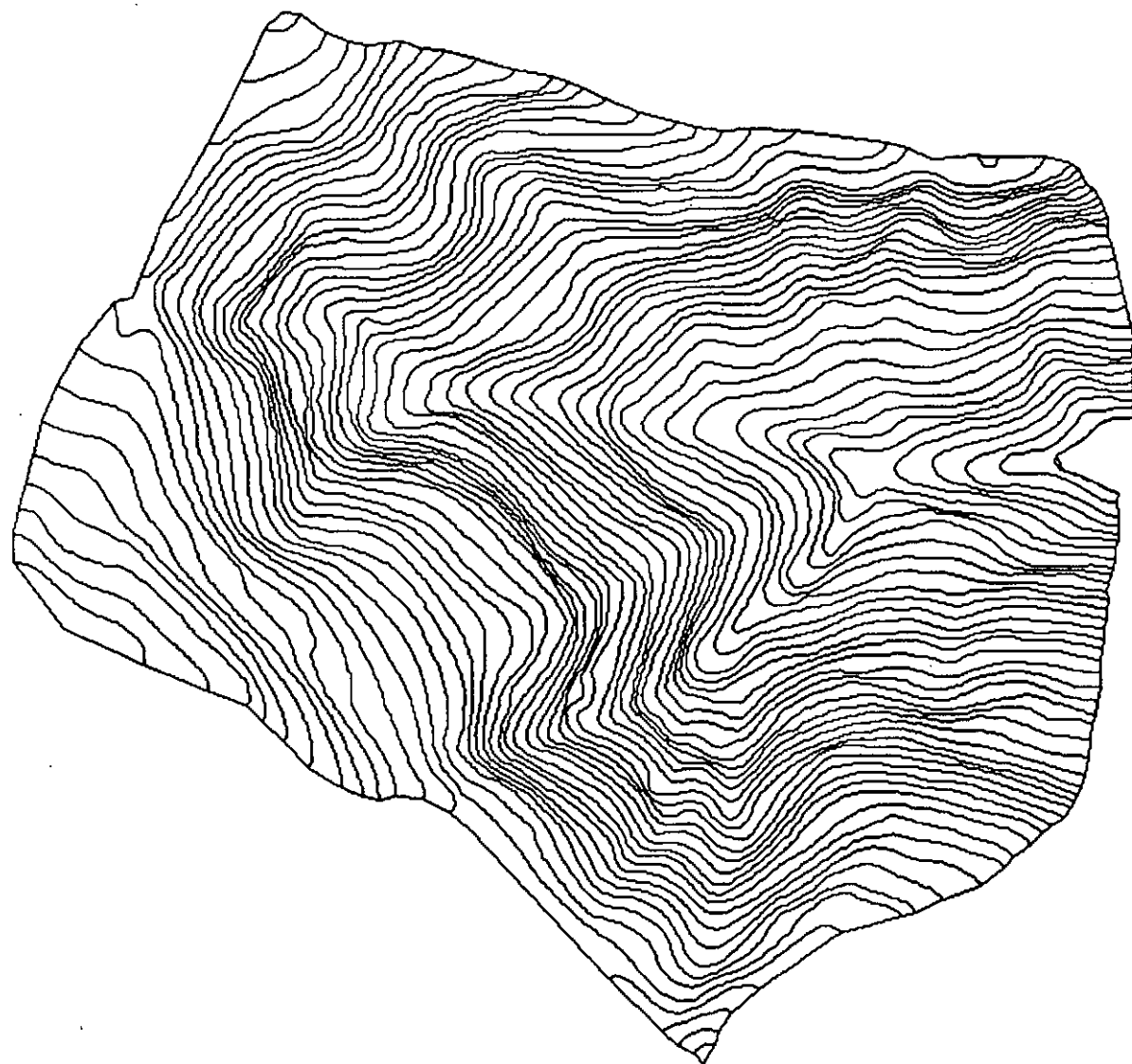


Figure 4A



loX = 1060.00
loY = 130.00
hiX = 1780.00
hiY = 930.00

Pickable files:

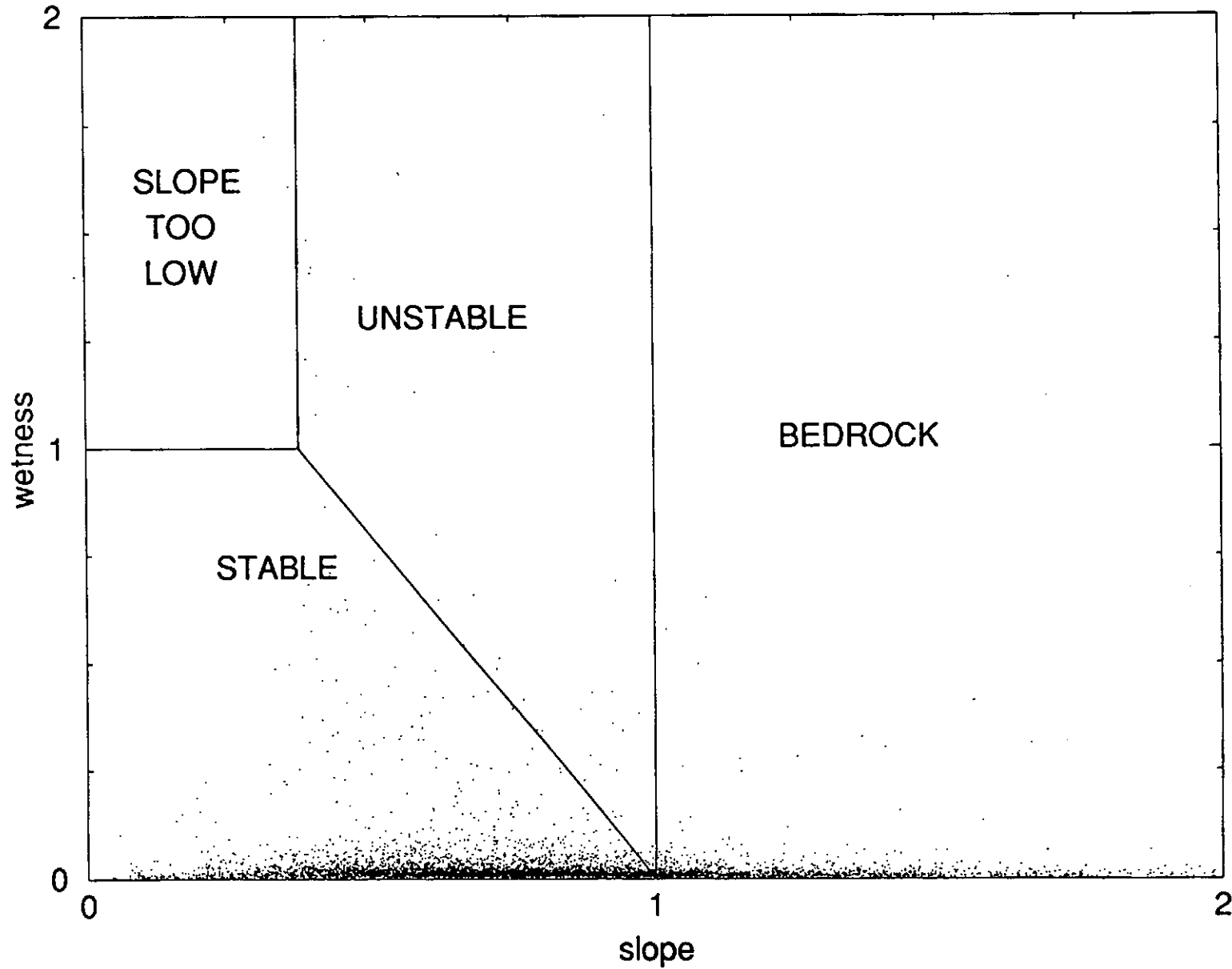
Other files:
net.sbd
net.son

100.0 meters

Figure 4B

Slope Stability

$\phi = 45, \rho = 1.6$

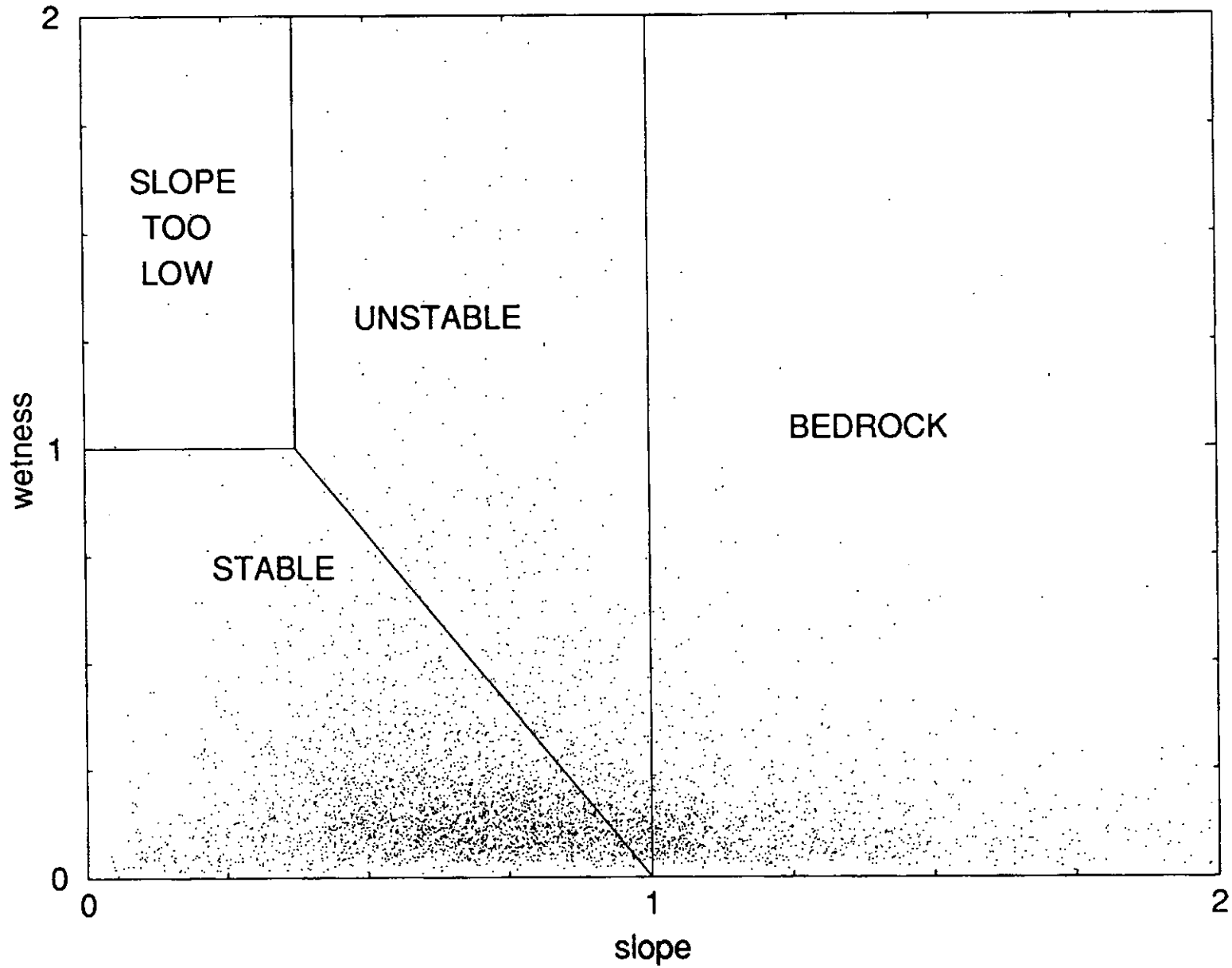


Points represent flow tubes for Mettman Ridge, $T=64.8, Q=10$.

Figure 5A

Slope Stability

$\phi = 45, \rho = 1.6$

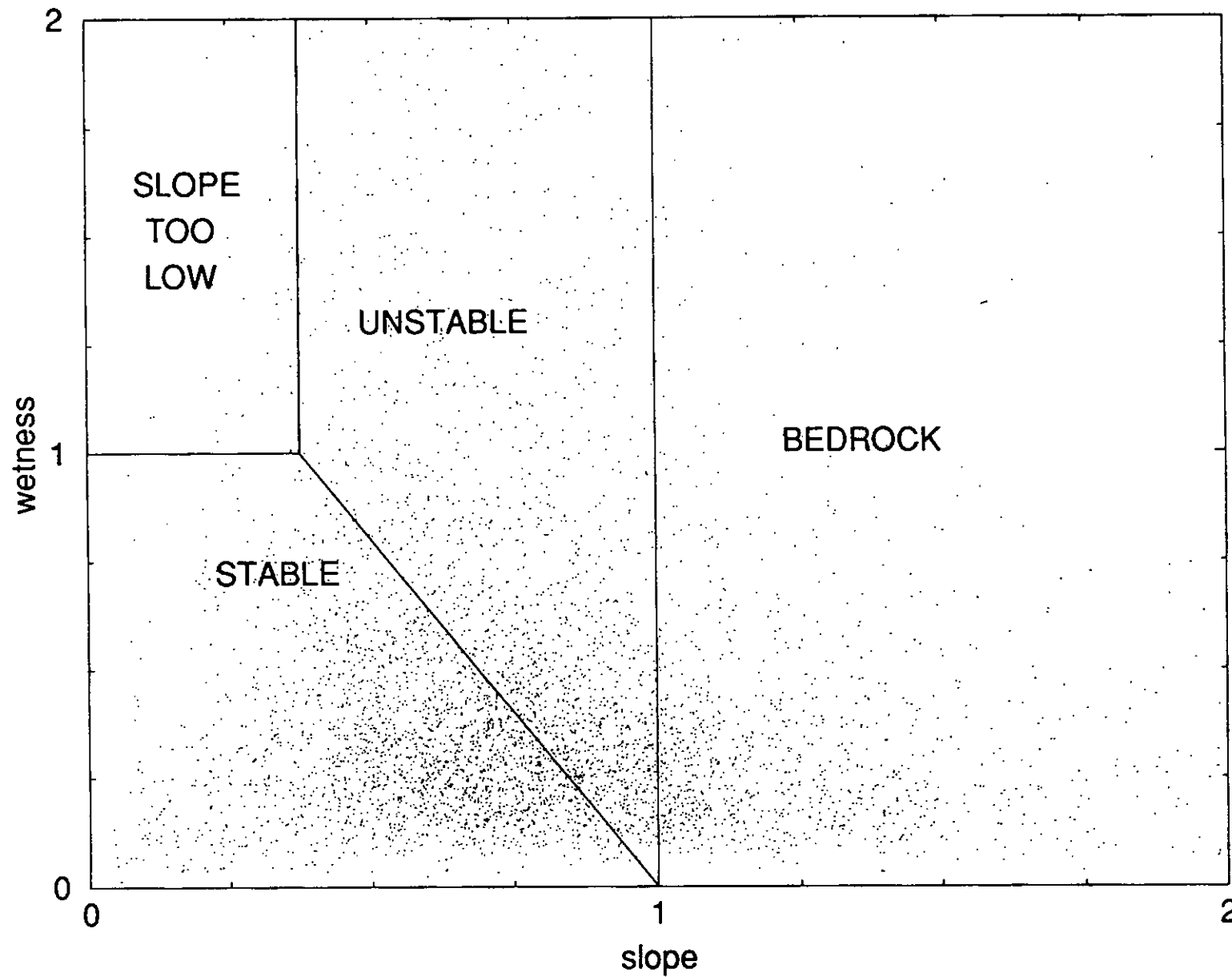


Points represent flow tubes for Mettman Ridge, $T=64.8, Q=100$.

Figure 5B

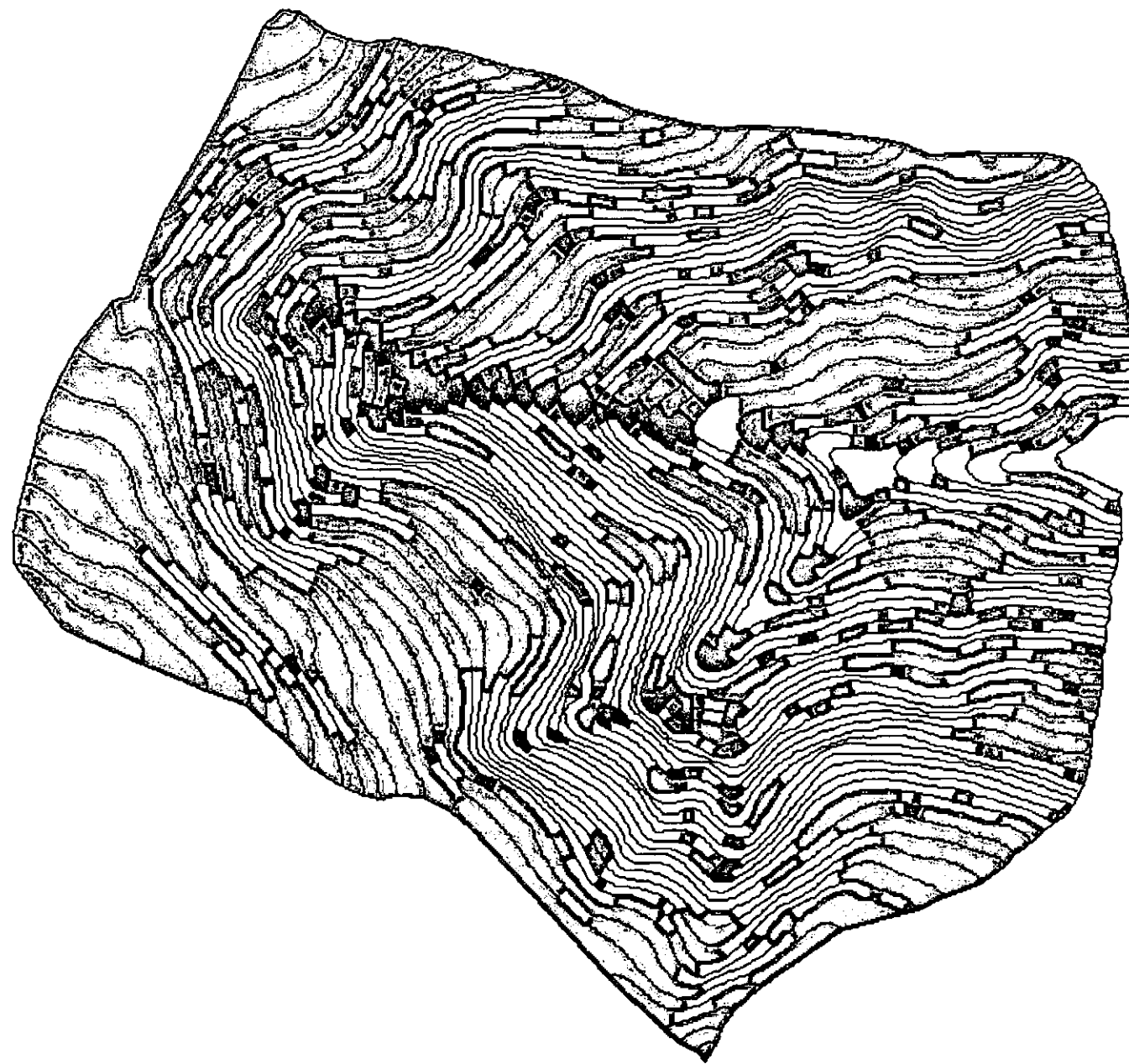
Slope Stability

$\phi = 45, \rho = 1.6$



Points represent flow tubes for Mettman Ridge, $T=64.8, Q=250$.

Figure 5C



Slope Stability

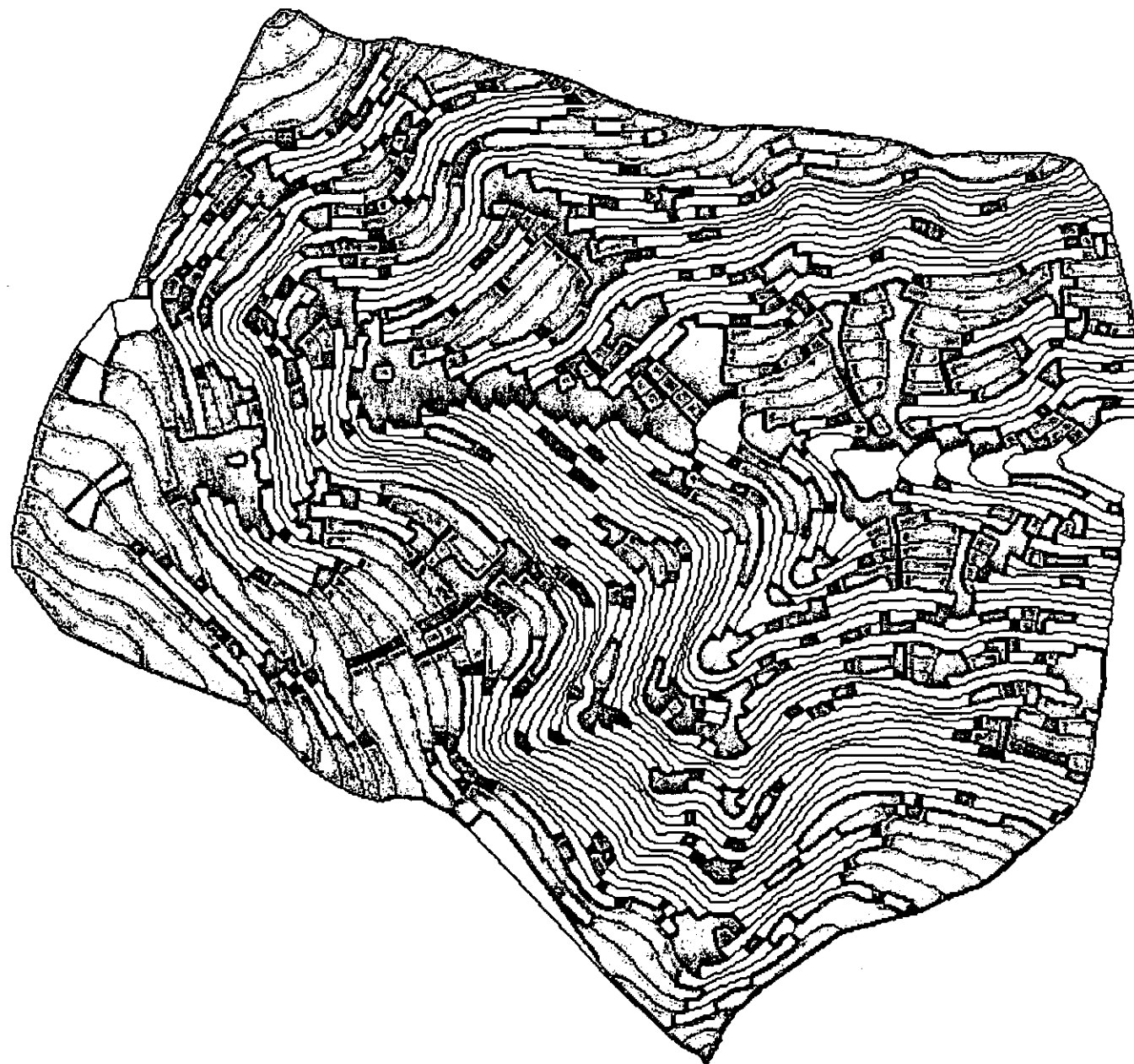
- stable
- pot. unstable
- unstable
- rock

Hettman Ridge
(Coos Bay)
Catchment 1





$T=64.8 \text{ mm}^2/\text{day}$
 $Q=10 \text{ mm}/\text{day}$
 $\phi=35 \text{ degrees}$
bulk density =
1.6 gm/cm^3

100.0 meters

Figure 6A



Slope Stability

-  stable
-  pot. unstable
-  unstable
-  rock

Mettman Ridge
(Coos Bay)
Catchment 1

$T = 64.8 \text{ mm}^2/\text{day}$
 $Q = 100 \text{ mm}/\text{day}$
 $\phi = 35 \text{ degrees}$
bulk density =
1.6 gm/cm^3

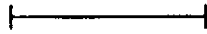
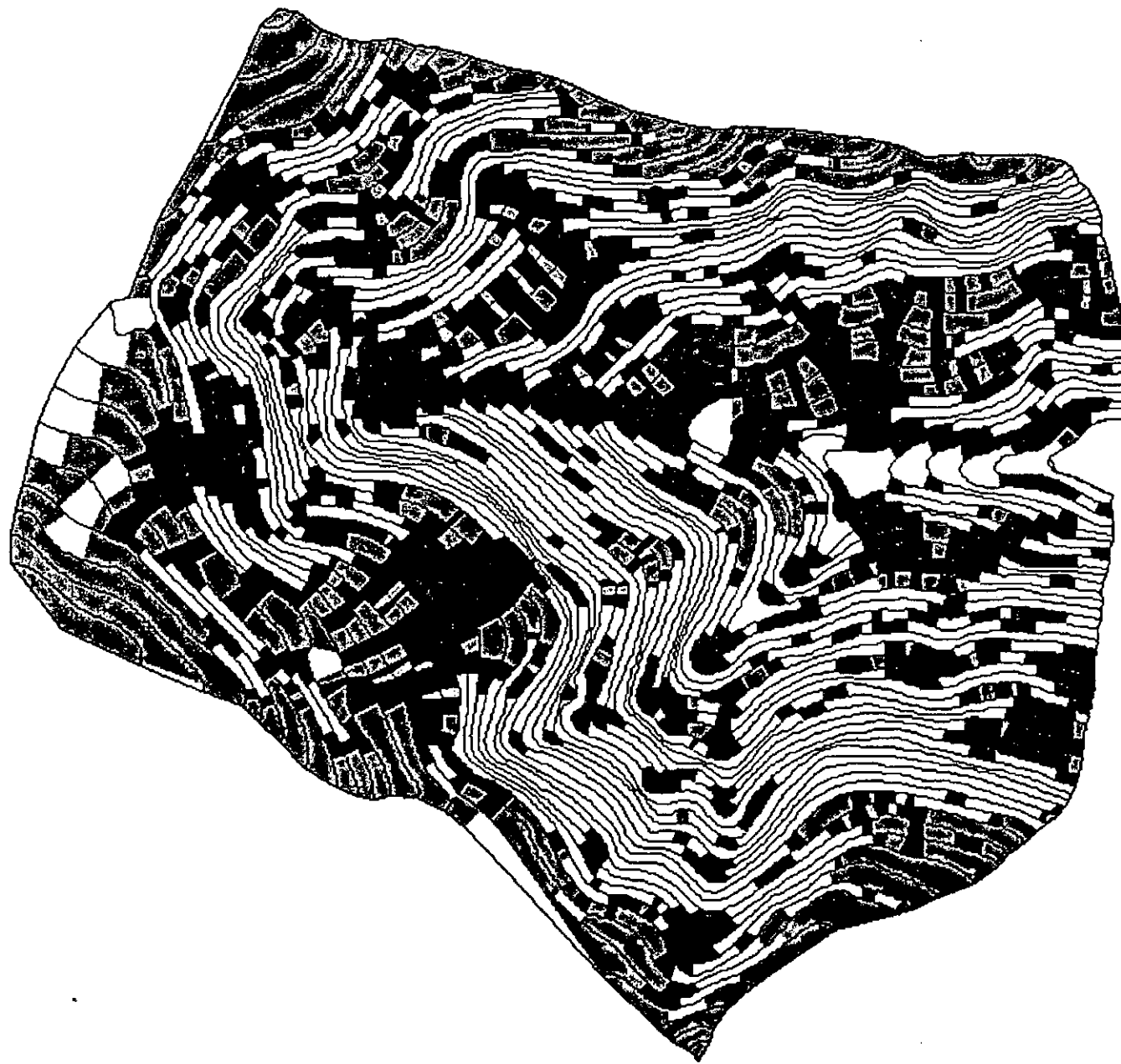





100.0 meters

Figure 6B



Slope Stability

-  stable
-  pot. unstable
-  unstable
-  rock

Mettman Ridge
(Coos Bay)
Catchment 1

$T = 64.8 \text{ mm}^2/\text{day}$
 $Q = 250 \text{ mm}/\text{day}$
 $\phi = 35 \text{ degrees}$
bulk density =
 $1.6 \text{ gm}/\text{cm}^3$


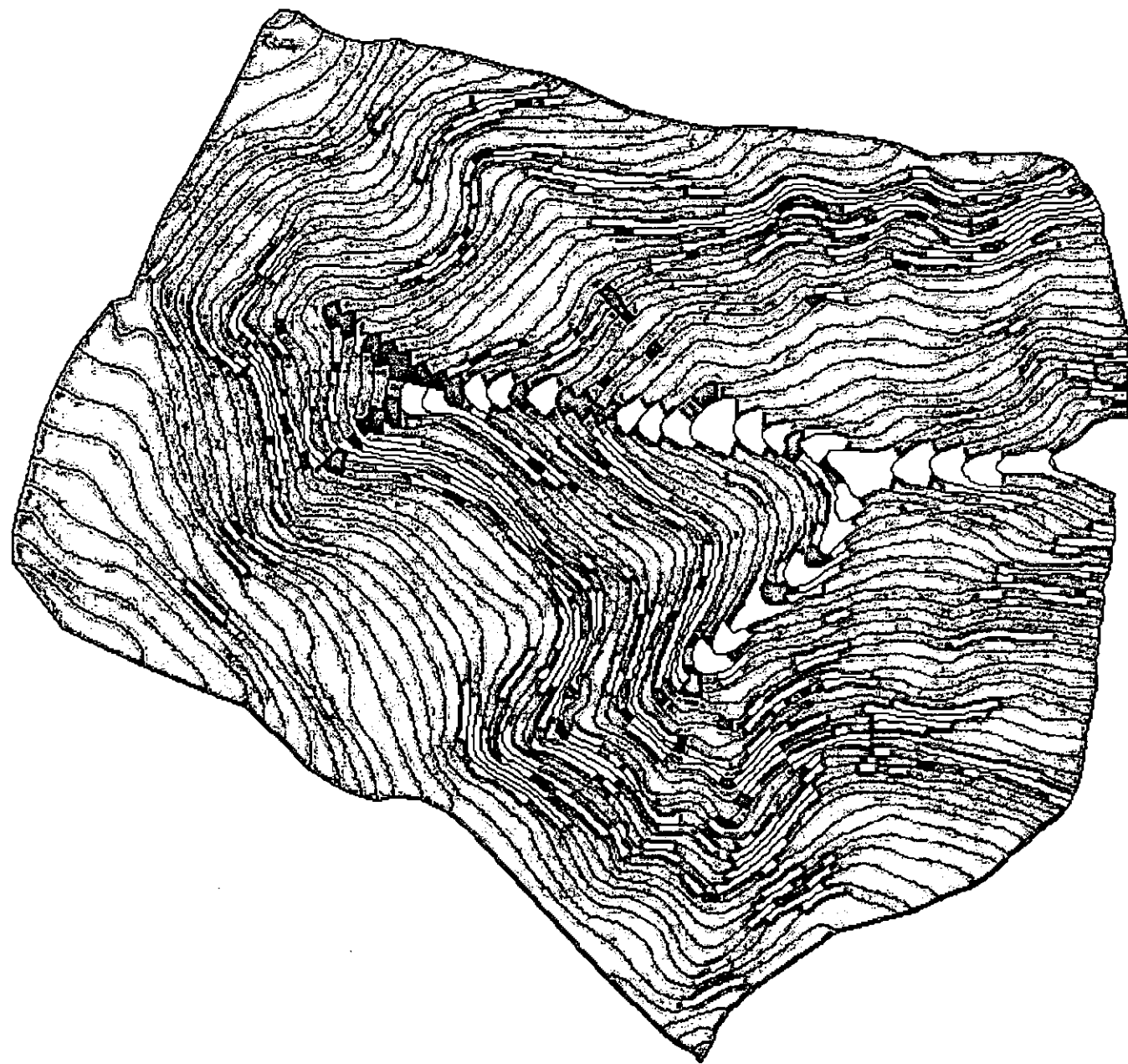





100.0 meters

Figure 6C



Slope Stability

-  stable
-  pot. unstable
-  unstable
-  rock

Mettman Ridge
(Coos Bay)
Catchment 1

$T=64.8 \text{ mm}^2/\text{day}$
 $Q=10 \text{ mm}/\text{day}$
 $\phi=45 \text{ degrees}$
bulk density =
 $1.6 \text{ gm}/\text{cm}^3$


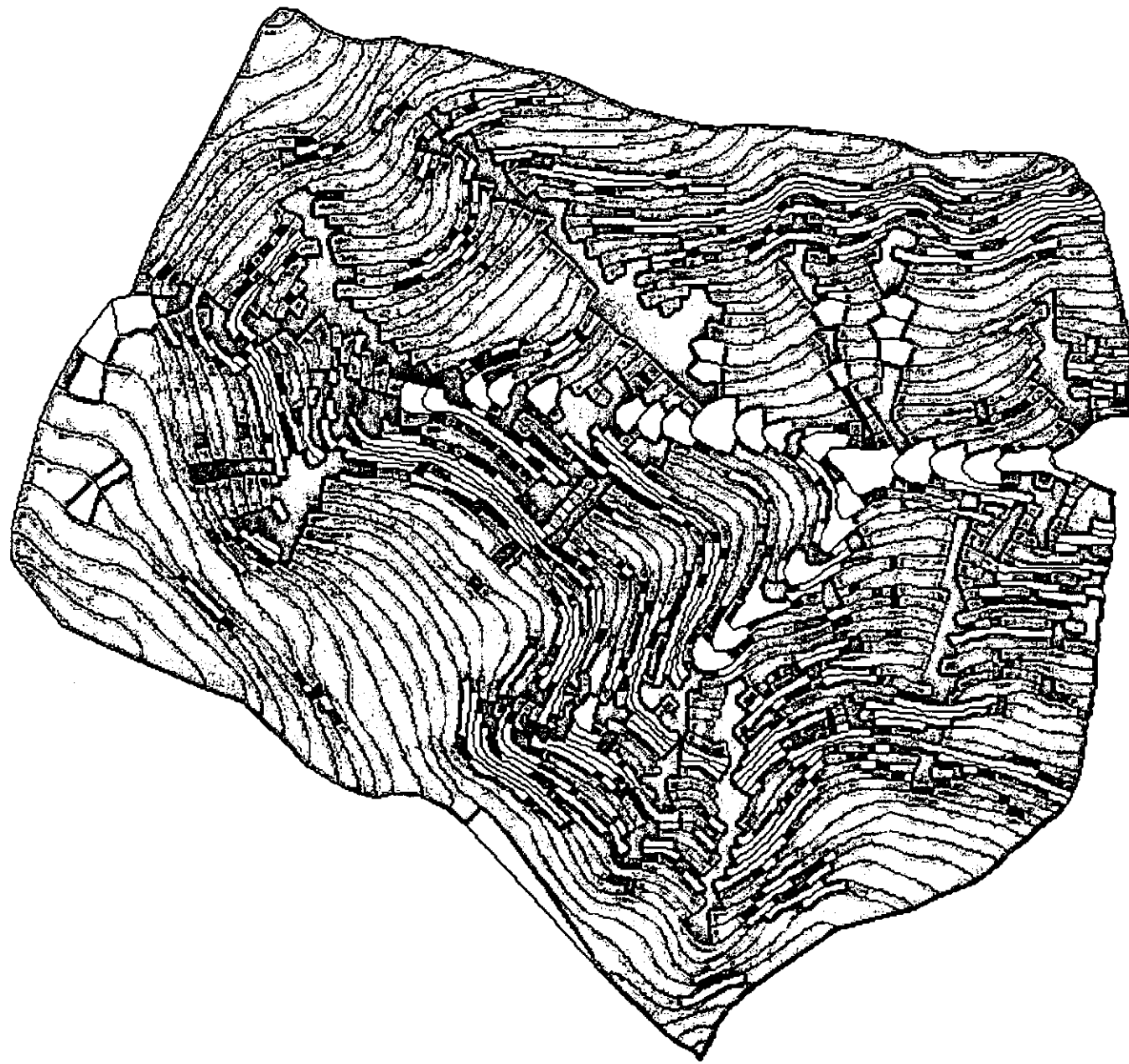

100.0 meters

Figure 7A



Slope Stability

- stable
- pot. unstable
- unstable
- rock

Mettman Ridge
(Coos Bay)
Catchment 1

$T = 64.8 \text{ mm}^2/\text{day}$
 $Q = 100 \text{ mm}/\text{day}$
 $\phi = 45 \text{ degrees}$
bulk density =
 $1.6 \text{ gm}/\text{cm}^3$

100.0 meters

Figure 7B



Slope Stability

- stable
- pot. unstable
- unstable
- rock

Hettman Ridge
 (Coos Bay)
 Catchment 1

$T = 64.8 \text{ mm}^2/\text{day}$
 $Q = 250 \text{ mm}/\text{day}$
 $\phi = 45 \text{ degrees}$
 bulk density =
 $1.6 \text{ gm}/\text{cm}^3$

100.0 meters

Figure 7C

Tennessee Valley

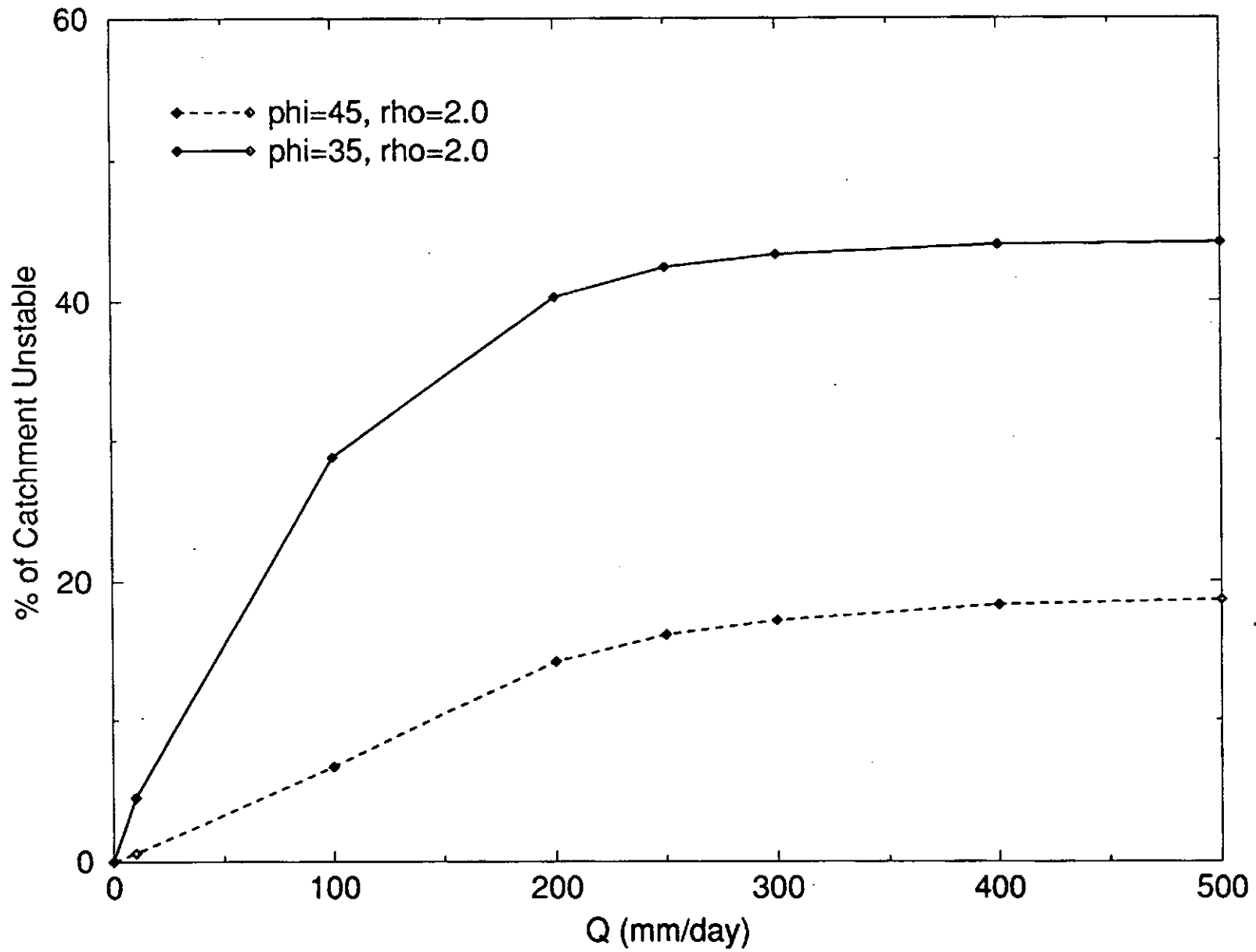


Figure 8A

Tennessee Valley

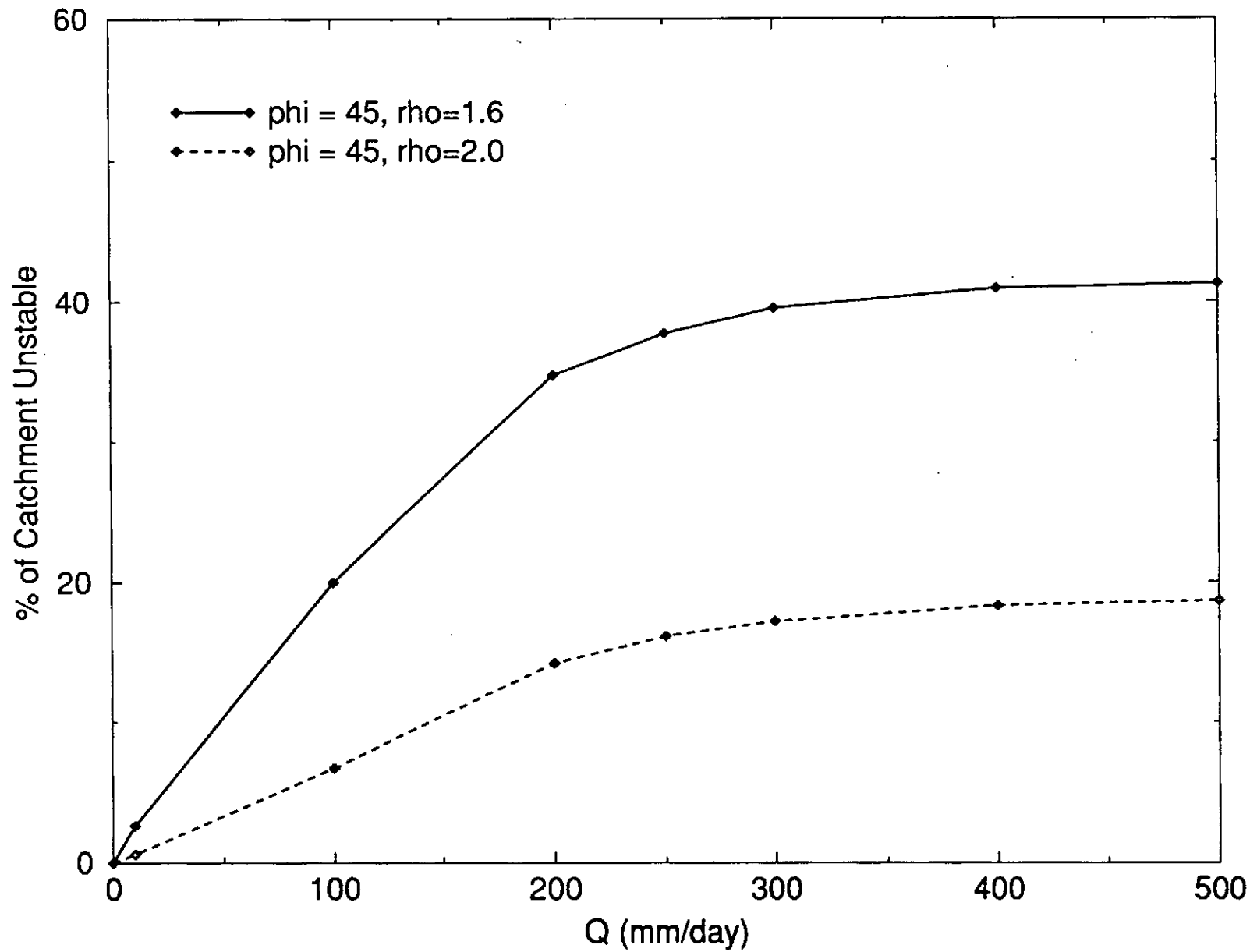


Figure 8B

Mettman Ridge

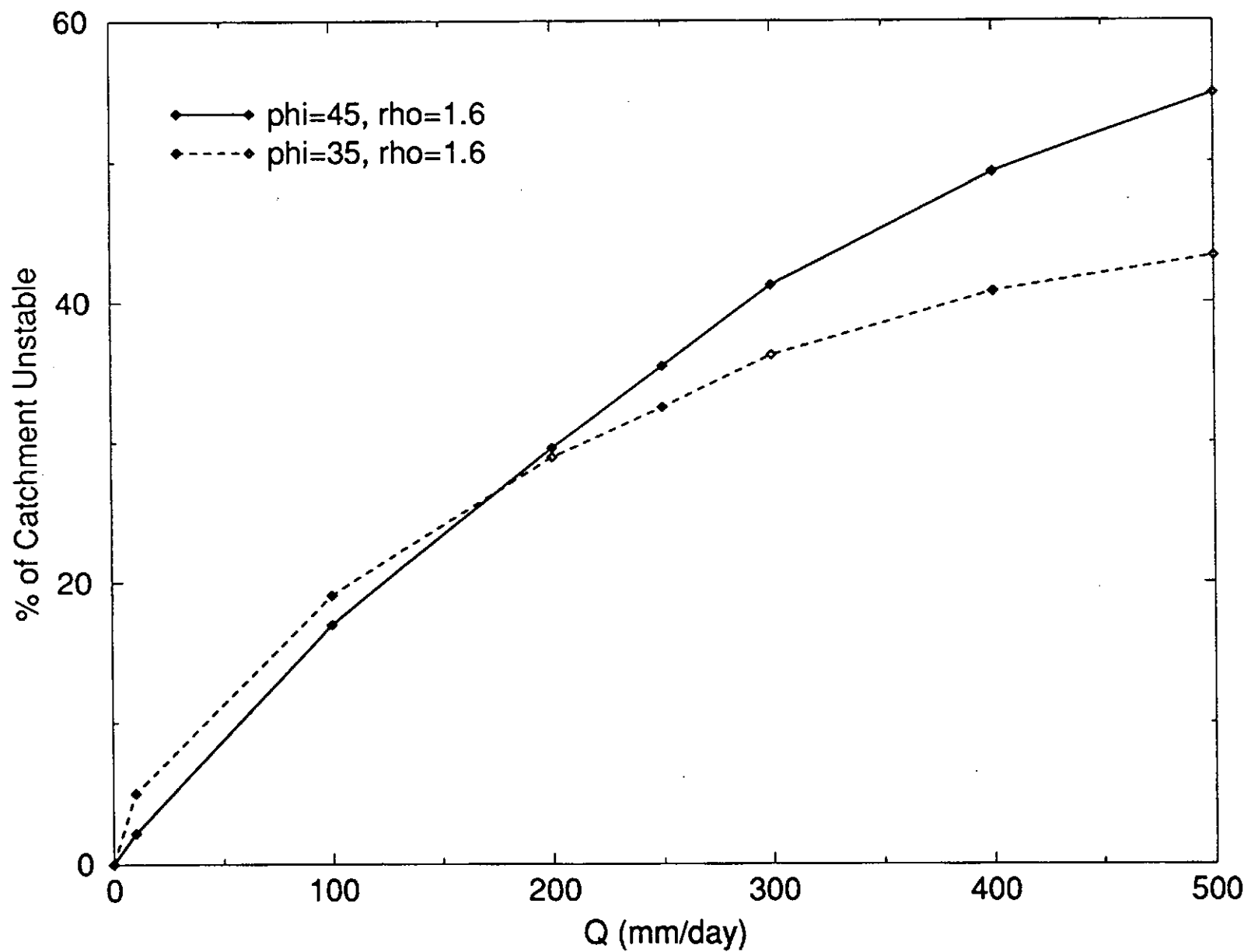


Figure 9A

Mettman Ridge

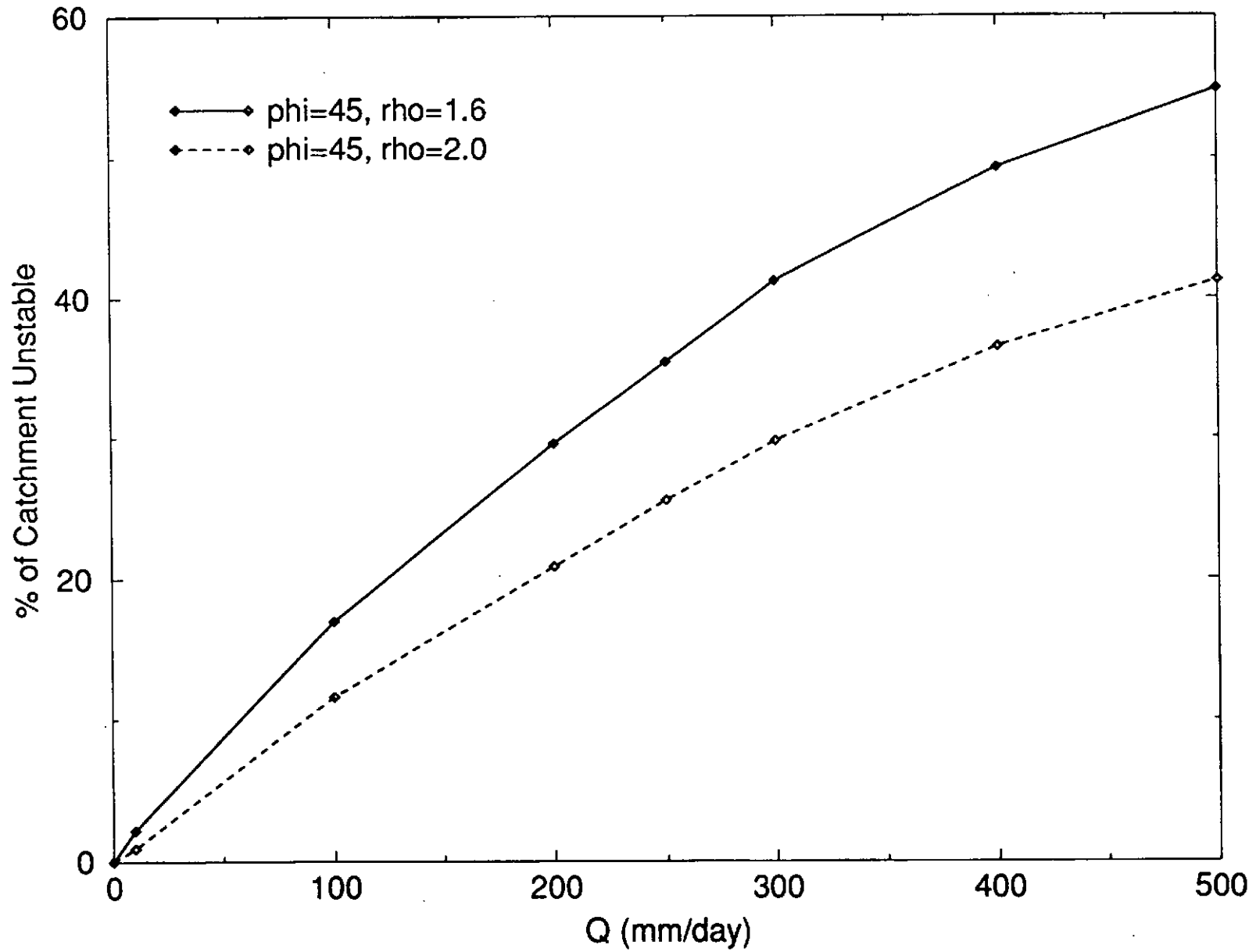
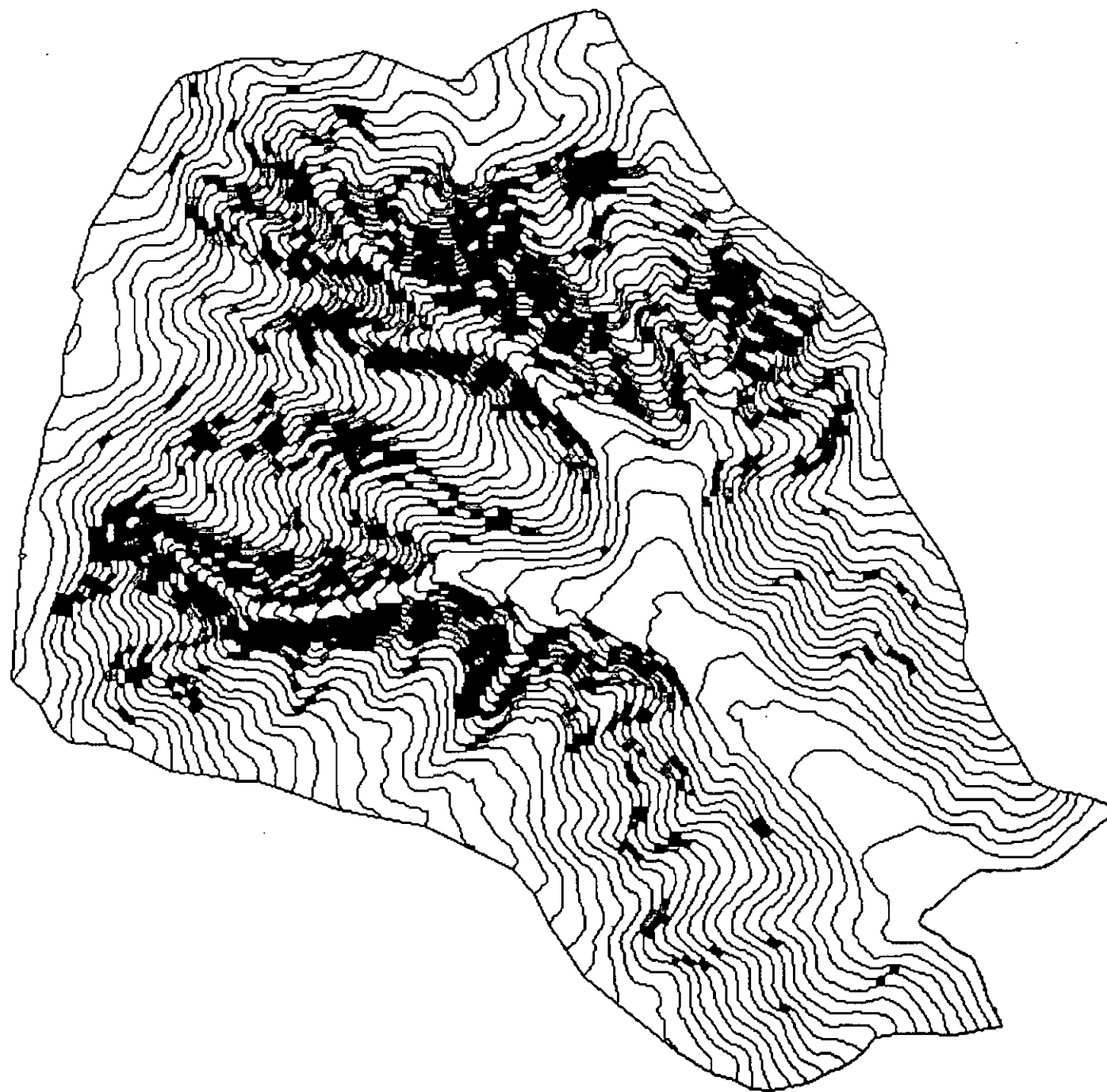


Figure 9B



Rain for Instability

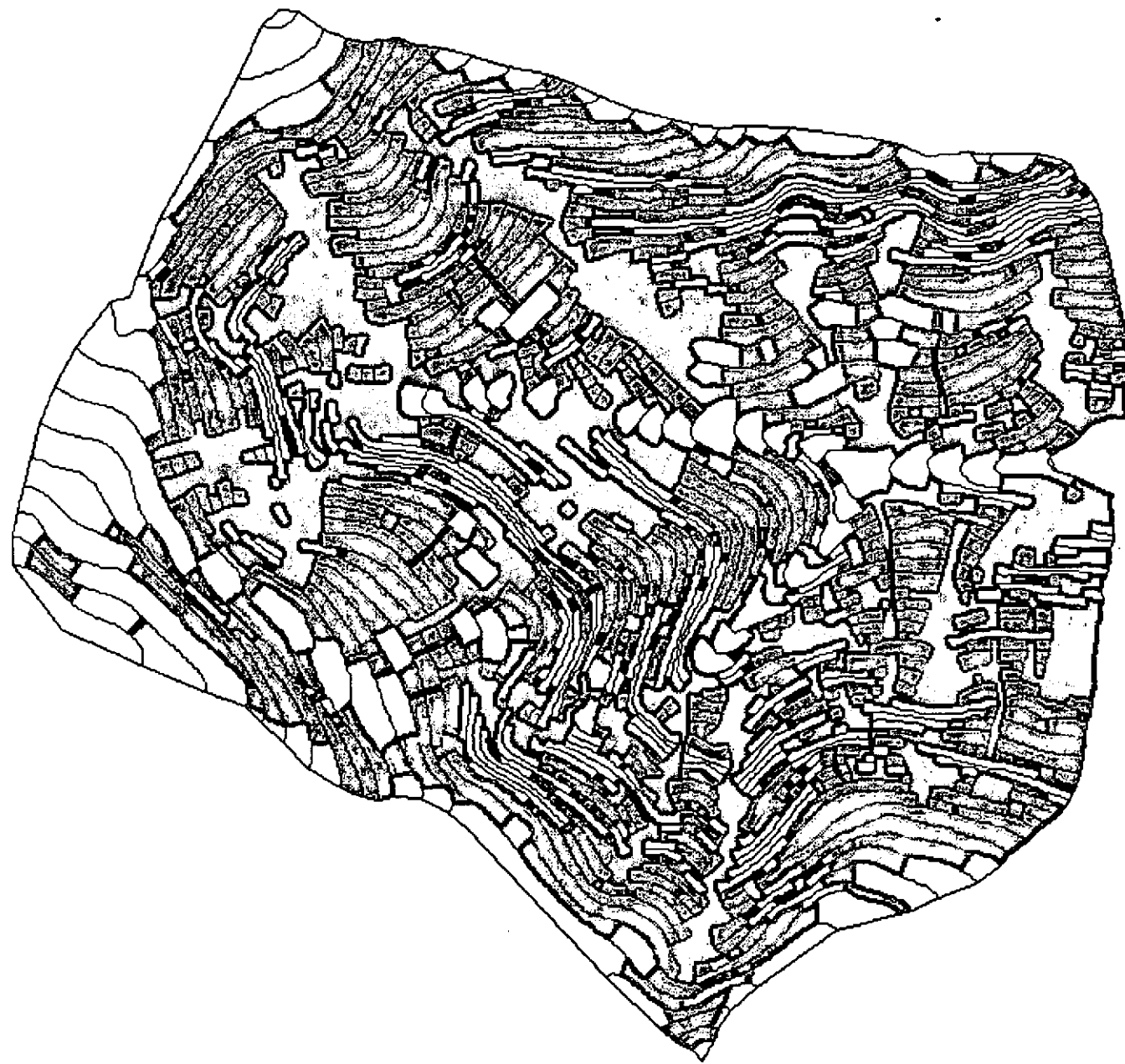
- slope too low
- > 200
- 100 - 200
- 0 - 100
- rock

Tennessee Valley
(Marin County)





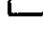
$T = 17.0 \text{ mm}^2/\text{day}$
 $Q = 100 \text{ mm}/\text{day}$
 $\phi = 45 \text{ degrees}$
bulk density =
 $2.0 \text{ gm}/\text{cm}^3$

200.0 meters

Figure 10



Rain for Instability

-  slope too low
-  > 200
-  100 - 200
-  0 - 100
-  rock

Hettman Ridge
(Coos Bay)
Catchment 1

Rainfall Needed
for Instability

$T = 64.8 \text{ mm}^2/\text{day}$
 $\phi = 45 \text{ degrees}$
 bulk density =
 1.6 gm/cm^3

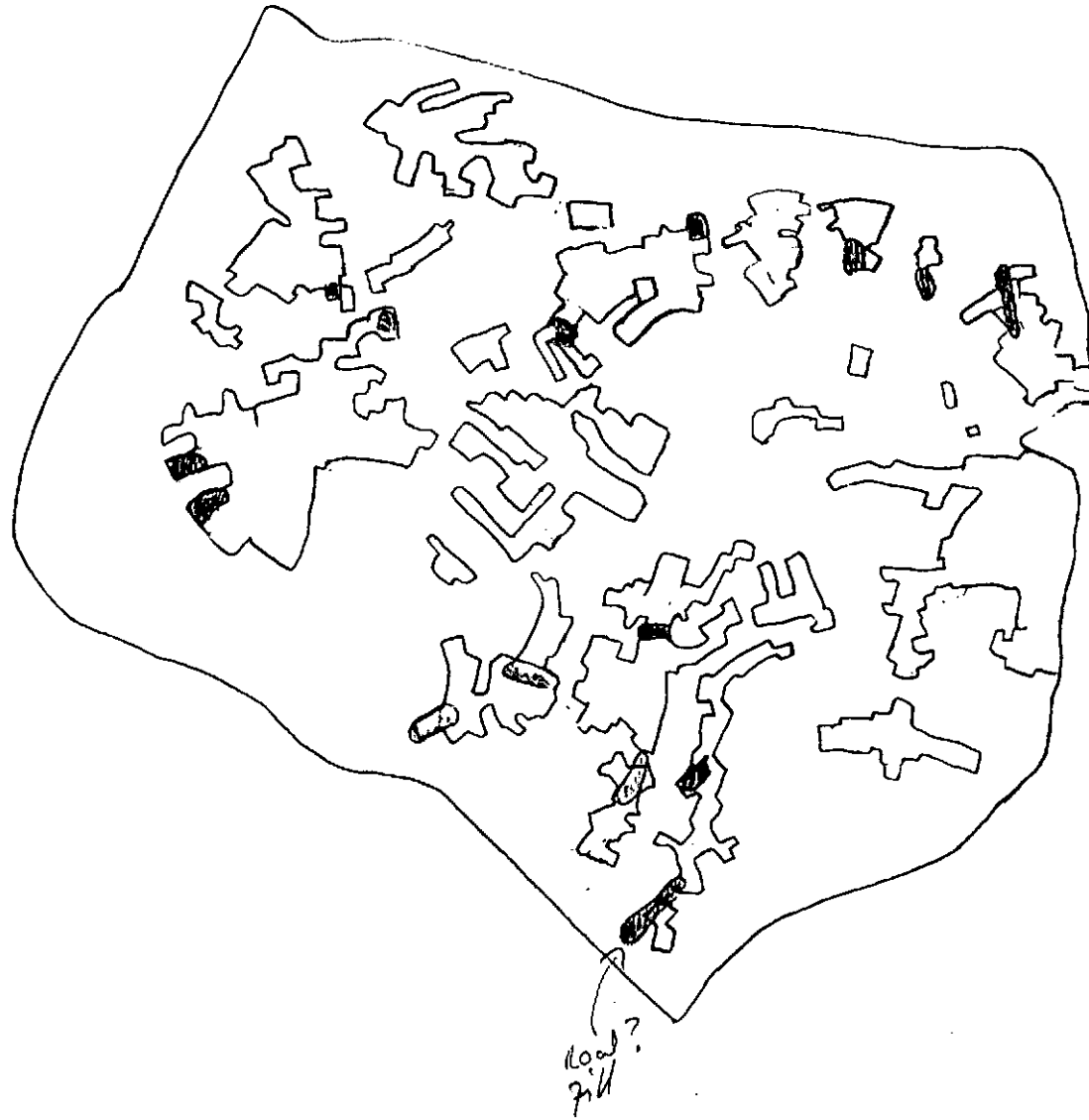
100.0 meters

Figure 11

4
R
explor
...



Figure 12










$q = 200 \text{ mm/day}$

Load?

Figure 13



Slope Stability

-  debris accumulate
-  scoured
-  stable
-  poten. unstable
-  unstable
-  rock
-  rock with flows

Tennessee Valley
(Marin County)

T = 17.0 mm²/day
 Q = 100 mm/day
 phi = 45 degrees
 bulk density =
 2.0 gm/cm³


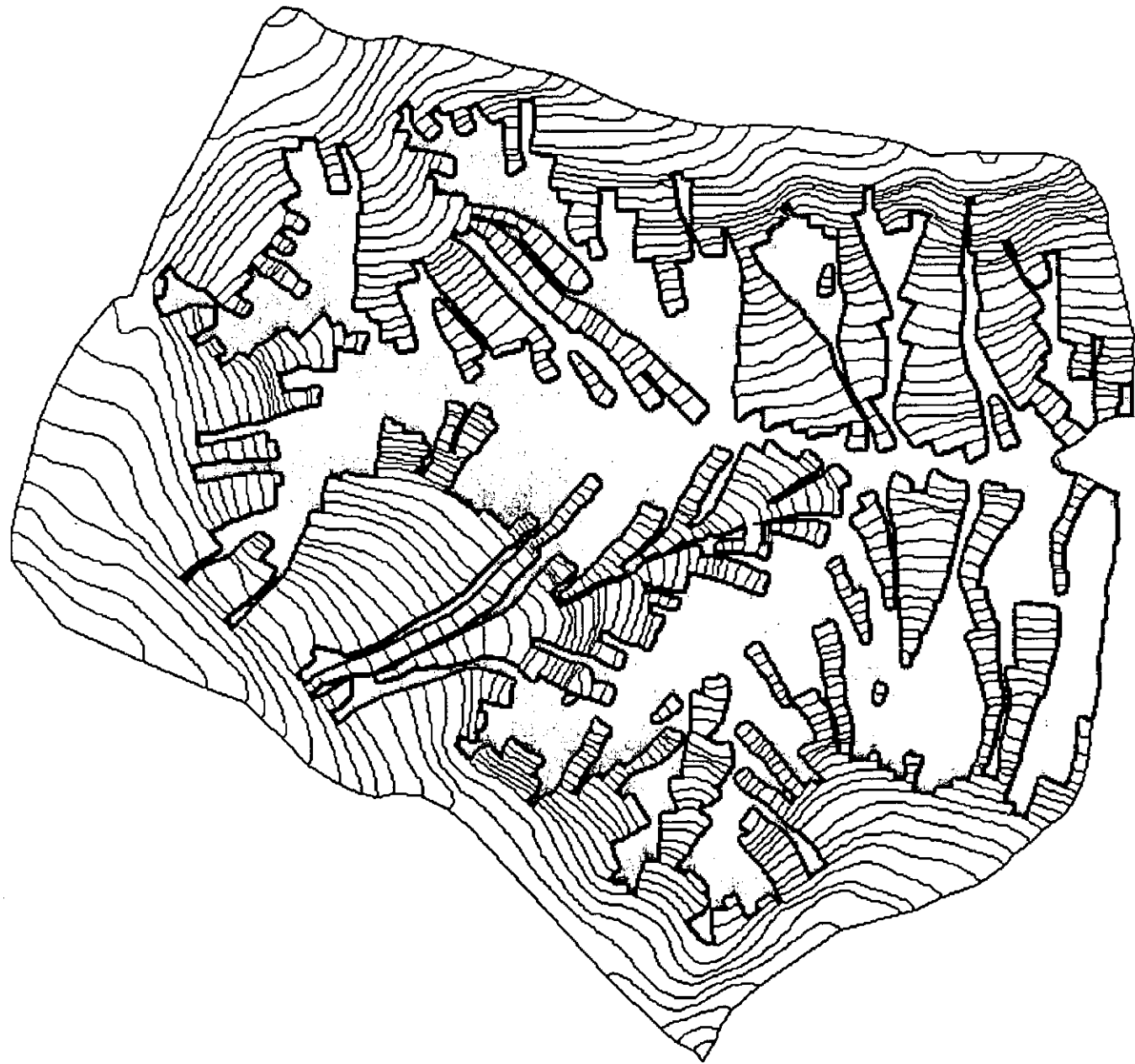








200.0 meters

Figure 14



Slope Stability

-  debris accumulate
-  scoured
-  stable
-  pot. unstable
-  unstable
-  rock
-  rock with flows

Mettman Ridge
 (Coos Bay)
 Catchment 1

$T = 64.8 \text{ mm}^2/\text{day}$
 $Q = 10 \text{ mm}/\text{day}$
 $\phi = 45\text{-degrees}$
 bulk density =
 $1.6 \text{ gm}/\text{cm}^3$

100

100.0 meters

Figure 15

7/8

Appendix 5

Application of Ridge Slope/Height Relationships to Identification of Deep-Seated Mass Failures

Kevin M. Schmidt
Department of Geological Sciences, AJ-20
University of Washington
Seattle, Wa. 98195

We hypothesize that for a given lithology, climate, and tectonic regime there is a limit to the size of stable hillslopes. This hypothesis is based on the observation that an increased slope height, in response to fluvial downcutting for example, results in increased shear stress over a potential failure surface. If the increased shear stress exceeds the shear resistance of the rock, deep-seated landsliding may occur. This suggests that some combination of slope gradient and slope height provides a limit to the stable local relief that we term the "limit to topographic development." Simple force balances can be used to predict the stable combinations of slope angle and maximum slope height for given lithologic geotechnical properties. Application of these concepts to real landscapes, however, is complicated by the heterogeneity of geologic materials at the scale of hillslopes and mountains. Idealized elastic continuum mechanics cannot be strictly applied because a rock mass is a discontinuum characterized by pervasive discontinuities such as faults, joints, and bedding planes. Thus, natural slopes rarely attain heights close to their theoretical maximum (Hoek and Bray, 1977). This study focuses on the relationships between observed ridge height and slope angle for stable and unstable ridges in order to examine the controls on deep-seated mass failures and limits to stable relief development in the discontinuum of real landscapes.

STABILITY ANALYSIS AND CRITICAL SLOPE HEIGHT

The Culmann or sliding-wedge method of slope stability analysis (Culmann, 1866) approximates a failure block as a wedge with a planar failure surface. The maximum stressed surface is a plane passing through the toe of the slope (Spangler, 1960). The force balance of shear stress and shear resistance for this geometric configuration leads to an equation for maximum slope height:

$$H = 4c/\gamma \{ \sin\beta \cos\phi / [1 - \cos(\beta - \phi)] \} \quad (\text{Eq. 1})$$

where c = cohesive shear strength of rock
 γ = unit weight of rock

β = hillslope angle measured with respect to horizontal
 ϕ = internal friction angle

This approach has been applied to clay strata in England by Skempton (1953), to friable loess deposits in Iowa by Lohnes and Handy (1968), and to weathered greywacke in New Zealand by Grant-Taylor (1964), but not in either larger-scale, relatively unweathered bedrock landscapes or in deeply dissected terrain.

STUDY AREA

The Chuckanut Formation, a 20,000 ft. thick stratigraphic package of subaerially deposited sediments, was selected for study because of its relative homogeneity, wide spread aerial extent, and its propensity towards large-scale landsliding. Classified as one of thickest fluvial sequences in North America (Johnson, 1982), this interbedded, well-cemented sandstone and shale extends from the Bellingham, Washington area east to the high relief mountains adjacent to Mt. Baker. These Eocene rocks have been deformed into plunging folds and are often truncated by local faults. Deeply incised glacial deposits are ubiquitous along the mountain fronts and locally form wide benches in the river valleys. Fiksdal and Brunengo (1981) previously mapped mass wasting features and landform types in the Middle Fork of the Nooksack River area. This study supplemented their previous work with stereoscopic mapping from color infra-red aerial photographs flown by N.A.S.A. in 1971. The locations of deep-seated landslides were mapped on 1:24,000 scale blowups and slope base lengths and heights were measured off the basemaps.

APPLICATION OF CULMANN WEDGE ANALYSIS

With the locations of landslide sites identified, a portion of the Nooksack River drainage basin was randomly sampled for the characteristics of: maximum slope angle, vertical slope height, and corresponding horizontal base length. These measurements extend from the ridgeline, down the mountain front to the valley bottom. Several theoretical envelopes define the empirical relations obtained from these transects (Fig. 1). Curve I, the "limit to topographic development," defines the maximum hillslope size present in the landscape. The limits to large-scale landsliding, (curves II & III), define the range over which large-scale landsliding is observed. Curves I-III were fit with Equation 1, uniquely defining combinations of cohesion and internal friction angle for this material. A number of stable ridges plot above the failures enclosed by curves II & III suggesting the destabilizing influence of joints and bedding

planes. The geotechnical properties implied by these threshold curves reflect the sum-total of all the stability influences, both in the present and observable past. The *in situ* properties characteristic of the Chuckanut Formation record the minimum strength mobilized since deglaciation. It should be noted that the geotechnical properties obtained through this method are quite conservative in that they represent response to the most destabilizing conditions present in the history of the slope. The space bracketed by thresholds I and III spans a range in the internal angle of friction of 40% and a 65% variation in cohesion.

The present stability of slopes above 2400 ft. in height can be partially explained by the buttressing of the lower portions of hillslopes with glacial-fluvial deposits. Of the fourteen sites in Figure 2 which plot above 6400 ft. in base length, eight sites are recognized landslides and six are presently stable, but are buttressed by glacial deposits at the toe of the slope. Prominent benches of glacial sediments are present along Clearwater Creek and the Middle Fork of the Nooksack River. Up to 500 ft. thick, this material decreases the average slope from ridge top to valley bottom and buttresses the toe of the slope, allowing higher ridges to be stable than might otherwise be possible. However, these glacial benches themselves are rapidly eroding. Undercutting by streams causes over-steepening of the channel banks inducing progressive slope failure. Along the middle reach of the Middle Nooksack River, slumping is common where the inner gorge has incised deeply with steep channel banks nearing 70 degrees. These unstable, incised reaches have high potential for impacting stream channels through rapid introduction of large volumes of sediment from slope failure.

PROPOSED FIELD WORK

Because of their proposed role in stabilizing bedrock slopes, threshold curves similar to those in Figure 1 should be defined for the glacially derived benches. To achieve this goal, higher resolution data than can be obtained from aerial photographs or U.S.G.S. 1:24,000 scale quadrangles is required. Field surveying along the banks of the Middle Fork of the Nooksack River has been planned for the summer of 1992. Subsequent application of stability thresholds will aid in assessing both the magnitude of the short-term sediment input from the channel banks as well as the long-term influence in buttressing the bedrock slopes.

WORK IN PROGRESS

The site locations depicted in Figures 1 & 2 are situated in unstable high relief terrain which plot close to the stability thresholds. Current mapping efforts will extend the classification of the stable and unstable sites west toward the city of Bellingham. This extension into low relief areas will help to fill in the balance of low slope/low height and high slope/low height space in Figure 1. Once the thresholds are properly defined, the method may be applied in a predictive sense to highlight areas of potential instability with the aid of digital elevation models.

REFERENCES

- Culmann, C., 1866, Graphische Statik: Zurich.
- Fiksdal, A.J. and Brunengo, M.J., 1981, Forest slope stability project phase II, Washington State Department of Ecology, WDOE 81-14, 62 p.
- Grant-Taylor, T.L., 1964, Stable angles in Wellington greywacke, New Zealand Engineering, vol. 19 (4), p. 129-130.
- Hoek, E. and Bray, J.W., 1977, Rock Slope Engineering (2nd ed): Institute of Mining and Metallurgy, London.
- Johnson, S.Y., 1982, Stratigraphy, Sedimentology, and Tectonic Setting of the Eocene Chuckanut Formation, Northwest Washington: Ph.D. dissertation, Department of Geological Sciences, University of Washington, Seattle Wa.
- Lohnes, R.A. and Handy, R.L., 1968, Slope angles in friable loess, The Journal of Geology, vol. 76, p. 247-258.
- Skempton, A.W., 1953, Soil mechanics in relation to geology, Proceedings of Yorkshire Geological Society, vol. 29 (1) #3, p.33-62.
- Spangler, M.G., 1960, Soil engineering (2nd ed): New York, International Textbook Co., 483 p.

FIGURE CAPTIONS

Figure 1

Plot of maximum slope versus ridge height for Chuckanut Formation sites in the Middle Fork of the Nooksack River

region. Large open circles denote recognized deep-seated landslide sites while solid circles represent currently stable ridges. Theoretical predictions based on equation 1 (curves I,II, and III) represent: the limit to topographic development (curve I), the apparent upper limit to large scale landsliding (curve II), and the lower boundary to large scale landsliding (curve III).

Figure 2

Plot of horizontal base length versus corresponding ridge height. Large open circles denote recognized deep-seated landslide sites while solid circles represent currently stable hillslopes. Above 6400 ft. in base length, all the presently stable slopes are buttressed by glacial deposits. The landslide sites above 6400 ft. in base length are easily recognized on aerial photographs, even though they may be thousands of years old.

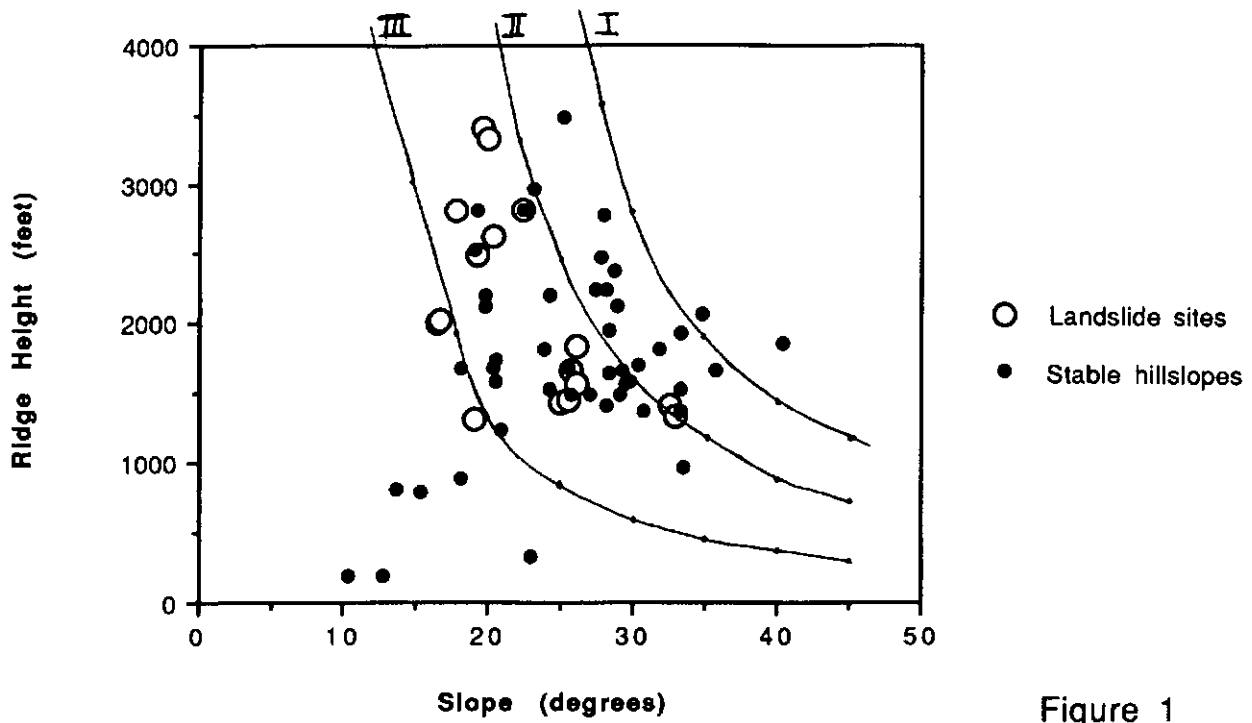


Figure 1

Threshold curve	Friction angle (degrees)	Cohesion (lb/sq. ft.)	Unit weight (lb/cubic ft.)
I	13	10000	160
II	11	7000	160
III	8	3500	160

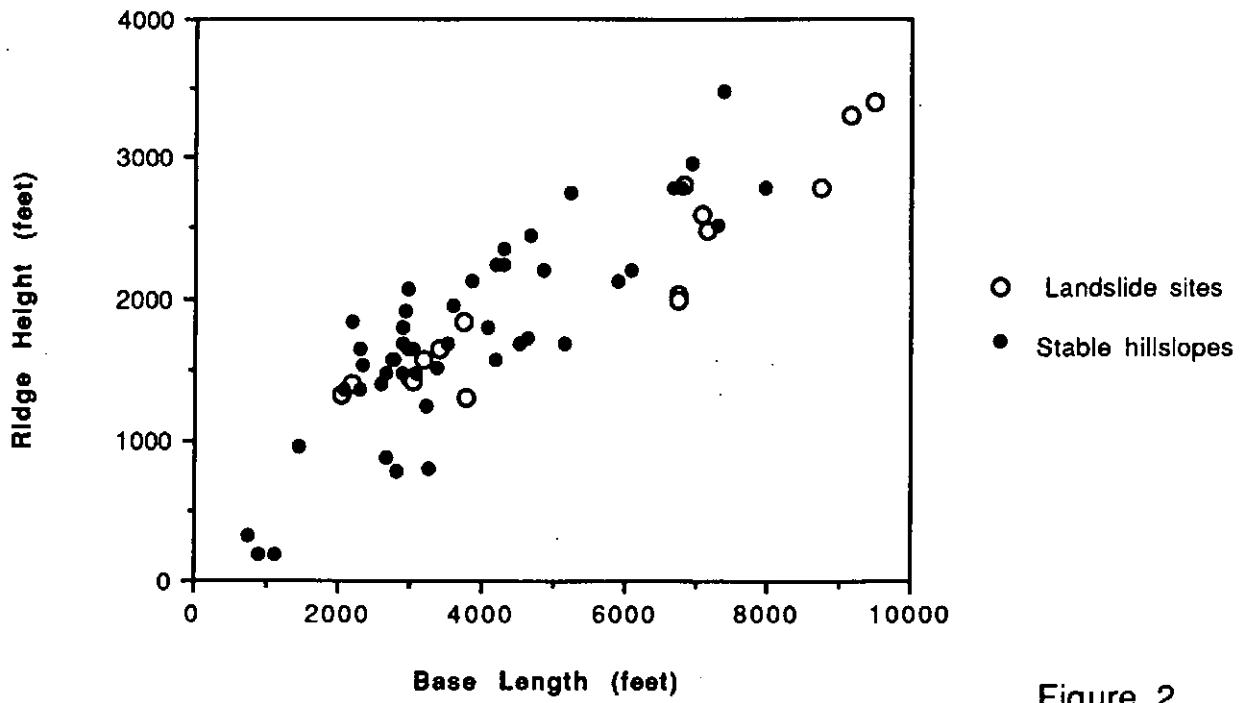


Figure 2

Appendix 6

Channel classification, assessment of channel conditions,
and the prediction of channel response.

David R. Montgomery and John M. Buffington
Department of Geological Sciences
University of Washington
Seattle, WA 98195

for submission to the SHAMW committee of the TFW agreement

ABSTRACT	1
INTRODUCTION	4
THEORETICAL BASIS FOR INTERPRETING CHANNEL ADJUSTMENTS	6
Conceptual Response Models	10
EMPIRICAL STUDIES OF CHANNEL CHANGES	13
Sediment Supply	13
Discharge	17
Dams	19
Vegetation	20
CHANNEL CLASSIFICATIONS	21
LANDSCAPE CLASSIFICATION	26
Hillslopes	26
Hollows	27
Channels	28
Sediment Supply and Transport Capacity	29
Channel Morphology	30
Colluvial Channels	31
Bedrock Channels	33
Alluvial Channels	33
Cascade Channels	34
Step-Pool Channels	36
Plane Bed Channels	38
Pool-Riffle Channels	39
Regime Channels	43
Braided Channels	44
Confinement	44
Large Woody Debris	46
Debris Flows	46
PROPOSED CHANNEL CLASSIFICATION SCHEME	48
HYPOTHESIZED ORIGIN OF CHANNEL TYPES AND VALLEY CONFINEMENT	51
RESPONSE TO ALTERED DISCHARGE REGIME AND SEDIMENT SUPPLY	54
Hillslopes	55
Hollows	55
Channels	56
Colluvial Channels	56
Bedrock Channels	57
Alluvial Channels	58
Cascade Channels	58
Step-Pool Channels	58
Plane Bed Channels	59
Pool-Riffle Channels	60
Regime Channels	61
Braided Channels	61
Large Woody Debris	61
Debris Flows	62
Confined vs. Unconfined Channels	63
Disturbance Frequency, Magnitude, and Recovery Time	64
Summary of Potential Channel Responses	64
ASSESSING PAST CHANNEL CHANGES	65
ASSESSING SUSCEPTIBILITY TO FUTURE CHANGES	69
SUMMARY	75
ACKNOWLEDGEMENTS	75
REFERENCES CITED	76
FIGURE CAPTIONS	93

ABSTRACT

A process-based landscape and channel classification system is proposed as a framework for assessing watershed response to natural and anthropogenic environmental change. Landscapes can be divided into hillslopes and valleys based on both morphological and process-based criteria. Hillslopes are the undissected radially divergent portions of the landscape characterized by downslope divergence of topographically-driven run-off and sediment transport. Due to the lack of topographic convergence, hillslope sediment transport processes are primarily slope and gravity-driven and independent of discharge. Consequently, hillslopes are relatively insensitive to changes in basin hydrology from either land use or climate change. Valleys, however, are regions of the landscape that focus runoff and sediment transport through downslope topographic convergence; they may be either channeled or unchanneled, but both are sensitive to changes in watershed hydrology. Hollows are the unchanneled valleys that occupy the upslope tips of drainage networks and temporarily store sediment delivered from surrounding hillslopes. Steep slopes, thick colluvial soils, and concentration of near-surface throughflow make hollows sites of periodic instability. Over geomorphic time scales, the colluvial soils that accumulate in hollows are intermittently destabilized resulting in a cyclic process of hollow filling and erosion. In contrast, channeled valleys are characterized by flow and sediment transport within defined banks, or channels. Fluvial sediment transport processes within channels are dependent upon both discharge and sediment supply. Sediment is delivered to channels at a relatively constant rate from hillslopes, intermittently from hollows, and may be eroded from the valley bottom by flow within channels. In a landscape context, the response of hillslopes, hollows, and channels to perturbations in sediment supply or hydraulic discharge is linked through sediment routing and storage; specifically in the style and frequency of sediment delivery to channels and the capacity of channels to transport the delivered sediment.

Hillslopes and hollows respond in relatively predictable ways to altered sediment supply or discharge, but channel response is more complicated and dependent on the specific channel morphology. Before any predictions can be made regarding channel response to perturbation, it is first necessary to discriminate channel morphologies in a process-based framework. We hypothesize that observed systematic and local downstream changes in channel morphology and channel roughness correlate with changes in sediment supply (size and amount of material available for transport) and transport capacity (essentially a function of the available shear stress). Furthermore, we recognize that although sediment transport dynamics differ for each channel type, a general distinction can be made between supply-limited and transport-limited channels.

Our proposed channel classification system relies on a process-based interpretation of channel bed morphology, confinement, and large woody debris loading. The most general channel classification distinguishes colluvial, alluvial, and bedrock channels. Alluvial channels may be subdivided into distinct channel types based on sediment transport characteristics, channel roughness elements, and bedforms. We suggest that these distinct bed morphologies reflect different roughness configurations related to downstream energy loss and sediment supply. Channels in which multiple scale mobile bedforms occur in response to hydraulic regime are termed regime channels; those with multiple longitudinal bars are termed braided channels; streams with predominantly stable laterally oscillatory bedforms are termed pool-riffle channels; those lacking distinct bedforms are termed plane bed channels; reaches with vertically oscillatory channel spanning bedforms are termed step-pool channels; while those in which tumbling flow over disorganized large clasts that provide the primary roughness are termed cascade channels. Preliminary data indicate that this suite of channel types may be distinguished on a plot of channel slope versus relative roughness, defined as the ratio of bankfull flow depth to the size of the coarsest bed material. Other channel types also are identified on the basis of bed morphology and sediment transport characteristics. Bedrock channels lack a continuous alluvial cover. Colluvial channels are those in which fluvial sediment transport maintains a channel, but in which colluvium tends to accumulate within the valley between intermittent scouring events.

We hypothesize that these channel types reflect relations between sediment supply and transport capacity. A bedrock channel bed implies an excess of transport capacity over sediment load. In contrast, colluvial channels have an excess of sediment supply and are primarily transport limited. Alluvial channels may be either supply or transport limited. Braided channels, for example, have abundant sediment available for transport and thus are transport limited. Regime, pool-riffle, and plane bed channels respond to increased sediment supply by channel or bedform modifications due to low transport capacity and thus also may be considered to be transport limited. Step-pool and cascade channels have a high transport capacity relative to sediment supply and rapidly transport increased sediment loads with little morphologic change. Consequently, sediment transport in them may be considered to be supply-limited.

Channel confinement may serve as an indication of the long-term balance between sediment supply and transport capacity. Channels confined by narrow valley walls do not accumulate sediment in floodplain storage and thus have a high transport capacity relative to sediment supply. In contrast, unconfined channels with significant floodplain storage indicate a long-term excess of sediment supply. Channel confinement thus serves as a

general indicator of potential channel response to changes in sediment supply or discharge. The supply of large woody debris (LWD) also influences channel morphology and potential channel responses. In large channels, LWD acts essentially as sediment and provides only temporary grain buttressing and storage. In contrast, LWD in small channels forms important roughness elements, provides significant sediment storage, and may influence channel morphogenesis.

Potential response to perturbations in discharge or sediment load can be examined by channel type and in the context of supply- or transport-limited regimes. Supply-limited channels will tend to maintain their morphology while transmitting increased sediment loads to downslope transport-limited channels. In contrast, transport-limited channels may change their geometry, bed morphology, or substrate in response to increased sediment loads. Changes in sediment supply and transport capacity may result in similar or opposing effects. Thus, neither can be realistically examined in isolation. Both need to be considered when analyzing watershed impacts. Assessing past changes in channel conditions and predicting likely responses to future changes may require different approaches. Moreover, it is vital to focus on aspects of channel morphology and dynamics that are sensitive indicators of perturbation. As different channel reaches have different response potential, it is imperative to consider the specific channel type, as well as its relation to the rest of the channel network. A number of quantitative and qualitative approaches provide insight into reconstructing watershed impacts and for predicting potential responses to continuing or anticipated watershed disturbance.

Appendix 7

**Channel Assessment and Relative Roughness Partitioning
In Gravel-bedded Streams**

**(Draft masters thesis proposal in conjunction with the
Geomorphological Watershed Analysis Project)**

**John M. Buffington
Geological Sciences, AJ-20
University of Washington
Seattle, Wa. 98195**

5/18/92

Introduction

An important problem in watershed analysis is quantitatively assessing the state of a given channel. We would like to know how "healthy" a channel is, and in particular how sensitive it is to increased sediment impacts (natural or anthropogenic). The first step in any sort of predictive channel response model is to assess the current state of the channel, and to recognize the limits of potential response. The principal investigators of the Geomorphological Watershed Analysis Project proposed the use of a bankfull threshold channel model in conjunction with an assessment of the channel efficiency (as proposed by *Dietrich et al., 1989*) in order to determine the condition of a channel.

Theory

Based on field observations the threshold for significant bedload transport in heterogeneous gravel-bedded channels occurs at the bankfull stage. The total bankfull boundary shear stress, τ_b , for this case is

$$\tau_b = \rho_w g h S \quad (\text{eqn 1})$$

where ρ_w is the density of water, g is the gravitational acceleration, h is the average bankfull depth, and S is the water surface slope, approximating the energy slope. The median bed grain size, D_{50} , is commonly used in sediment transport equations to characterize the shear stress necessary to mobilize a bed of mixed grain sizes. Thus, τ_b is the critical shear stress required to mobilize D_{50} . The corresponding dimensionless shear stress, τ_* , is

$$\tau_* = \tau_b / (\rho_s - \rho_w) g D_{50} \quad (\text{eqn 2})$$

where ρ_s is the sediment density. Combining these two equations produces an expression relating D_{50} to depth, h , and slope, S :

$$D_{50} = 13.47 (hS) \quad (\text{eqn 3})$$

such that ρ_s and ρ_w are equal to 2.65 and 1.0 g/cm³ respectively, g is the gravitational constant, and τ_* is empirically determined to be 0.045 (*Komar, 1987*). Equation (3) allows one to predict from simple channel geometries the D_{50} for a bankfull threshold channel. This

model assumes that all of the channel roughness is caused by the grain roughness (a common assumption for gravel-bedded rivers).

It has been observed that stream beds fine in response to increased sediment supply and coarsen (armor) if deprived of sediment (*Dietrich et al., 1989; Kuhnle & Southard, 1988; and others*). *Dietrich et al. (1989)* argued that bed fining is a dynamic response that allows the channel to carry the imposed load without significant aggradation. They (*Dietrich et al., 1989*) proposed a dimensionless ratio, q_* , that assesses the efficiency of a channel to carry the load imposed on it (i.e. assessing the channel condition in terms of transport capacity and sediment supply):

$$q_* = \left(\frac{\tau_b - \tau_{cs}}{\tau_b - \tau_{cl}} \right)^{1.5} = \left(\frac{\tau_b - \alpha \frac{D_{50s}}{D_{50l}}}{\tau_b - 1} \right)^{1.5} \quad (4)$$

such that

$$q_b = k(\tau_b - \tau_c)^n \quad (\text{eqn 5})$$

where q_b is the bedload transport rate, k and n are empirically determined (n is approximately equal to 1.5), τ_{cs} and τ_{cl} are the critical boundary shear stresses of the surface and sub-surface, α is a constant equal to 1 for gravel with uniform specific gravity, and D_{50s} and D_{50l} are the median grain sizes of the surface and load respectively; here the bedload and sub-surface grain size distributions are assumed equal. This ratio normalizes the surface transport rate by the transport rate for a surface as fine as the sub-surface or load. D_{50l} represents the limit of possible bed fining (without aggradation). Equation (4) gives an index to the channel competence, in that as channels approach q_* values of 1 they are close to their capacity in terms of sediment load; channels with low q_* values are much more resilient to increased sediment supply (Fig. 1).

A quantitative channel assessment in terms of sediment supply can be made by combining the q_* theory with the threshold channel prediction (eqn. 3). The τ_c value of equation (3) is representative of well armored (low sediment supply) heterogeneous bed surfaces. Thus, equation (3) provides a theoretical reference point from which to analyze impacts to the channel from increased sediment load, while q_* provides an independent measure of the state of the channel. Putting q_* in terms of the bankfull threshold model, a 1 m deep channel with a low q_* value (low sediment supply and armored bed) would plot very close to the predicted 1 m threshold curve (Fig. 2), while similar channels with progressively higher q_* values (high

sediment supply and bed fining) would plot progressively further from the predicted curve (Fig. 2). The bankful threshold channel curves set the physical limit to bed armoring due to decreased sediment input, while the sub-surface grain size distribution of a given site limits the maximum bed fining response (without aggradation) to increased sediment load.

Research Investigation of the Theory

In order to test the validity of the bankful threshold channel model a literary search of previous stream studies providing relevant information was conducted; some preliminary results follow. Figure 3 compares the ratio of surface D_{50} to sub-surface D_{50} versus the difference between the threshold channel predicted surface D_{50} and the observed surface D_{50} . It is clear that the well armored beds ($D_{50s}/D_{50ss} > 1$) show the smallest deviation of observed D_{50} from predicted D_{50} ; similarly the beds that have fined ($D_{50s}/D_{50ss} \approx 1$) show the largest deviation from the predicted surface D_{50} . There are a few anomalous points that show actual D_{50} values greater than predicted; this may reflect the range of uncertainty in the empirically derived value of τ_* .

Figure 4 shows the same data plotted as the channel depth-slope product versus D_{50} . Again note that in general the D_{50ss} values plot below the D_{50s} values; with the magnitude of difference reflecting the degree of surface armoring. Note that while there is some scatter around the predicted threshold channel curve, most of the surface D_{50} values plot below the predicted curve. We have interpreted this to indicate surface fining, but it could also be argued that there are other roughness elements (e.g. bedforms and obstructions, Fig. 2) that need to be considered in the energy balance of the channel. It is commonly assumed that grain roughness is the dominant form of channel roughness in gravel bedded rivers. This is true for the flume data shown in Figure 4. *Kuhnle and Southard (1988)* conducted flume experiments in which they varied channel slope, width, discharge, and sediment feed rate. They found that runs with low feed rates produced armored beds (points closest to the predicted curve, Fig. 4), while a run with a high feed rate caused surface fining to the point of approximating the bedload D_{50} size (Fig. 4). During their experiments bedforms began to develop only for the run with the highest sediment feed rate. *Kinerson's (1990)* study (Fig 4) controlled for channel sinuosity and obstructions, but the relative effect of bedforms on the data is uncertain.

In Figure 5 data from old growth and clear cut gravel-bedded channels in southeast Alaska are presented. The clear cut channels were cut down to their banks and have had most of the in-channel debris removed, as was common practice in the 1960's. The clear cut channels have had about 25 years to recover (the data was collected during 1988-1990), and while there are distinct morphological differences between the channels it is believed that these differences are predominantly due to the relative differences in LWD loading (*Smith and Buffington, 1991*). Interestingly, Figure 5 clearly shows that the debris-poor channels have

coarser median grain sizes than the old growth debris-rich channels. In other words, the old growth channels may be plotting below the debris-poor channels and the predicted threshold channel curve, because of the additional roughness effects and energy dissipation caused by the LWD. Although there is a lot of scatter, Figure 6 shows that there may be some potential in empirically describing the relative effects of LWD and other obstructions on channel morphology and response.

The data found to date in the literature are all plotted in Figure 7. There is an obvious distinction between the data for gravel channels and that for sand bedded rivers; the bankful threshold channel model does not apply to sand bedded rivers, because the roughness elements for those channels are dominated by bedforms and not by grain roughness. Again most of the gravel bedded streams plot below the predicted threshold curve. Nevertheless, there is a gross trend to the data, lending credence to the concept of a consistent relation of slope and grain size. Although Figure 7 is a log-log plot and the scatter is significant, there may be more distinct slope/grain size relations along a given channel or for channels in regionally similar environments. Figure 8 is the same plot with the 1990 TFW/Ambient Monitoring Project data superimposed. The Ambient data shows considerably more scatter. This greater scatter may be real, but may also reflect the effects of small pebble count sampling sizes and averaging of data over long reaches with potentially varied morphologies.

Discussion

The flume data of Figure 4 indicate that the bankful threshold channel model serves as a useful theoretical reference point for assessing the state of a channel in terms of sediment supply. While it may be attractive to interpret *Kinerson's (1990)* data as also validating the threshold model, the effects of other roughness elements on channel response are not well known. The Alaska data further suggest that LWD and other obstructions may play an important role in energy dissipation and channel response to perturbation. In order to properly partition the kinematic energy of the channel over the various roughness elements, detailed studies aimed at isolating each effect are warranted. This will involve evaluating an effective bankfull boundary shear stress as modified by roughness elements in addition to grain roughness. This effective shear stress will replace the depth-slope shear stress in equation (3) and define the theoretical D_{50} for a well armored bankful threshold channel; essentially defining a threshold channel curve lower than that predicted for a channel where grain roughness characterizes the total channel roughness. A q_* channel assessment of sediment load impacts will then be relative to the effective threshold curve. While a general examination of variation in typical D_{50} sizes between channels with distinctly different roughness elements may empirically determine characteristic zones of response (e.g. Figs 5 and 6), an evaluation of the effective boundary shear stress is necessary to truly partition roughness elements and properly assess channel

response to increased sediment supply. Theoretical calculations that describe the mechanics and predict the effects of roughness partitioning would also provide a valuable addition to understanding the problem. This sort of channel evaluation is essential to predicting stream response to changes in sediment supply and would be valuable in a watershed sediment budget model.

Proposed Data Collection

Following the suggestions above, data collection will involve:

- 1) An initial characterization of channel geometries (bankful width, depth, and slope) to be used to predict the theoretical D_{50} for an equivalent armored threshold channel in which roughness is characterized by grain roughness.
- 2) Detailed surveys of actual gravel bed textures aimed at quantifying spatially averaged bed response to the introduction of roughness elements. Bed textures will be mapped in progressively more complex channels with progressively more roughness elements (i.e. starting from a straight plane bed channel and progressively adding bedforms, sinuosity, and LWD and other obstructions).
- 3) Characterization of typical surface and sub-surface grain size distributions for each of the texture mapping units in (2) to assess spatially averaged response to sediment loading.
- 4) Evaluation of typical effective basal shear velocities affecting sediment transport and creating the observed bed textures.

Although the data will be gathered in some detail, they will essentially be used to characterize roughness partitioning and sediment supply impacts over reach scales.

References

Dietrich, W.E., Kirchner, J. W., Ikeda, H., and Iseya, F., Sediment supply and the development of coarse surface layer in gravel-bedded rivers, *Nature*, v. 3340, no. 6230, p. 215-217, 1989.

Florsheim, J. L., Fluvial requirements for gravel bed formation in northwestern California, unpublished MS thesis, Humboldt State University, Ca., 1985.

Kinerson, D., Bed surface response to sediment supply, unpublished MS thesis, University of California, Ca., 1990

Komar, P. D., Selective grain entrainment by a current from a bed of mixed sizes: A reanalysis, *J. Sed. Petrology.*, v. 57, no. 2, p. 203-211, 1987.

Kuhnle, R. A. and J. B. Southard, Bed load transport fluctuations in a gravel bed laboratory channel, *Water Resources Res.*, v. 24, no. 2, p. 247-260, 1988.

Smith, R. D. and J. M. Buffington, Effects of LWD on channel unit distribution in southeast Alaska, extended abstract, presented at Watershed 1991, USFS conference, Juneau, Ak., unpublished ?, 1991.

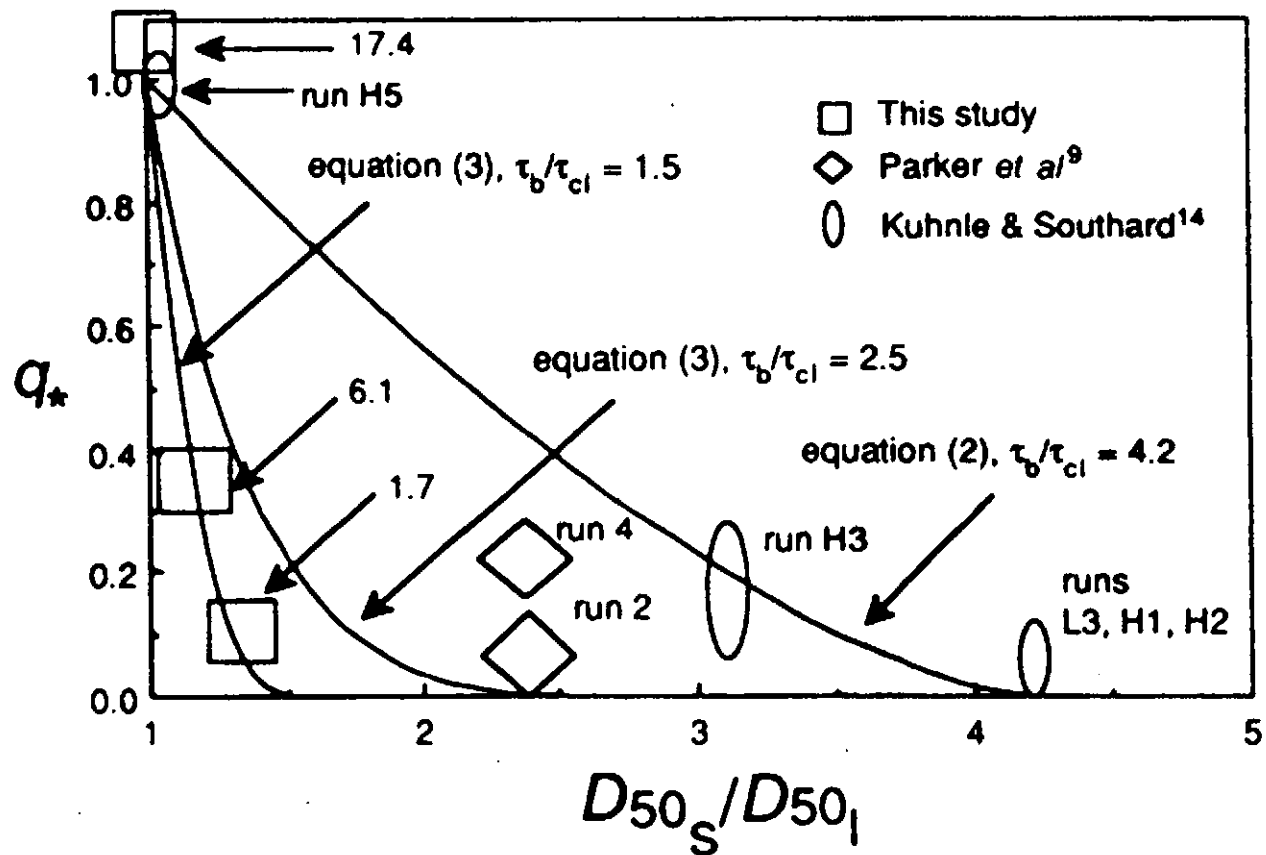


FIG. 1

Comparison of the predicted transport ratio q_* as a function of median grain diameter (D_{50}) ratio, with the observed transport ratio and grain ratio at transport rates of 17.4, 6.1, and 1.7 g min^{-1} per cm width. The symbol size represents the approximate range of observed values for each run. (TAKEN FROM DIETRICH ET AL., 1989)

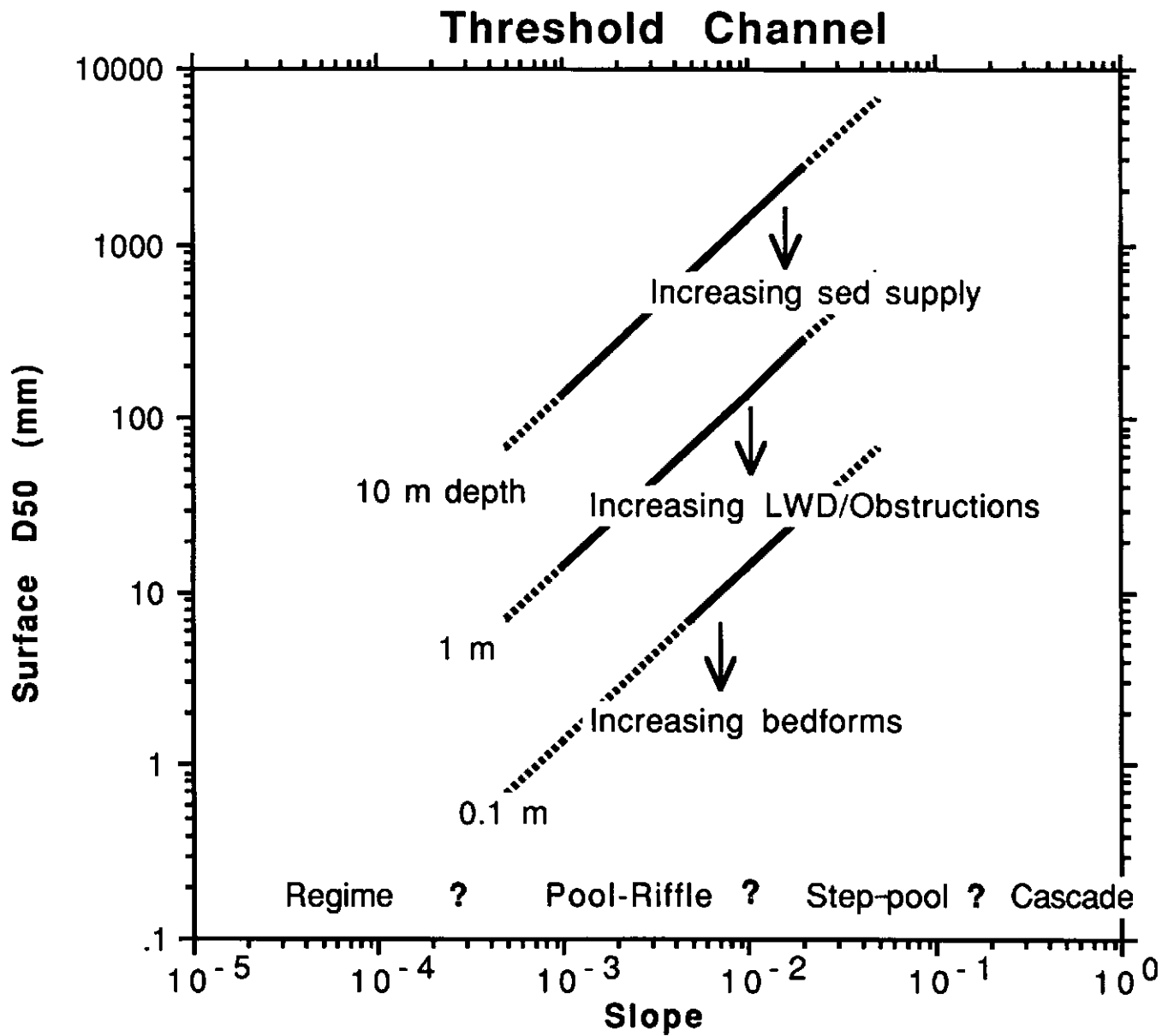


FIG. 2

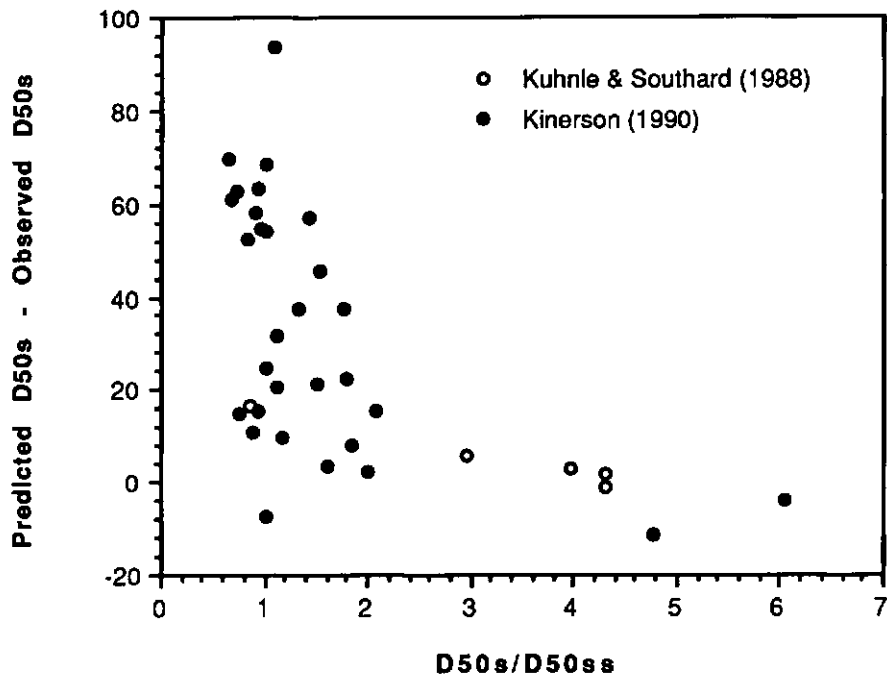


Fig. 3

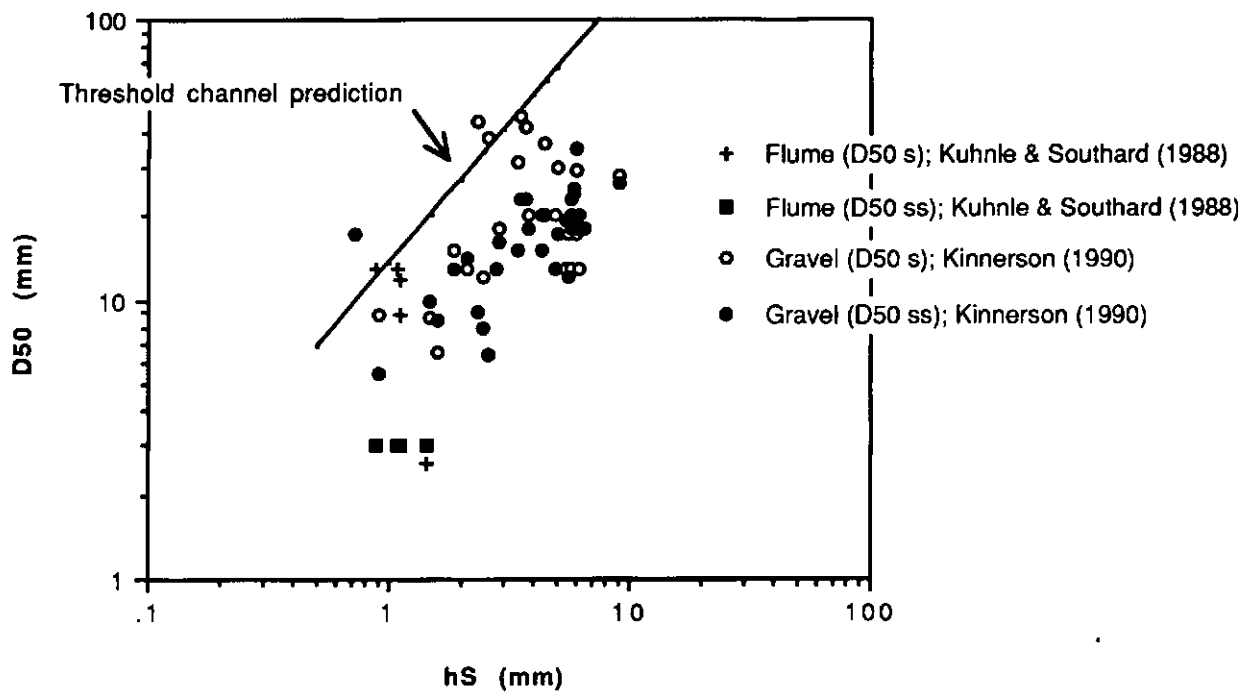


Fig. 4

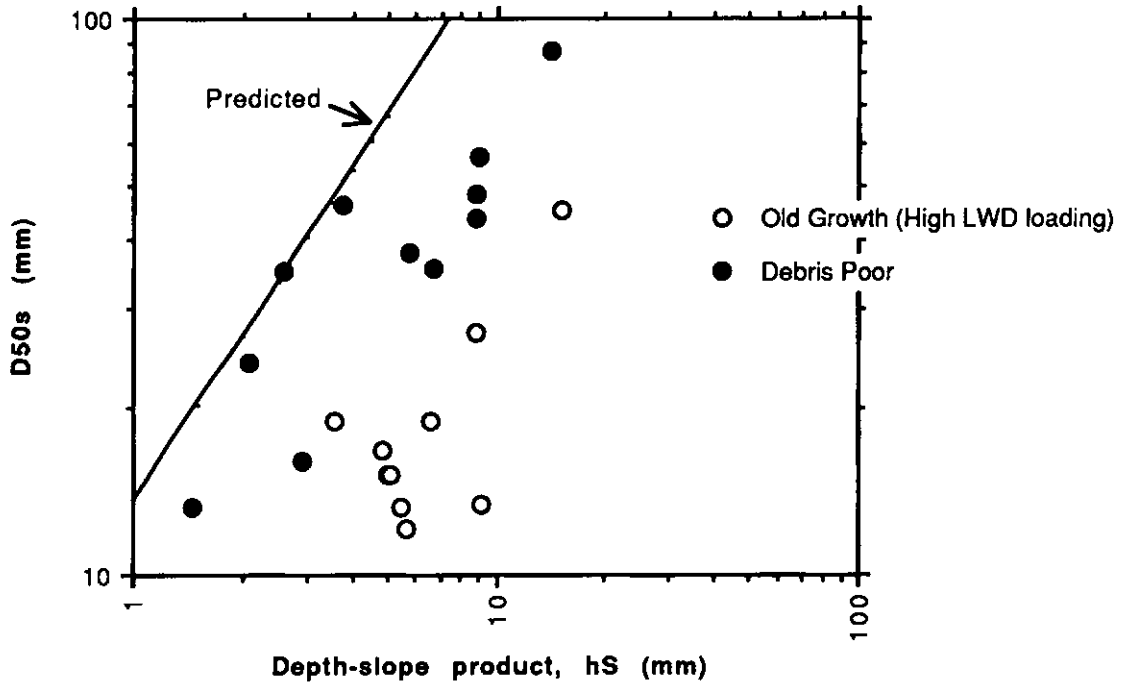


Fig. 5

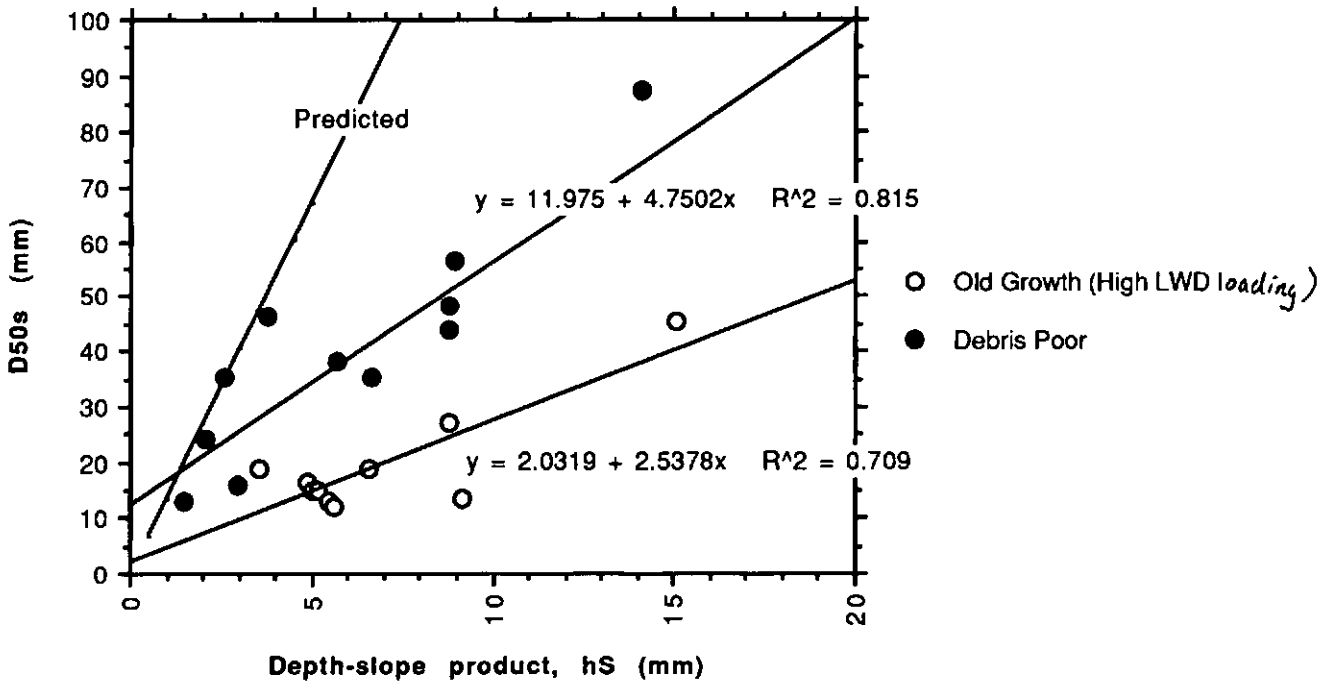


Fig. 6

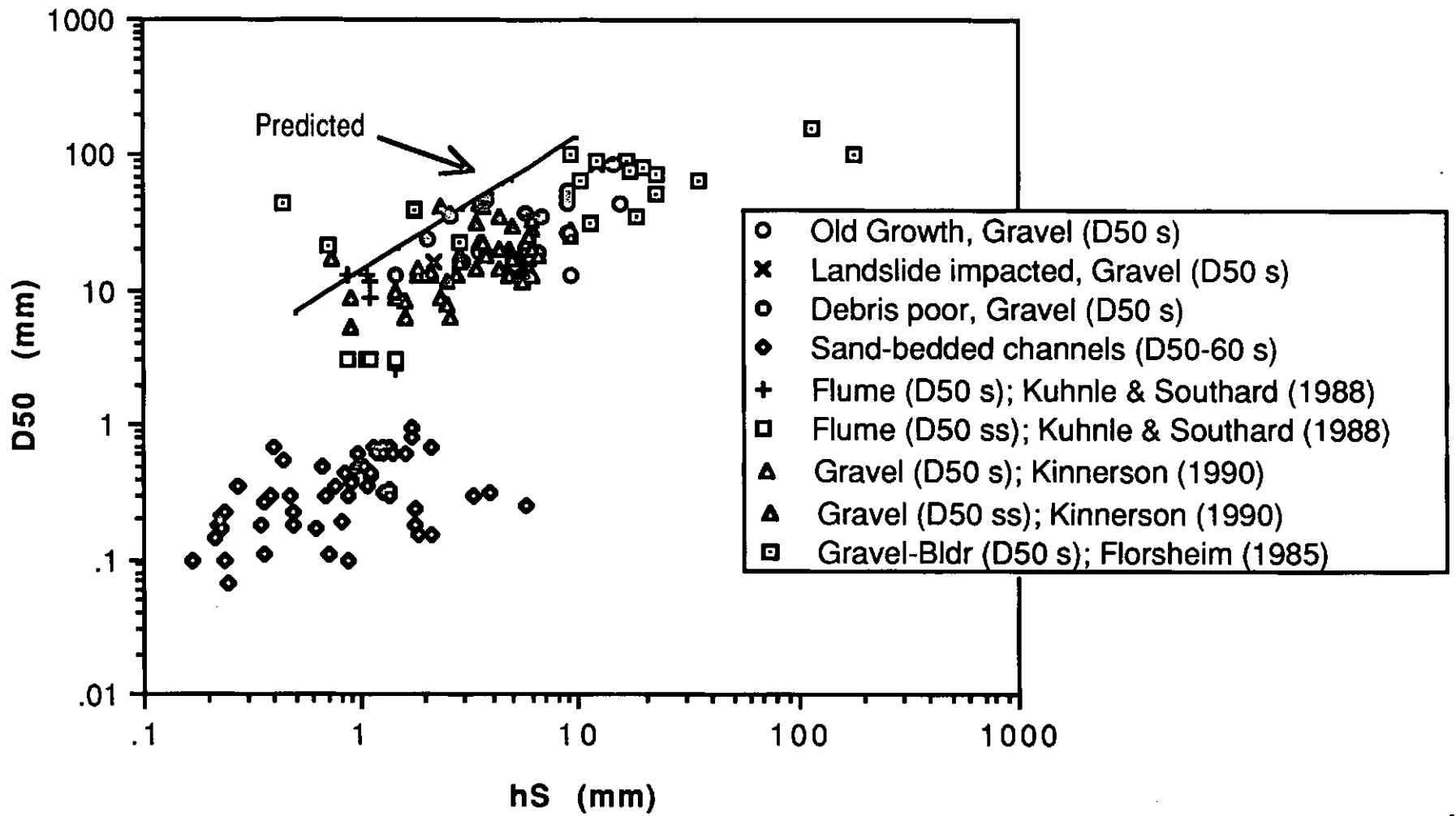


Fig. 7(a)

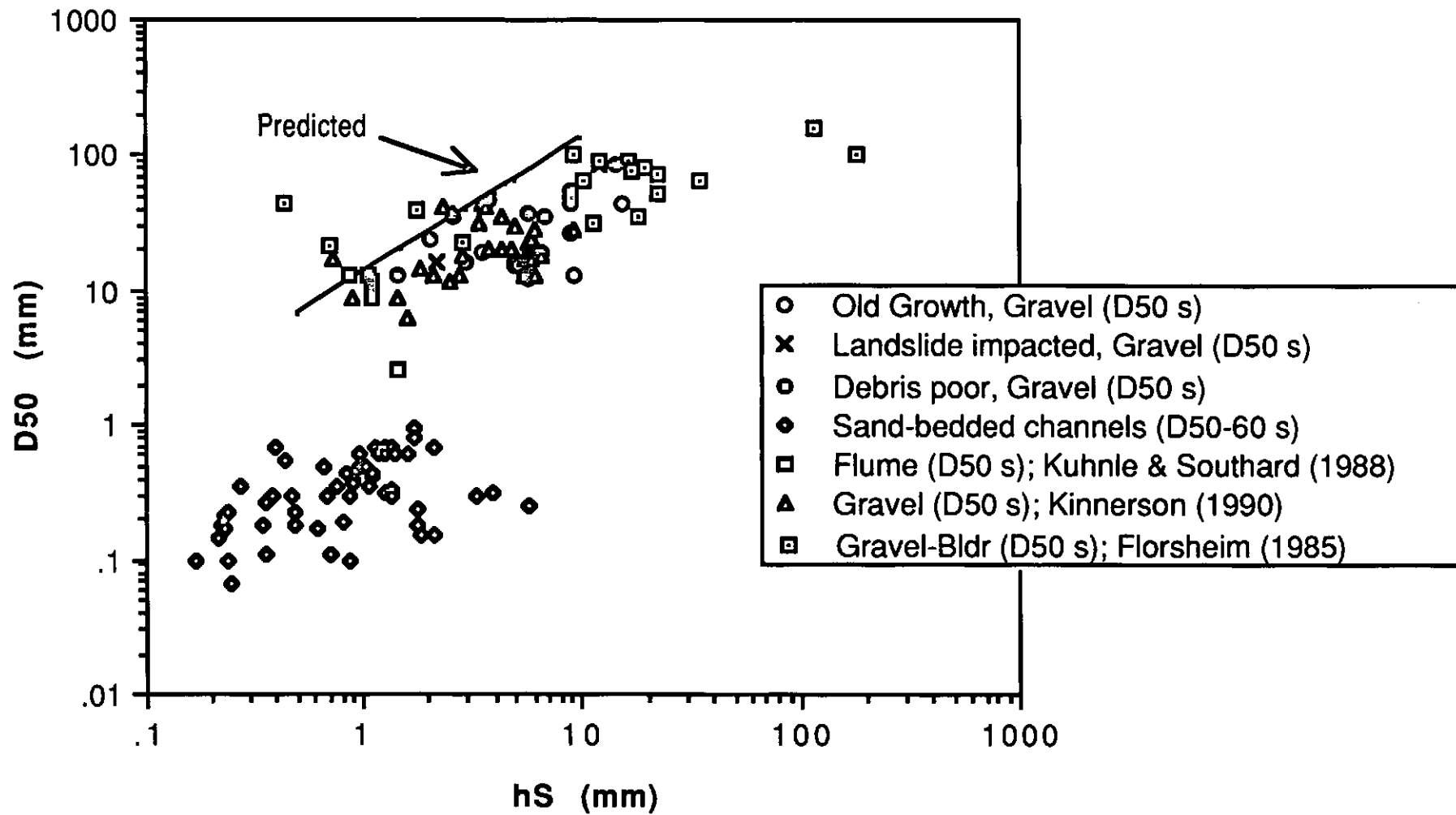


Fig. 7(b)

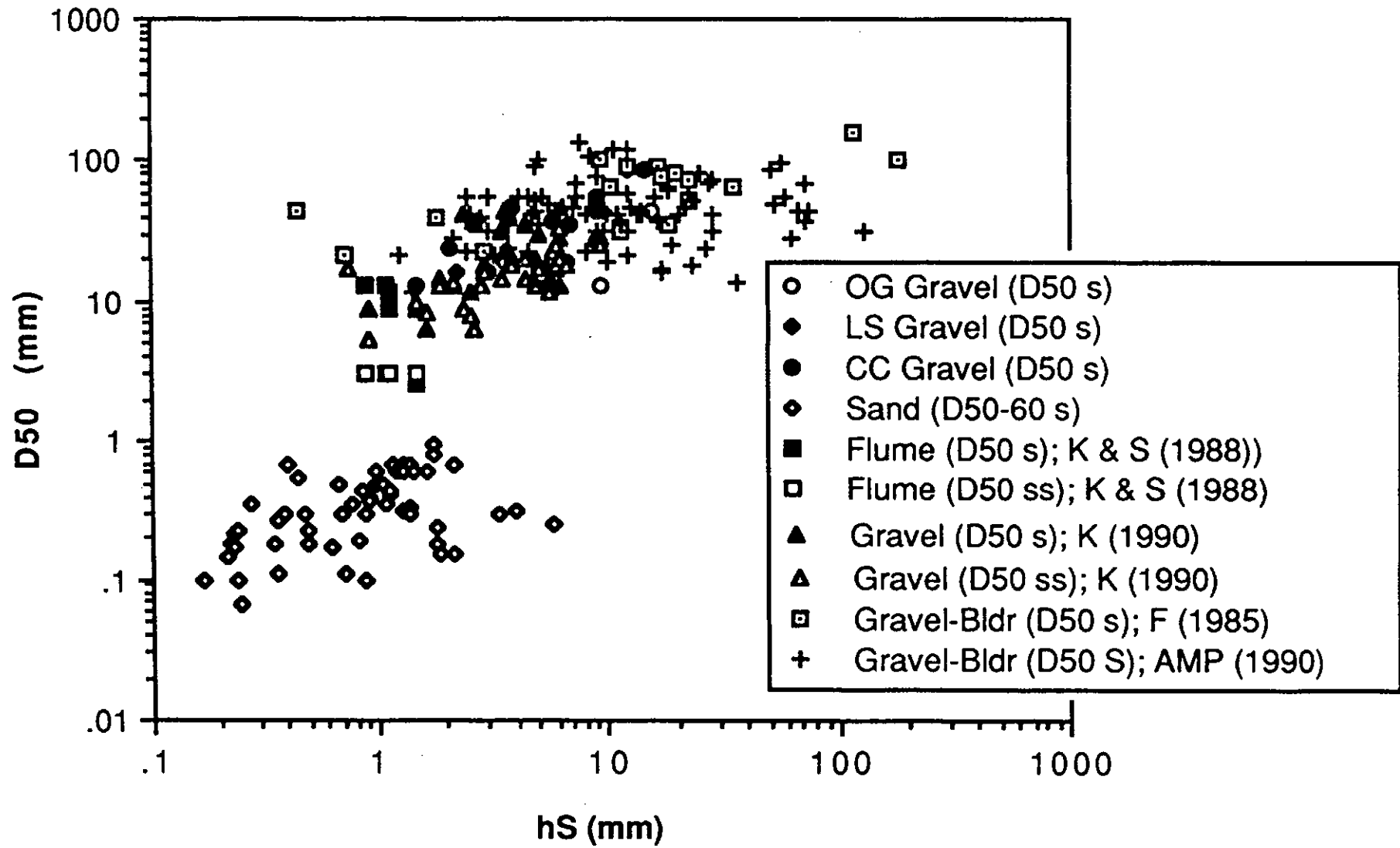


Fig. 8(a)

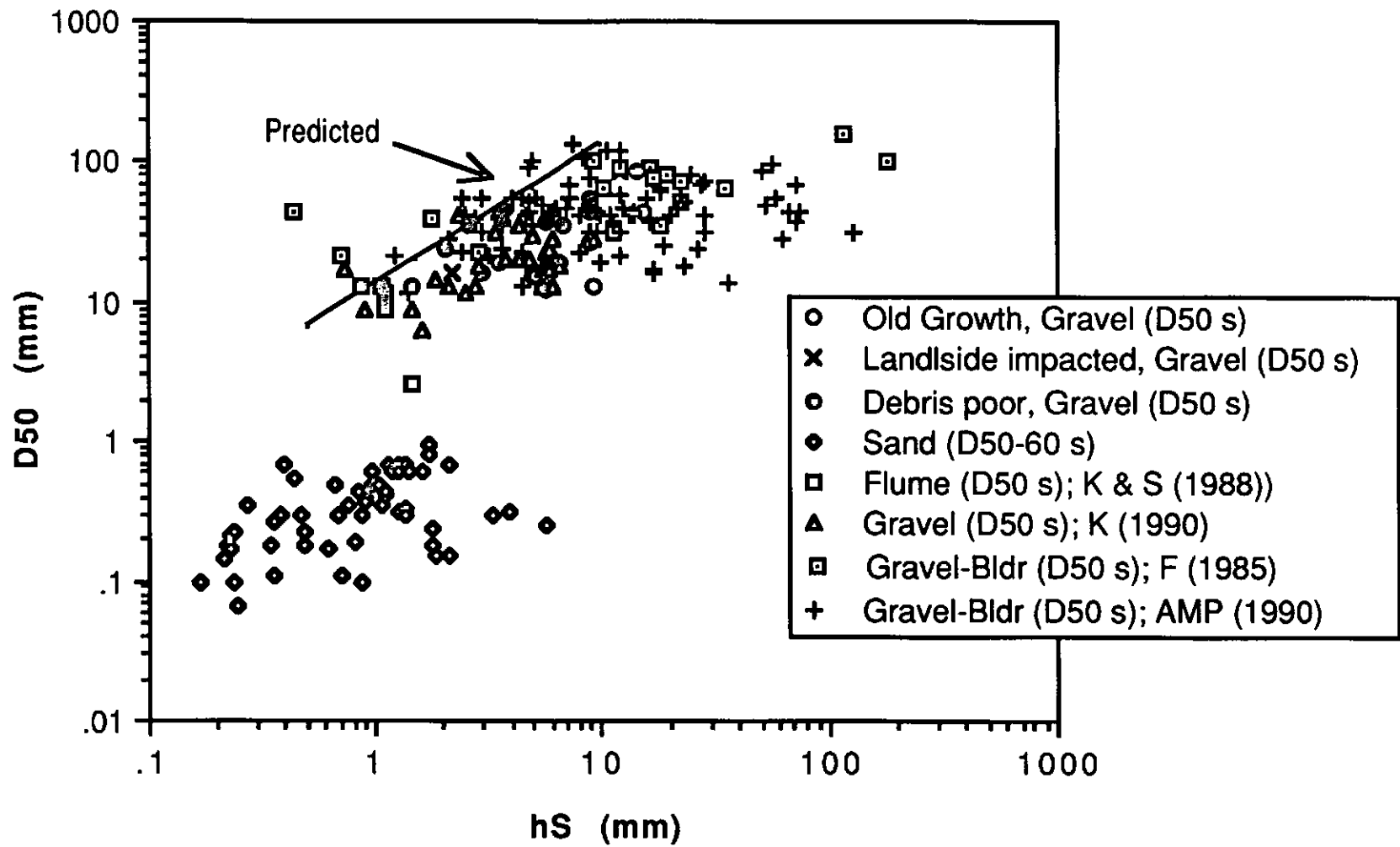


Fig. 8(b)

Appendix 8

Soil depth, slope stability and sediment production

a progress report for TFW - FY92-010

William E. Dietrich
Department of Geology and Geophysics, UC Berkeley, CA 94720

May 1992

Introduction

The use of digital terrain models in watershed analysis points out the need for relatively high spatial resolution information about the properties of the ground surface that effect hydrologic and erosional processes. Soil depth influences subsurface runoff and, if roots of vegetation or soil cohesion contribute strength to soil, then soil depth also influences slope stability. In landscapes where overland flow is absent, soil discharge to channels is dominated by mass transport, and a significant portion of the sediment yield to channels may occur through slow, diffusive-like transport of the shallow soil mass to the channel. In this case the soil thickness can be visualized as analogous to flow depth in rivers, in which soil is moving progressively downhill toward channels. Soil depth in this case is the balance between the rate of change of soil transport downslope and the addition of new material from weathering of the bedrock surface.

While it is impractical to conduct extensive investigations of the spatial pattern of soil depth, it may be possible to predict soil depth based on some simple principles. The project described here is focused on the prediction of soil depth on real landscapes using a digital terrain model and a simple sediment transport law. We propose that a relatively simple model that takes an initial uniform soil depth and predicts the evolution of a spatially variable soil depth may give satisfactory estimates of local soil depth for the purposes of watershed modelling. Preliminary findings look very promising. We envision this theory for soil depth being incorporated into a larger model enabling prediction of runoff, shallow slope stability and sediment production as influenced by vegetation change associated with landuse. The results to date, however, have also dictated a major revision of our digital terrain model in order to more satisfactorily predict the soil transport and deposition. This revision is currently in progress.

Model for prediction of soil depth

Figure 1 shows an idealized slice of a soil-mantled hillslope. This model is most readily applied to the coastal mountains of the Northwest and to the inland mountains unaffected by glaciation. Soil in this case is the material overlying the bedrock which lacks the relict rock structure (equivalent to the "solum" in pedology). The soil depth is modelled as a consequence of a simple mass balance. Written at the top of the figure is

$$I - O = \Delta S \quad (1)$$

which is simply the conservation of mass equation, i.e. input, I, minus output, O, must equal the change in storage, ΔS . The discharge per unit width into the soil "box" of depth, h, consists of the soil movement from upslope labelled here Q_1 and the addition to the soil from below due to the conversion of bedrock into soil, labelled here Q_3 . The output from the box is the downslope transport, Q_2 . If the input and output are not equal then the soil thickness will change, hence $\Delta S = (\Delta h/\Delta t)\Delta x$. This analysis is performed on a per unit width or contour length basis, hence lateral variation does not come into the analysis shown. If Q can be predicted from the digital terrain model then soil depth evolution with time can be performed.

The digital terrain model we currently use (see other papers in this annual report) divides the land surface into discrete elements with area, a_e and slope, $\tan\theta$. Equation (1) can be written to be used in TOPOG, the digital terrain model, as follows:

$$(q_s b)_{in} + (-\rho_r \frac{\partial z}{\partial t}) a_e - (q_s b)_{out} = \rho_s \frac{\partial h}{\partial t} a_e \quad (2)$$

in which

- q_s = the soil transport rate (mass/contour length per time, i.e. M/L-T)
- b = contour length (i.e. width of box in figure 1)
- in = upslope end of the element
- out = downslope end of the element
- ρ_s = soil bulk density (mass/cubic length)
- ρ_r = bulk density of underlying (usually weathered) bedrock (M/T³)
- z = vertical coordinate (L)
- t = time (T)
- a_e = horizontal area of the element (L²)
- h = element averaged soil depth (L).

Equation (2) can be written more generally as

$$\nabla \cdot \vec{q} = -\rho_r \frac{\partial z}{\partial t} - \rho_s \frac{\partial h}{\partial t}$$

in which \vec{q} is the local rate of sediment transport per unit width (a vector), but the version used in TOPOG is shown here to make it clearer what we have done. Equation (2) can be rearranged to yield

$$(q_s b)_{out} - (q_s b)_{in} = a_e \left[\left(-\rho_r \frac{\partial z}{\partial t} \right) - \rho_s \frac{\partial h}{\partial t} \right] \quad (3).$$

Equation (3) shows that we need an expression for sediment transport rate, q_s , and an expression for soil production rate from rock, $-\frac{\partial z}{\partial t}$ in order to solve for soil depth, h . It is widely held that soil transport rate by such processes as creep and biogenic is essentially a slope dependent transport process, hence we can propose

$$q_s = \rho_s K \tan\theta$$

in which $\tan\theta$ is the ground slope and K is a coefficient setting the rate of transport which is equivalent to a diffusion coefficient. Based on radiocarbon dating of colluvial soils in hollows and measurements of hillslope form, K has been estimated for parts of California and Oregon (Dietrich, et al. in prep.). Although G.K. Gilbert in his various papers about the West in the late 1800's and early 1900's proposed that bedrock weathering and by inference soil production rate should vary with the thickness of the soil mantle, few studies have addressed the issue of soil production rates and no data exist that define the functional form of a transport law. We propose that soil production rate should vary with soil thickness. In general, as the soil thickens, the probability of mechanical disturbance due to animal, insect and plant root growth disruption of the weathered rock structure should decline and, consequently, rate of soil production should decline.. It is debated about whether very thin soil would favor high or low production rate (low would occur if the soil is so thin it does not retain water for infiltration into the rock thereby inducing weathering, and if it is too thin to host organisms that would dig into the weathered rock). Hence, we can propose

$$-\frac{\partial z}{\partial t} = f(h) \quad (4)$$

and equation (4) becomes

$$\frac{\rho_s K}{a_e} [(b \tan \theta)_{out} - (b \tan \theta)_{in}] = \rho_r f(h) - \rho_s \frac{\partial h}{\partial t}$$

if $\rho_s, \rho_r, K \neq f(x, y, t)$.

Solving for h yields

$$h_{t_{i+1}} = h_t + \left[f(h_t) - \frac{K \rho_s}{a_e \rho_r} \left((b \tan \theta)_{out} - (b \tan \theta)_{in} \right) \right] \Delta t \quad (5)$$

where $h_{t_{i+1}}$ = depth at some time step, t_i and Δt = the time step. We have begun an investigation of this prediction of soil depth using two different models for soil production rate (equation 4). One assumes that soil production rate monotonically declines with increasing soil depth, while the other assumes that the production rate peaks at a depth of 25 cm. Soil production rate at 25 cm depth was fit to equal that estimated based on radiocarbon dating in the grasslands in Marin County, California. The two production laws are:

$$f(h) = 6.34 \times 10^{-3} - 6.85 \times 10^{-5}h - 3.23 \times 10^{-7}h^2$$

and

$$f(h) = 5.27 \times 10^{-4} + 4.85 \times 10^{-4}h - 1.61 \times 10^{-5}h^2 + 1.94 \times 10^{-7}h^3 - 1.02 \times 10^{-9}h^4 + 1.99 \times 10^{-12}h^5$$

in which soil depth is in centimeters.

The digital terrain model, TOPOG, is not set up to allow for elevation change as a consequence of surface erosion, consequently modelling of soil depth based on equation 5 is most realistic as long as predicted erosion and deposition did not cause large topographic change. This limit will be overcome with the development of our grid-based digital terrain model.

Soil depth modelling: trial runs for a small watershed

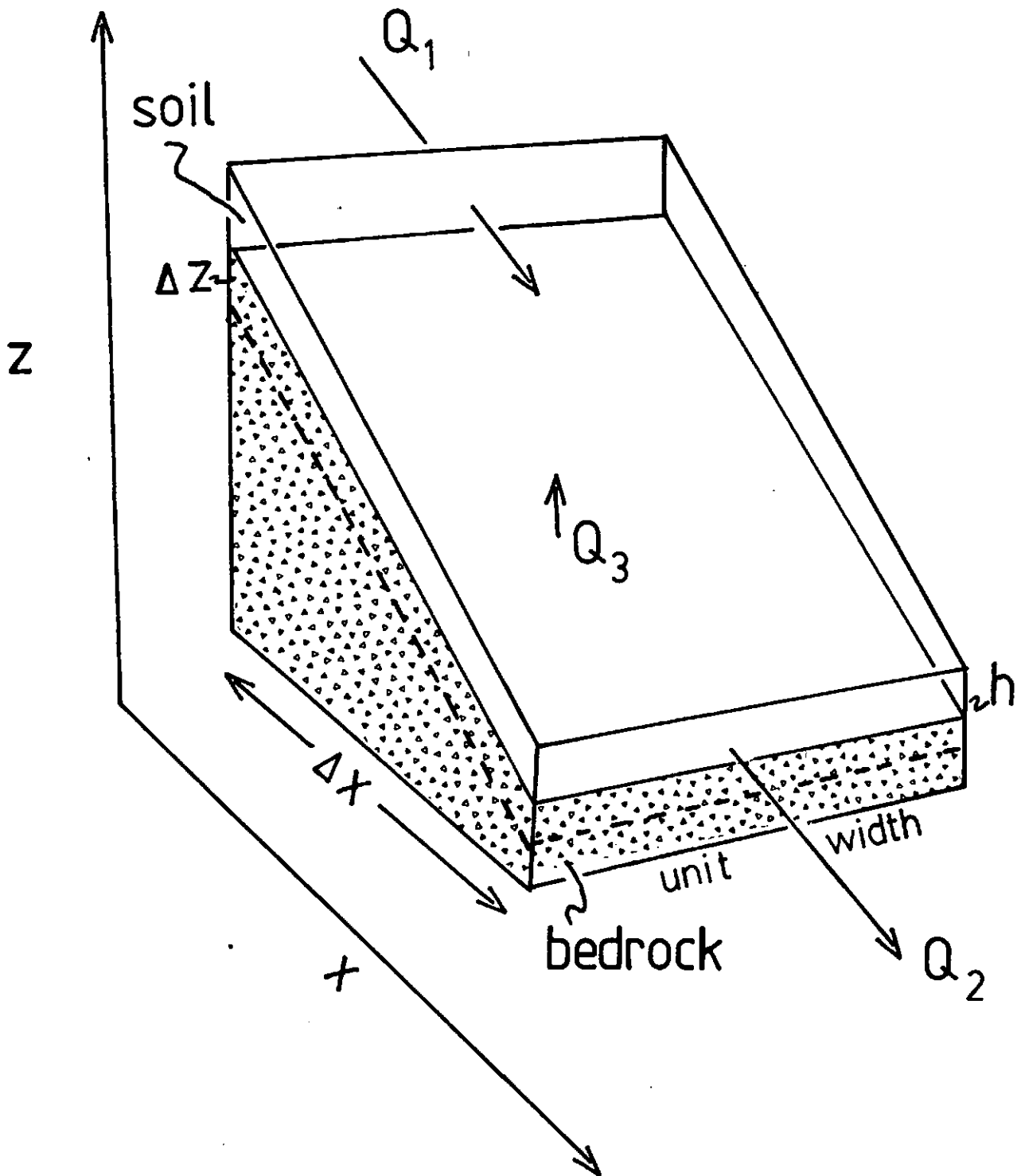
We ran the soil depth prediction model for a variety of initial soil depths, diffusion coefficients and for the two proposed soil production laws. Figure 2 shows a typical result of the model. In this case the initial soil depth is 60 cm, and the diffusion coefficient is 45 cm²/yr. We used the second order polynomial for production rate and ran the model for the equivalent of 10,000 years. This choice of model time was based on limiting soil depth variation to generally small changes so that the surface topography would not have changed significantly. Also 10,000 years is a period of roughly constant climate.

In general soil depth prediction is consistent with field observations. The thin soils correspond well to regions where bedrock outcrops occur. The thick soils occur at the break in slopes at the boundary between hillslopes and valley bottom and in hollows. We did not see the relatively thin soils in the model on the narrow ridges that are found in the field. Also the pattern of hollow infilling is not entirely consistent with what we find in the field in that the model tends to underpredict soil depth along the hollow axes. Some of these inconsistencies are associated with how the model performs calculations. The grid-based model which we are currently building should eliminate this problem and allow the model run for a longer period.

Conclusions

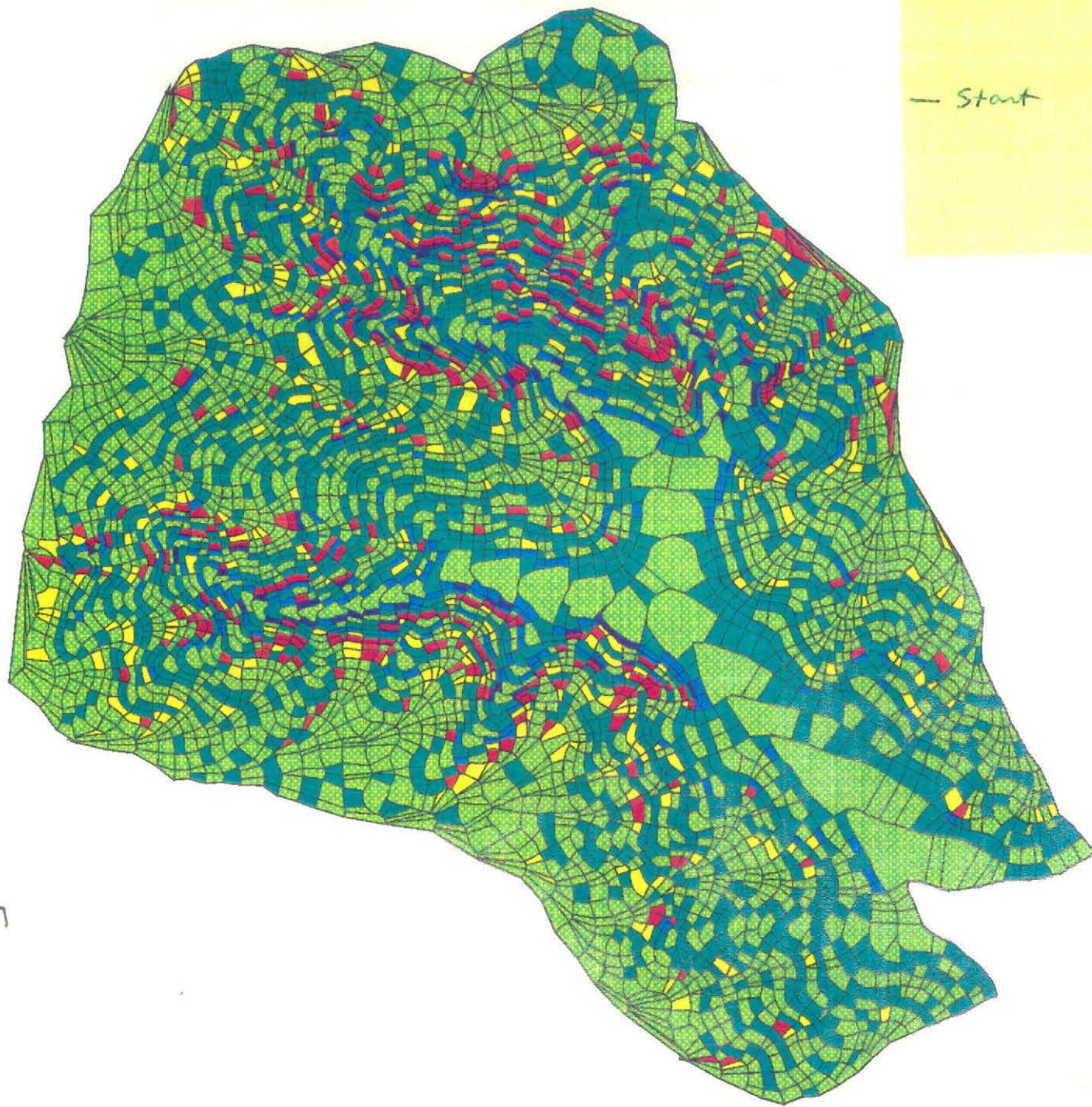
Preliminary modeling of soil depth variation in a watershed appears promising. Successful development of such a model would have great value in improving the hydrologic, slope stability and sediment flux models for watershed analysis. Once a new digital terrain model is completed that will allow for topographic change over time, further analysis of the soil model will be performed. We can test the specific predictions of the model by conducting field surveys of soil depth. We will also analyze other, forested environments, where adequate digital elevation data exist.

$$I - O = \Delta S$$



$$Q_1 + Q_3 - Q_2 = \frac{\Delta h}{\Delta t} \Delta x$$

Figure 1.



Height cm

- Above 400
- 200 - 400
- 80 - 200
- 35 - 80
- 15 - 35
- 5 - 15
- Below 5

— Start →

Sediment Transport

$k = 45$

Init Height = 60 cm

Poly = 2nd Order

Run Time = 10,000 years

Figure 2.